United States
Department of
Agriculture

Forest Service

Pacific Northwest
Research Station

General Technical
Report
PNW-GTR-251
March 1990

Airborne Monitoring and Smoke Characterization of Prescribed Fires on Forest Lands in Western Washington and Oregon: Final Report

Lawrence F. Radke, Jamie H. Lyons, Peter V. Hobbs, Dean A. Hegg, David V. Sandberg, and Darold E. Ward

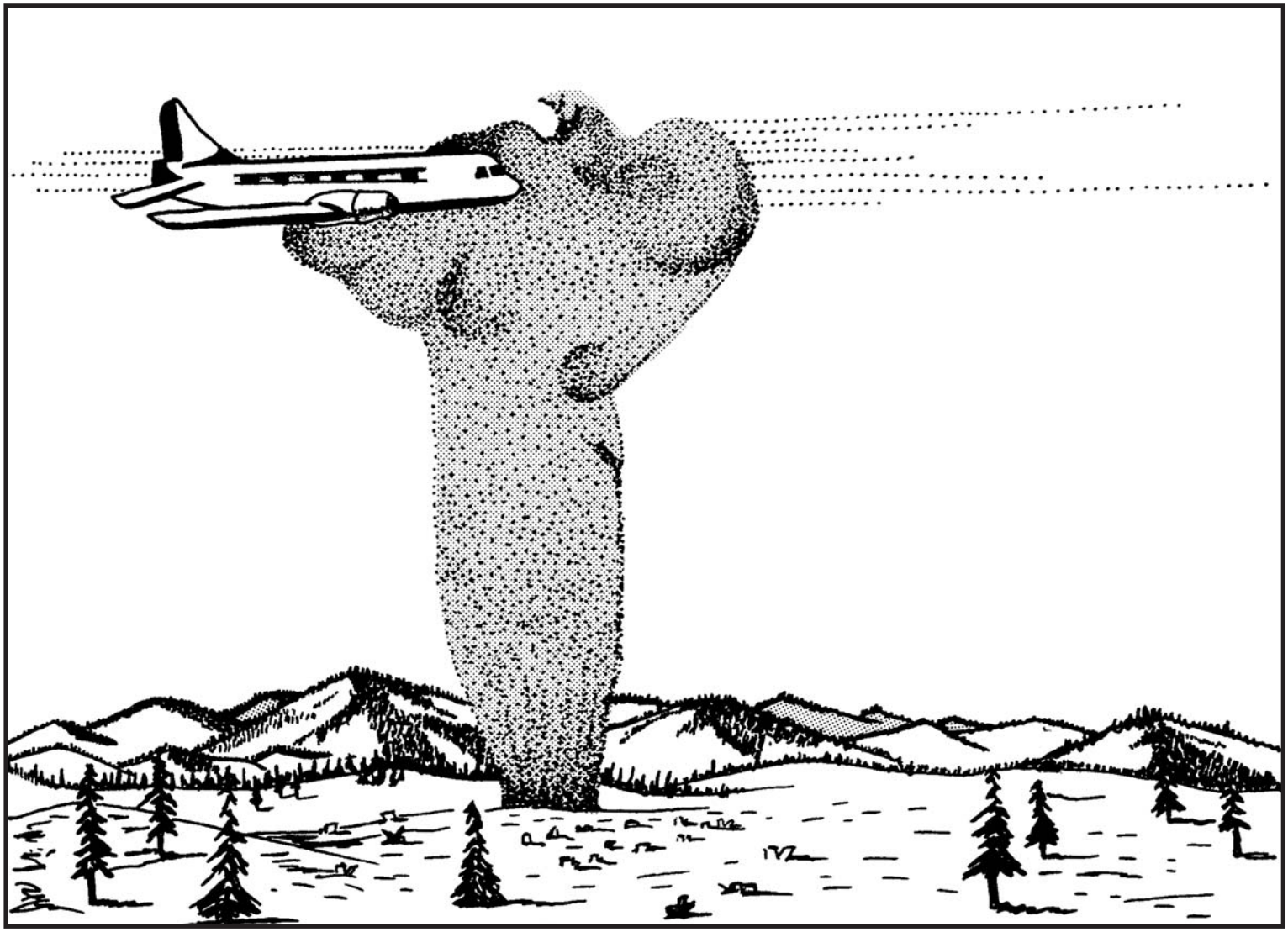

Authors

LAWRENCE F. RADKE is research professor, JAMlE H. LYONS is meteorologist, PETER V. HOBBS is professor, and DEAN A. HEGG is research associate professor, University of Washington, Department of Atmospheric Sciences, Seattle, WA 98195; DAVID V. SANDBERG is supervisory research forester, Pacific Northwest Research Station, Forestry Sciences Laboratory, 4043 Roosevelt Way, NE, Seattle, WA 98105; and DAROLD E. WARD is supervisory research chemist, lntermountain Research Station, lntermountain Fire Science Laboratory, P.O.Box 8089, Missoula, MT 59807.

The material was prepared for Lockheed Engineering and Management Services Company, Inc., Las Vegas, NV 89114, under EPA contract no. 68-03-3050, U.S. Environmental Protection Agency, Office of Research and Development, Environmental Monitoring Systems Laboratory, Las Vegas, NV 89114. This report supersedes two previous drafts.

Abstract

Radke, Lawrence F.; Lyons, Jamie H.; Hobbs, Peter V.; Hegg, Dean A.; Sandberg, David V.; Ward, Darold E. 1990. Airborne monitoring and smoke characterization of prescribed fires on forest lands in western Washington and Oregon. Gen. Tech. Rep. PNW-GTR-251. Portland, OR: U.S. Department of Agriculture, Forest Service, Pacific Northwest Research Station. 81 p.

Detailed airborne measurements of smoke plumes from seven prescribed burns of forest biomass residues leftover from timber harvests in Washington and Oregon are described. Measurements of particle size distributions in the plumes at ≈3.3 km downwind of the burns showed a prominent peak in the mass concentration for particles ≈0.25-0.30 μm in diameter. The total mass of particles in the plume was dominated, however, by supermicron-sized particles. The particle number distributions were dominated by large numbers of Aitken nuclei (median number diameter ≈0.15 μm).

Based on numerous airborne measurements from six burns, the following average emission factors were determined using the carbon balance method: for total suspended particulates 1.2±0.4 percent, for particles ≤43 μm in diameter 0.6±0.3 percent, and for particles <0.2 μm in diameter 0.4±0.2 percent. Particle mass fluxes for total suspended particulates, particles ≤43 μm diameter, and particles <2 μm diameter ranged from 0.1 to 2.4 $kg \cdot s^{-1}$, 0.1 to 1.1 $kg \cdot s^{-1}$, and 0.1 to 0.8 $kg \cdot s^{-1}$, respectively, for the smaller Oregon burns and from 1.1 to 11.7 $kg \cdot s^{-1}$, 0.6 to 7.0 $kg \cdot s^{-1}$, and 0.4 to 14.1 $kg \cdot s^{-1}$, respectively, for the larger Washington burns.

Other samples collected in conjunction with the airborne work included those for trace gas analysis, particulate matter for trace element analysis, and gas concentration measurements for carbon-mass analysis (oxides of nitrogen, ozone, and hydrocarbons). Mass concentration-to-light scattering coefficient algorithms and ratios, which can be used to convert integrating nephelometer response to mass concentration units, are also reported.

Keywords: Emissions, prescribed burning, smoke management.

Contents

1. Introduction

Forest fires, prescribed burning of forest logging wastes, and agricultural burning create a portion of the particles injected directly into the atmosphere (SCEP 1970). Ward and others (1976) noted that about 10^7 ha of forest land are burned annually in the United States and that estimates of the quantity of particles emitted into the atmosphere from this source range from 0.5 to 50 million metric tons per year. The Environmental Protection Agency (EPA) has estimated the total direct emission of particulate matter from all sources in the United States to be 20 million metric tons per year (SCEP 1970). The upper limit for estimates of particles from the burns of forest land clearly is inconsistent with the EPA estimate for total emissions. The uncertainties are due to the limited data base and also to the difficulty in obtaining good measurements of particle emission rates from large areal sources such as forest fires.

This paper reports on part of a larger study to characterize particle emissions from the prescribed burning of forest biomass (residues from harvesting) as functions of time, combustion character, fuels, and forestry practices. Measurements were made of the plumes from seven prescribed burns conducted during 1982 in Washington and Oregon. Five of the tests were designed to increase knowledge of the effects of residue removal—to various size specifications—on emissions (one of the problem areas being studied by the USDA Forest Service, Pacific Northwest Research Station, Forest Residues and Energy Program). The other two tests were conducted to examine mass-ignition techniques (such as heliotorch) as emission-reduction methods. It was hypothesized that rapid ignition may be one way to reduce the composite emissions factor and to limit the period of smoldering combustion. The combined data set supplements work completed during 1981, in which two prescribed fires were sampled (Anderson and others 1982, Sandberg and Ward 1982, Ward and Sandberg 1982).

This report deals only with the airborne measurements of the emissions from the seven prescribed burns as obtained by the Cloud and Aerosol Research Group at the University of Washington (UW). Some preliminary analyses are also presented of samples collected by UW but analyzed by Lockheed Engineering and Management Services Company (LEMSCO), the Oregon Graduate Center (OGC), and the Crocker Laboratory, at the University of California at Davis. We will characterize the fires as to plume dimensions, particle size distributions, particle densities, and particle emission fluxes. This report was prepared without detailed information on ignition techniques, "yarding" preparation, fuel moisture, and other surface measurements related to the prescribed burns so that our analysis of the emissions could be as independent as possible.

Besides the emissions characterizations that are discussed, several other types of data were collected by cooperators working under the leadership of the U.S. Department of Agriculture (USDA) Forest Service, Pacific Northwest Research Station. The data collection, data reduction, and analysis were coordinated by the USDA Forest Service, (see Ward and Sandberg 1982). The study was cooperatively funded and administered by the USDA Forest Service PNW Research Station; EPA Region X; the U.S. Department of Energy, Region X,

through the Bonneville Power Administration; and the EPA Environmental Monitoring Systems Laboratory.

2. Aircraft Instrumentation System

The aircraft used in this study was a Douglas B-23[1] which is maintained and operated by the Cloud and Aerosol Research Group of the Atmospheric Sciences Department at UW, Seattle.

2.1 Overview

The trace gas and aerosol instrumentation aboard the aircraft is shown in figure 1, and descriptions of the instruments are given in table 1. The measurements of interest in this study included descriptions of particle size distributions and the masses of suspended particulates. The masses of suspended particulates were measured by weighing filters exposed to the air and by a microbalance cascade impactor (with a diffusion dryer) and-a mass monitor (with a 2- μm diameter cutoff inlet impactor and diffusion dryer). The overall performance of the complete measuring system was excellent during the several experiments.

2.2 Particle Measuring System

The particle light-scattering coefficient of air was measured with an in-house modified, MRI 1567 integrating nephelometer, which sampled from a 30-L plenum chamber maintained at 5 °C above ambient temperatures. Outside ambient air was brought into this chamber isokinetically by means of a pump connected to a static pressure transducer that maintained zero overpressure in the head and line of the sample probe to the plenum chamber. The above-ambient temperature of the plenum chamber ensured that only dry particles entered the integrating nephelometer.[2]

The main filter sampling system consisted of a ≈500-L polyethylene bag, which was filled nearly isokinetically by ram air through a 6.3cm diameter sample port, a filter sampling manifold with flowmeter, and an engine-driven vacuum pump. The bag took ≈5 seconds to fill and entrained all particles <5 μm in diameter (the collection efficiency of the system for particles >5 μm was not quantified). After the bag was filled, a sample of the air in the bag was pulled through a Teflon filter 37 mm in diameter. Sample flow rates and mass flow volumes were measured by a TSI 2013B mass flow sensor interfaced with a microprocessor. Postflight analysis of the filters was done at the Crocker Laboratory. The results of these analyses will be discussed.

---

[1] Use of a trade name does not imply endorsement or approval of any product by the USDA Forest Service to the exclusion of others that may be suitable.

[2] Air from the plenum chamber was automatically passed through a set of filters when the light-scattering coefficient indicated that the aircraft was in the plume from a burn. These filters were sent for analysis to the Crocker Laboratory, University of California at Davis.

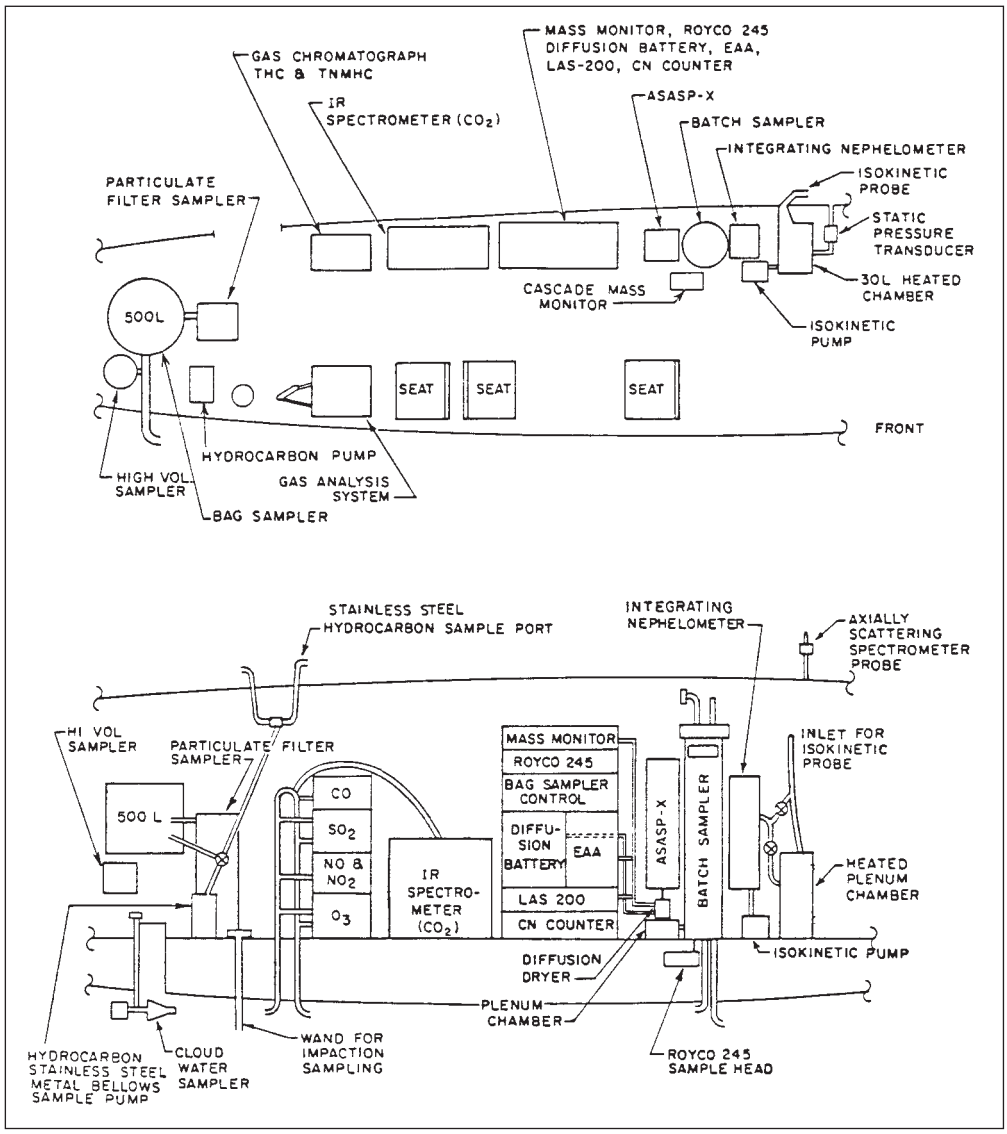

Figure 1—Aerosol and trace gas instrumentation aboard the University of Washington's B-23 research aircraft. Meteorological, navigational, cloud, and precipitation instrumentation are not shown.

A major subunit of the UW particle-measurement system measures size spectra of the atmospheric aerosol. Because the particles spanned a size range on a logarithmic scale of nearly four decades in diameter, several different sensors had to be used. This is illustrated in figure 2 where a typical volume distribution for a power plant plume is shown with the various instruments used to measure the sizes of the particles in the distribution.

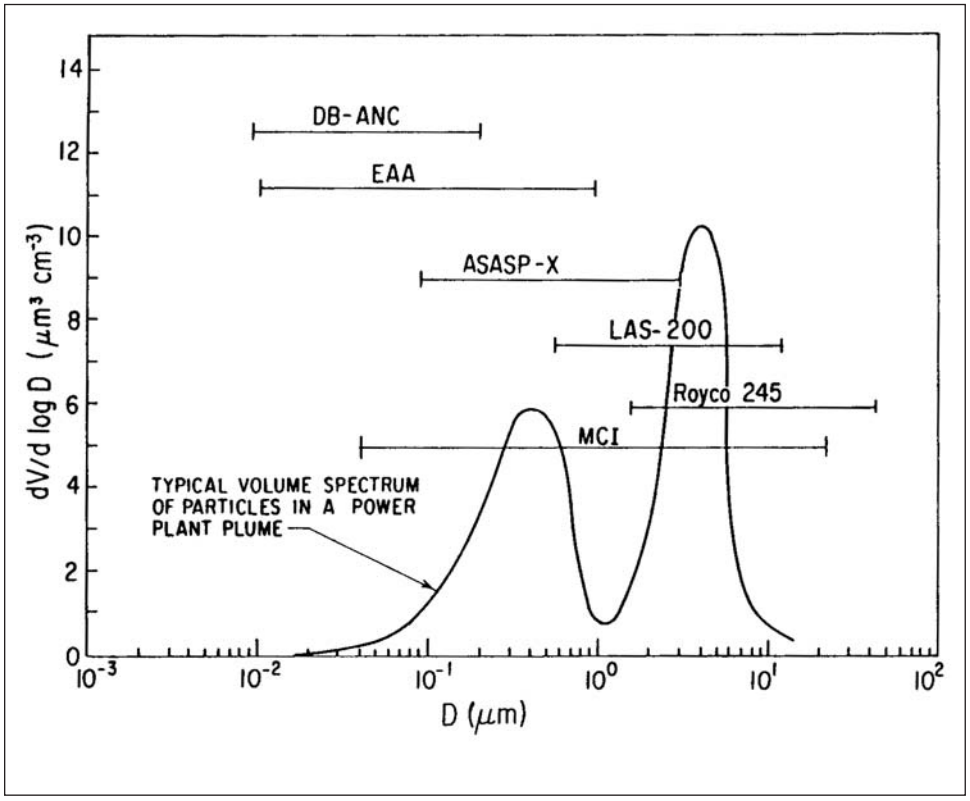

Figure 2—Diameter (D) ranges of the particle sizing instruments aboard the University of Washington's B-23 aircraft shown with respect to the volume (V) distribution of particles in a power plant: DB-ANC = diffusion battery coupled to an Aitken nucleus counter; EAA = electrical aerosol analyzer; ASAS = active scattering laser probe; LAS-200 = laser aerosol spectrometer; Royco 245 = forward light-scattering optical device; and MCI = microbalance cascade impactor.

These instruments have widely differing response and analysis times. This variability requires that all instruments sample from a common batch sample of air to obtain comparable measurements. A batch sample is also necessary if sharp concentration gradients of particles exist in the air, such as the smoke plumes described here. The batch sampler used on the B-23 consisted of a ≈90-L cylinder (≈150 cm high) with a freely floating piston to cap the sample. Air pressure forces the piston up, which fills the cylinder with ambient air. Because the sample offers negligible resistance to the incoming air, sampling is essentially isokinetic. After the cylinder is filled, the various particle-sizing instruments sample from the base of the cylinder (to avoid loss or sedimentation). A schematic of this batch sampler is shown in figure 3.

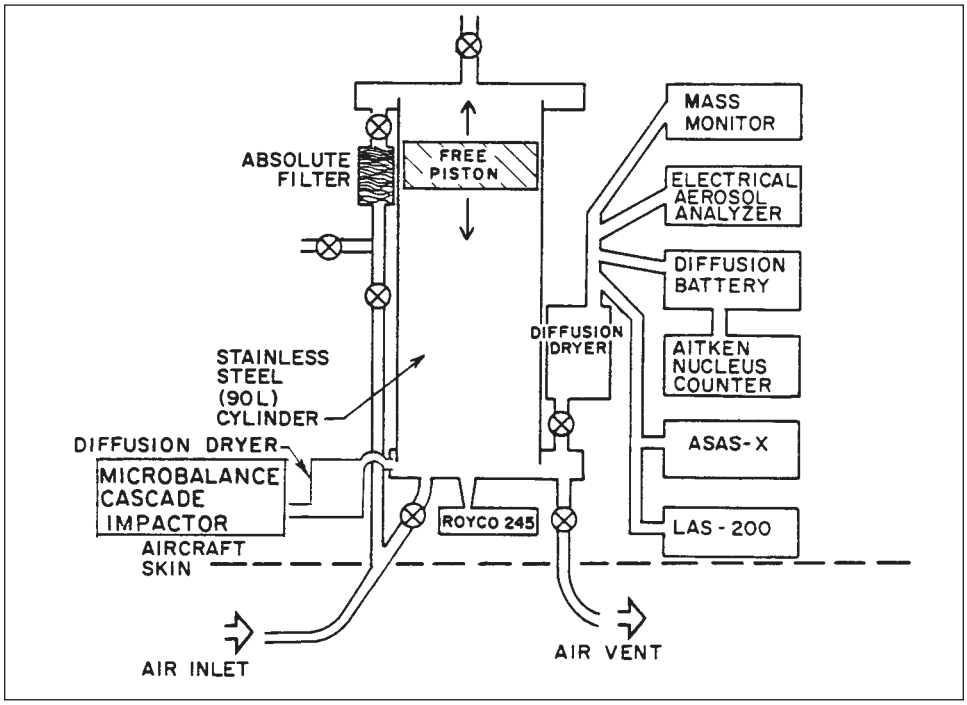

Figure 3—The batch air sampler aboard the University of Washington B-23 aircraft.

The smallest particles measured are sized by an electrical aerosol analyzer (EAA) and a diffusion battery coupled to an Aitken nucleus counter. The EAA operation is based on the relations among the charge, size, and electrical mobility of a particle. Particles entering the instrument are charged, their mobilities in an electrical field are measured, and their sizes are deduced. The diffusion battery measures particle sizes by determining the number of fine-mesh screens the particles can pass through. The greater the screen "penetration," the larger the size of the particles. Particle detection is achieved with an Aitken nucleus count er. In this study, the EAA generally functioned well; therefore, the diffusion battery data, which require extensive computer processing, were not analyzed.

Particles of intermediate size (see fig. 2) were measured with a particle-measuring system (PMS) active scattering laser probe (ASAS). This device is essentially an open-cavity laser; the measuring principle is based on the fact that a particle passing through the pumping cavity of a laser will "detune" the laser to an extent proportional to the size of the particle. Medium- to large-sized particles are measured with a PMS laser aerosol spectrometer (LAS-200) and a forward light scattering spectrometer (Royco 245). The LAS-200 determines particle sizes by measuring the quantity of light scattered in the forward direction with a laser, and the Royco 245 does so with filament light source.

A microbalance cascade impactor (MCO, supplied by EPA, was fitted with a diffusion dryer and placed near the inlet port of the large diffusion dryer. The total length of plumbing from the MCI to the batch sampler port was about 30 cm with a residence time of less than 1 second. The MCI had 10 stages, between 0.05 and 24 μm; however, because of the sampling inlet, only a small fraction of the aerosol <10 μm should have reached the MCI. The MCI was easily overloaded with aerosol, and it was not practical to clean it in flight. The number of samples taken with the MCI therefore was deliberately restricted.

2.3 Trace Gas Measuring System

Trace gas analyzers aboard the B-23 provided continuous measurements of the concentrations of SO_2, O_3, and NO_X in the atmosphere. Excess ethylene was supplied to a reaction chamber through which ambient air was drawn, and the O_3 instrument measured ozone by monitoring the chemiluminescence from the ozone-ethylene reaction.

The NO/NO_2 monitor is a dual-reaction chamber device; in one chamber, measurements are made of the chemiluminescence of the $NO+O_3$ reaction by supplying excess O_3 to ambient air drawn into the chamber. In the other chamber, excess O_3 iS Supplied to the ambient air that has passed over a catalytic-reducing agent to reduce to NO any NO_2 present. The difference between the NO concentrations measured in the two chambers is attributable to NO_2.

The regular sampling system for halocarbons and hydrocarbons aboard the B-23 aircraft consisted of one stainless steel sample loop 1.3 cm in diameter and about 25 m long that air was pumped through into a stainless steel canister with electropolished interiors. An overpressure of roughly 1 atmosphere was pumped into each canister. Some canisters filled through this system were supplied to the OGC for analysis. Because we required most of the canister samples to be coincident with the filter samples, the canisters were generally filled from the 500-L polyethylene bag (rather than from the stainless steel system). These samples were analyzed after each flight by LEMSCO by using gas-chromatography coupled with appropriate detectors. Use of the polyethylene bag compromised the measurements of some trace constituents (see section 4.3).

Measurements of the concentrations of CO_2 in the air (in real time) were made with a Miran/Foxboro long-path IR sensor. Carbon monoxide (CO) measurements were made with an Ecolyzer electrochemical oxidation instrument.

2.4 General Meteorological Instrumentation

The general meteorological instrumentation aboard the B-23 for measuring temperature, humidity, horizontal and vertical winds, and ultraviolet light intensity is listed in table 1. It is all standard equipment.

2.5 Data Processing System

Data flow charts are shown in figures 4, 5, and 6. In-flight comments by the pilots and crew were recorded on the aircraft instrumentation tape (fig. 4). Later, these were reproduced for transcript typing. High-resolution data and computer serial

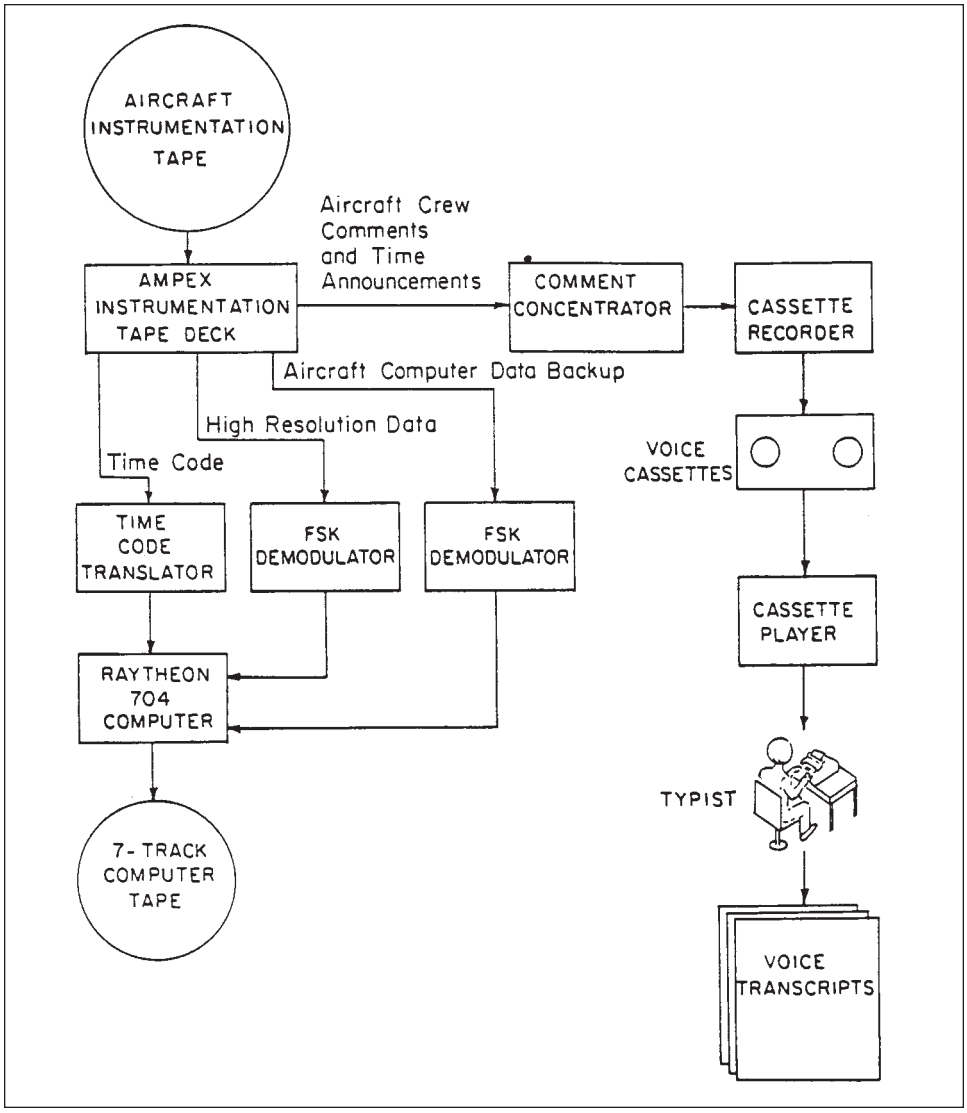

Figure 4—Flow chart for aircraft instrumentation tape to seven-track computer tape and voice transcripts.

digital products (backup to disk data) were frequency-shift-keyed, demodulated, and processed into appropriate engineering units on a Raytheon 704 mini-computer (fig. 4). The seven-track computer tape from the Raytheon can be directly reprocessed into printouts or strip charts of the high-resolution data or transferred, via a PRIME 400 minicomputer, to nine-track tapes for further processing (fig. 5).

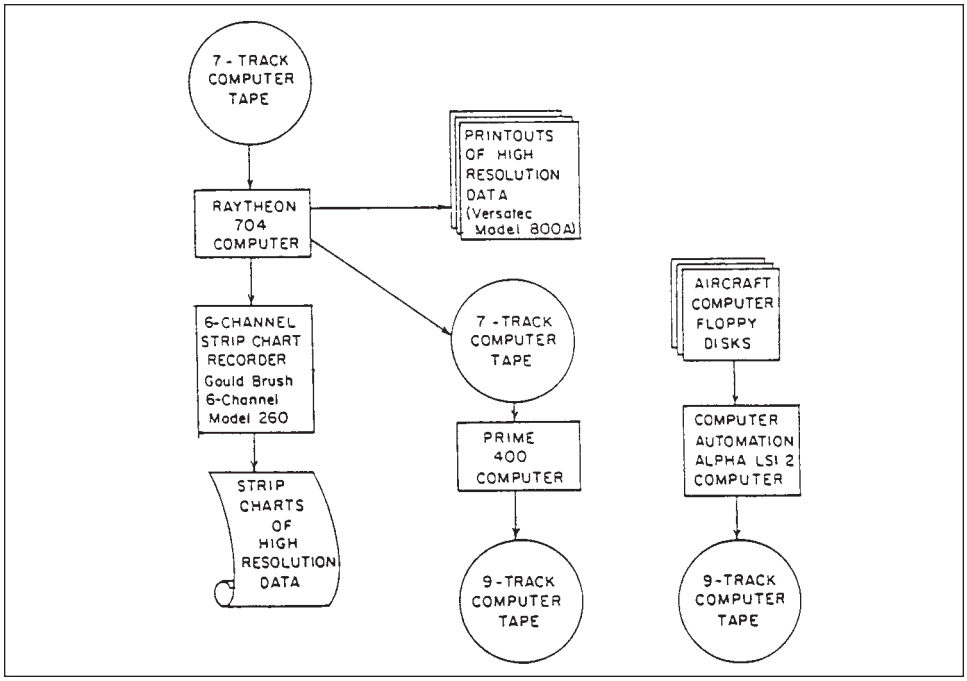

Figure 5—Flow chart for conversion of seven-track computer tapes and floppy disks to nine-track tapes and preliminary analysis hard copies.

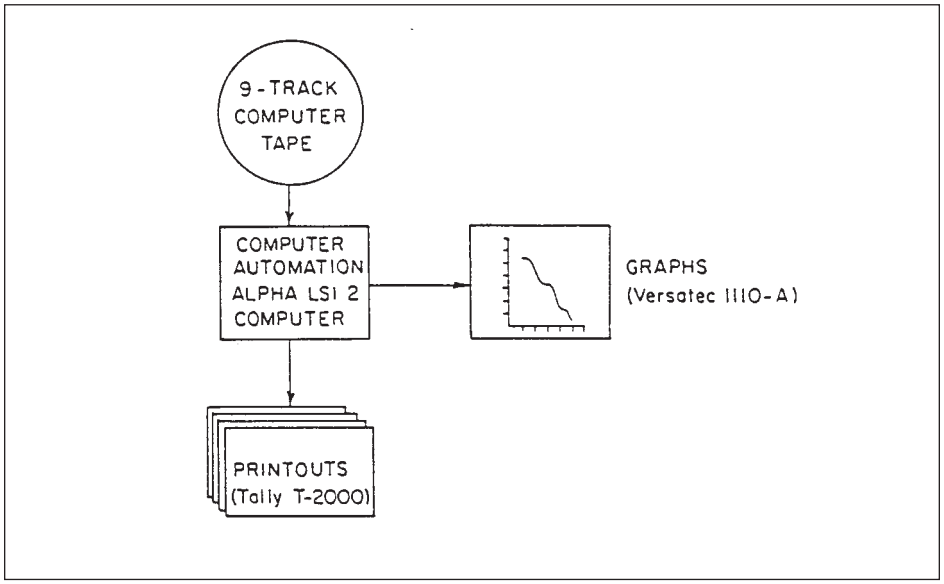

Figure 6—Flow chart for processing nine-track tapes into final hard copy printouts and graphics.

The serial digital stream from the aircraft computer normally was not recovered from the instrumentation tape but was taken directly from floppy disks (fig. 5) and converted to nine-track tape via a Computer Automation's A-LS1-2 minicomputer. Major computational efforts and graphics products were handled on the A-LSI-2 computer from a nine-track tape (fig. 6). This is a well-proven system that provides both flexibility and redundancy in data recording and processing.

3. Summary of Research Flights

On July 2, 1982, a preliminary quality control check was made of the instrumentation aboard the B-23 aircraft. The period between July 22 and July 27, 1982 was spent in Eugene, Oregon, to make four research flights through smoke plumes over the area of prescribed burning of timber harvest residues (broadcast slash burning) on units harvested to different size specifications in the Willamette National Forest (Joule Sale area). During this period, a second quality control check was completed on the airborne instrumentation system. Two research flights were made during September 1982 over two prescribed burns in the Twin Harbors area of Washington State. Table 2 summarizes the research flights made in support of this project.

4. Instrument Calibration and Data Quality Control

The interim calibration was performed in-house on June 29, 1982.

4.1 Interim Calibration Performed In-House

Ozone—The ozone analyzer was calibrated against a Monitor Labs 8510 Permacal O_3 source (UV irradiation), which was calibrated against neutral-buffered potassium iodide. Eight points were used in the calibration. The data produced the following calibration equation:

$$PO_3 \text{ (real)} = 1.08\ PO_3 \text{ (indicated)} - 1.46 \text{ ppb ;}$$

where PO_3 (real) and PO_3 (indicated) are, respectively, the actual concentrations of ozone and the concentrations as indicated by the instrument in parts per million. The correlation coefficient for the calibration equation was 0.998.

Nitrogen oxides—The NO_X analyzer (both channels) was calibrated against a Monitor Labs Permacal calibration source (permeation tube and span gas dilution), which was calibrated against gas-phase titration. Four points per channel were used in the calibration. The resulting calibration equation was:

$$PNO_X \text{ (real)} = 1.65\ PNO_X \text{ (indicated)} - 7.876 \text{ ppb ;}$$

where the concentrations are in parts per billion. The correlation coefficient in this case was 0.97.

Carbon dioxide—The carbon dioxide analyzer was calibrated against an in-house dynamic dilution system employing concentrated CO_2 and ultrapure NP_2 Although seven calibration points were employed, the inherent nonlinearity of the instrument rendered a single linear calibration over the entire range of

calibration (0-4000 ppm) impractical. For example, the calibration equation for the entire range (based on linear regression) was:

$PCO_2 = 7.395 \times 10^3$ (absorption) - 323.6 ppm ;

with a linear regression coefficient of 0.937. This equation predicts values of PCO_2 as much as 68 percent too high at lower PCO_2 (relative to the actual calibration values). If the linear regression is applied only up to 1000 ppm (a value still much in excess of any CO_2 measured during the study) the calibration equation becomes:

$PCO_2 = 3.6514 \times 10^3$ (absorption) - 7.939 ppm ;

with a correlation coefficient of 0.99. This equation predicts PCO_2 to within 16 percent of the actual calibration values and was used in the data reduction for this project.

Carbon monoxide—No attempt was made to calibrate the carbon monoxide analyzer before the audit by the Research Triangle lnstitute (RTD. The RTI audit therefore constitutes the calibration. This instrument suffers from excessive zero drift and must be constantly rezeroed to obtain accurate readings.

Integrating nephelometer—The integrating nephelometer was calibrated by comparing the instrument output when viewing clear air and Freon 12 with the expected b_{scat} (light-scattering coefficient) values for these substances. The following results were obtained:

	Clean air	Freon 12
Observed	$(1.8 \pm 1.0) \bullet 10^{-5} \bullet m^{-1}$	$3.4 \bullet 10^{-4} \bullet m^{-1}$
Expected	$1.5 \bullet 10^{-5} \bullet m^{-1}$	$2.4 \bullet^{-4} \bullet m^{-1}$

The differences between the observed and expected values were used to adjust the data collected in this field project.

4.2 RTI Field Audit

The results of the second audit of the instrumentation used aboard the B-23 and by LEMSCO are summarized in table 3.[3] The audit was made at Mahlon Sweet Airport, Eugene, Oregon, July 26-27, 1982.

[3] Data taken from: Murdock, R.W. [1982]. Second audit of airborne monitoring prescribed fires in the Willamette National Forest. RTI Report No. RTI/NIX 26/00-02F. No unresolved differences were noted between first and second audit.

Airborne instrumentation—The ambient air quality analyzers aboard the B-23 were audited for measurements of the concentrations of CO_2, CO, NO_X, and O_3. The measurements of CO_2, CO, and the total NO_X were satisfactory. The ozone analyzer read systematically 15 percent higher than the RTI standard with excellent traceability (correlation coefficient 0.9999). If the RTI standard is accepted, then the ozone concentrations reported hereafter should be reduced by 15 percent. The audit showed the flow rates on the quartz crystal microbalance and the Ghia filter sampler to be satisfactory. The Rosemount temperature sensor, Cambridge lnstruments dew point sensor, and the integrating nephelometer aboard the B-23 exhibited satisfactory performance.

The problem with the nitrogen oxides analyzer was not resolved; we accepted the analysis by RTI that the converter (NO to NO_2) did not function linearly, which resulted in NO_2 measurements that were systematically low relative to the calibration values. The error would be of order 10 percent for concentrations of NO_2 in the sub-part-per-million range. The measurements of NO_X were, however, in excellent agreement with the calibration. These problems have no impact on the data presented in this report.

LEMSCO Instrumentation—The Byron Model 401 gas chromatograph operated by LEMSCO was audited for measurements of the concentrations of carbon monoxide, carbon dioxide, methane, total hydrocarbons, and non-methane hydrocarbons. The carbon dioxide channel gave excellent performance; and the methane, total hydrocarbon, and carbon monoxide channels gave satisfactory performance. The nonmethane hydrocarbon channel was unsatisfactory (based on the intercept of the linear regression equation).

4.3 Comparison of Plume Minus Ambient CO_2 Concentrations

The data available for the comparison of the CO_2 measurements as made by OGC and LEMSCO from air samples collected in the stainless steel canisters via the polyethylene bag are shown in table 4. Each of the canister samples listed was analyzed by both systems with the indicated results. These results suggested an analytical discrepancy of about $\pm$20 percent.

Two samples were available to compare the polyethylene bag sampling system (employed most of the time) with the stainless steel sample loop system (used for some of the OGC samples). The results of these comparisons are shown in table 5. They suggest an additional discrepancy, this time systematic, of ≈20-60 percent, with the LEMSCO concentrations greater than those of OGC. This might be a bag-contamination problem, although it is unclear how such a large discrepancy could arise. The quantity of data is insufficient to warrant further discussion.

5. Flight Procedures and Data Processing

5.1 Flight Procedures

Each plume was studied by flying the UW B-23 aircraft at various altitudes across the width of the plume, generally at a range of 3.3 km (2 nautical miles) from the burn. The range was initially determined by use of visual terrain references and quadrangle maps. In cases where the plume fanned, or ground references became obscured, the range from the burn was computed in real time using data; from the doppler radar aboard the aircraft. Our position repeatability appeared, overall, to be excellent.

5.2 Data Processing

The traverses of the plume at various altitudes at a given distance downwind of a burn were labeled A, B, C, D, and E; where A, C, and E were the top, center, and bottom penetrations, respectively. The top and bottom penetrations were chosen visually such that ≈10 percent of the vertical dimension of the plume was above A and below E. The center of the plume was estimated visually, but it was generally about halfway between A and E. If the plume had sufficient vertical extent to sample at five levels, the B and D samples were taken midway between A and C and between C and E, respectively. When the plume lacked sufficient vertical depth for five traverses, the B and D samples were omitted.

Each cross section of the plumes presented in this report consisted of at least the A, C, and E traverses. The next cross section (in time sequence) at the same range used the previous traverse (either A or E) as the first traverse of the new cross section. It is assumed that the burns were of sufficiently steady states so that each cross section can be considered as if each of the plume traverses that comprise it were made simultaneously. The bag and batch samples were obtained as close as possible to the center of the plume. Because they were taken over a path with a minimum length of 300 m and required some degree of anticipation, they can be considered as located randomly about the central region of the plume. Because each filter required at least two bag samples, at least two traverses of the plume were made at each altitude. A canister sample and particle-size-distribution measurement were obtained coincident with each filter bag sample. The canister and size-distribution data are averaged when they are compared with the filter data.

The light-scattering coefficient (b_{scat}) as measured by the integrating nephelometer, was the parameter selected to be representative of the plume boundaries. Plume cross sections were created graphically by plotting the value of b_{scat} every 2 seconds (130-m path length) for each altitude traversed. Plume center was defined as that where b_{scat} reached peak values. Multiple traverses at the same altitude were averaged. In documented cases of substantial plume fanning with height, or with multiple plume cores, the cross sections were made logically consistent with the available data.

To calculate emission fluxes of any parameter, we assumed that the parameter could be linearly scaled to b_{scat}. High-resolution data (13 samples per second)

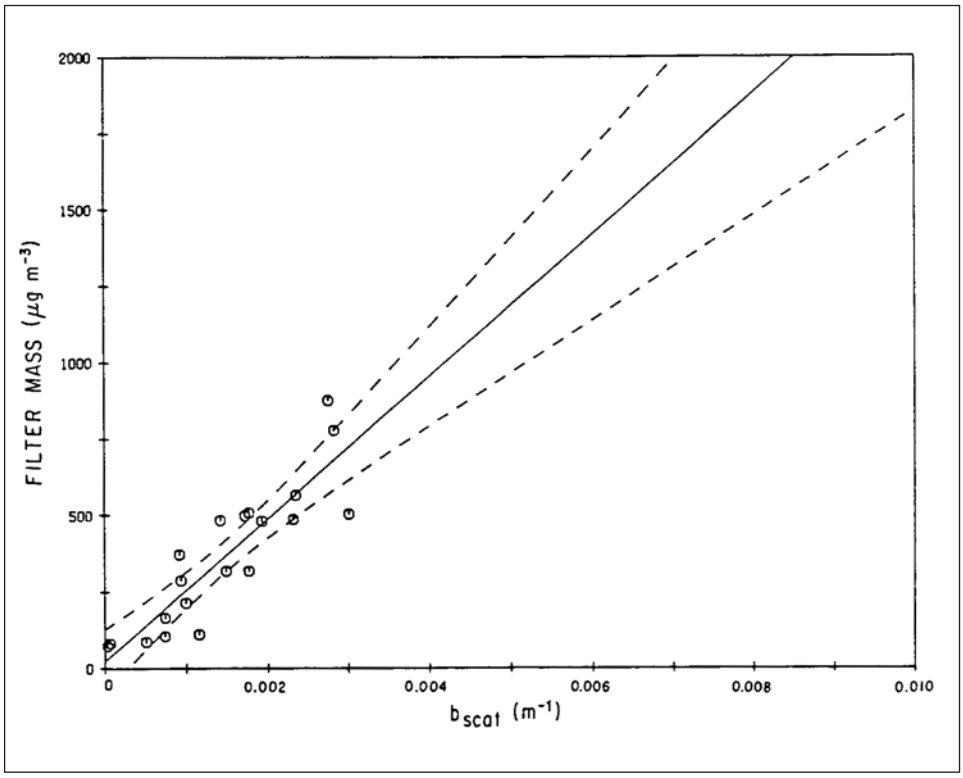

Figure 7—A plot of the weighed filter mass concentration versus the light-scattering coefficient (b_{scat}) with linear regression and the 95-percent confidence intervals for the Oregon data set.

were used for b_{scat} averages, which were computed for times when the batch sampler switch was in the “fill” position. By using a least-squares fit, an algorithm was derived for the relation between the average value of b_{scat} and each flux parameter.

In the cases of the mass fluxes derived from the filters and the mass monitor, separate algorithms were developed for the Washington and Oregon units. The b_{scat} cross sections were contoured, and the grid areas, or areas between b_{scat} contours, were determined. The cross sections were then divided elevationally by windspeed (which was interpolated from soundings taken with the pilot balloon released closest to the time of the cross section). An average windspeed was determined for each grid area. The emission flux is given by:

$$\text{Flux} = \Sigma_i (\text{grid area})_i \times (\text{windspeed})_i \times (\text{average parameter concentration in grid area})_i$$

where i indicates the b_{scat} contour level.

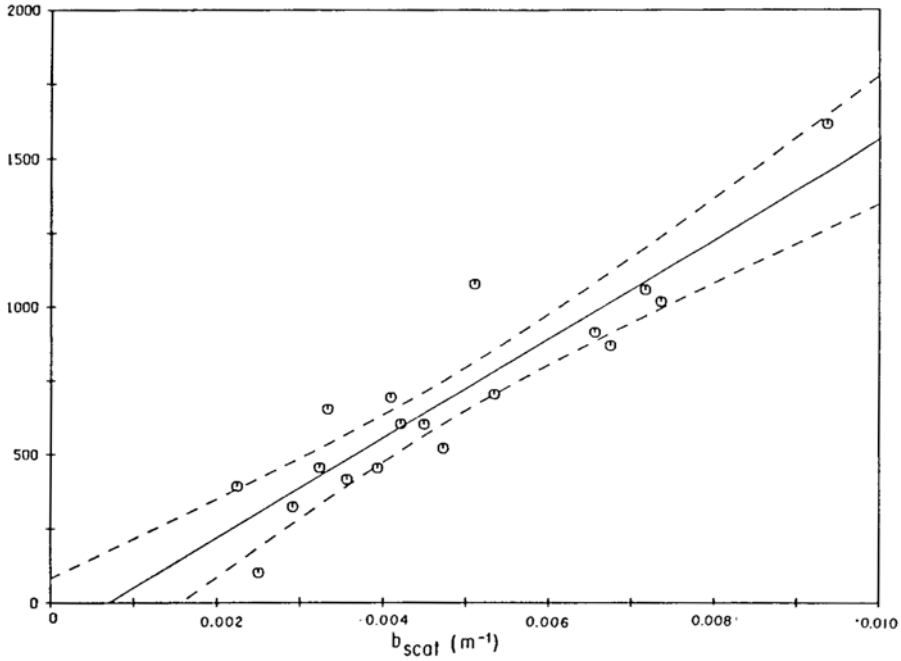

Figure 8—A plot of the weighed filter mass concentration versus the light-scattering coefficient (b_{scat}) with the linear regression and the 95-percent confidence intervals for the Washington data set.

Mass fluxes were derived from linear equations relating measurements of b_{scat} to the data from the weighed filters, the mass monitor (<2 μm in diameter) and the total aerosol volume (≤43 μm in diameter). These relations are given in table 6. Least-squares-fit linear regression equations on b_{scat} were used to derive the mass flux by using data from the mass monitor and total aerosol volume. The mean mass concentration divided by the mean b_{scat} value was also used to derive the mass flux from the filter data. Six extreme values from the weighed-filter data were excluded from analysis. FiRer data, mass monitor data, linear regressions, and 95-percent confidence intervals are plotted in figures 7, 8, 9, and 10.

5.3 Physical Interpretation of b_{scat} Algorithms

The relations between b_{scat} and aerosol mass reported in the literature have usually been the result of a very limited data set, and the authors have merely made a ratio of b_{scat} and aerosol mass and averaged the result (called the ratio method). For example, in our earlier work we found values between 1.3 and 5.8 m2•g^{-1} for this ratio. White (1981) reports a range of values from 1.5 to 15.4 m^2•g^{-1} for various sources. Anderson and others (1982) report b_{scat} to-aerosol mass ratios of 1.9 to 3.4 m^2•g^{-1} from a study similar to the present one. In the present study, the mean value was 5.6 m^2•g^{-1},with mean values of 4.1 and 6.9 m^2•g^{-1} for the Oregon and the Washington fires, respectively. The ratio method assumes that each particle contributes to b_{scat} in proportion to its mass; in fact, we know this is not the case. As described in more detail in section 6.2, the submicron particle mass completely dominates bscat for the size distributions observed in this study.

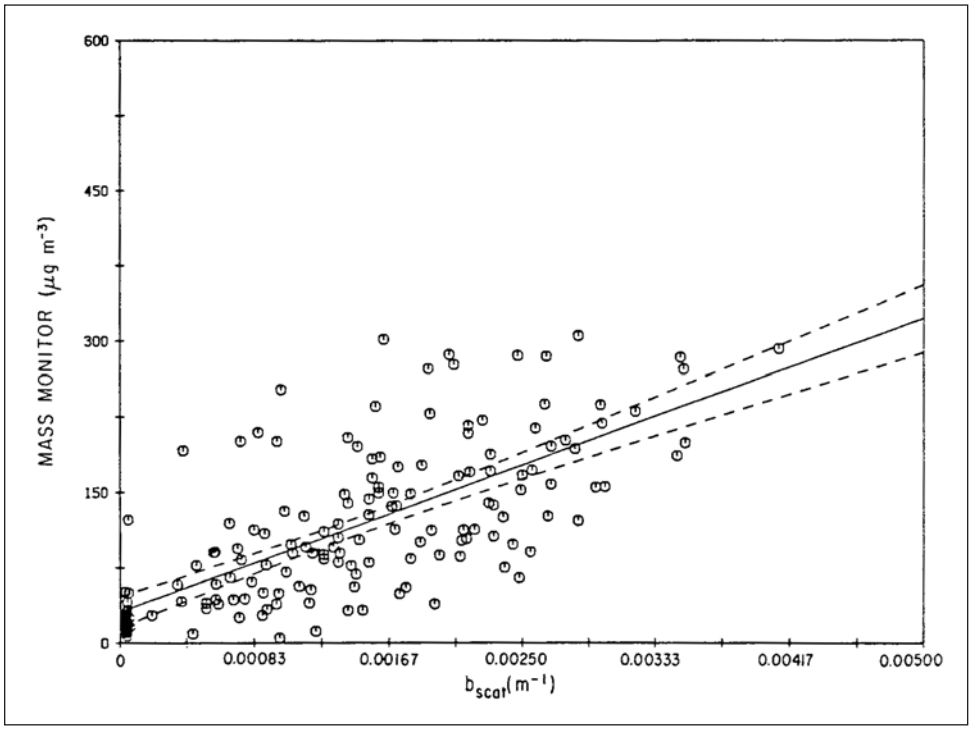

Figure 9—A plot of the mass concentration as measured using the mass monitor instrument versus the light-scattering coefficient with the linear regression and the 95-percent confidence interval for the Oregon data set.

It is some combination of the distribution of supermicron particles and the inherent noise of the data that produces the significantly nonzero intercepts of the algorithms in table 6. That this departure from a 1:1 relationship is mathematically secure for the filter data is indicated by the number of samples (44) and the satisfactory correlation coefficient (0.78). The correlation coefficients are significantly improved if the data are divided into sets for Washington and Oregon and six "extreme" values are excluded. The correlation coefficients for the Washington and Oregon data sets are 0.92 and 0.88, respectively. No apparent basis for excluding the extreme values exists other than they appear to be "outliers." Thus, for the bums studied, the b_{scat}-linear-fit algorithm provides, in some ways, a superior predictor of smoke mass than does the ratio method. The disadvantage of the algorithm is its questionable value at the edges of plumes where bscat is small.

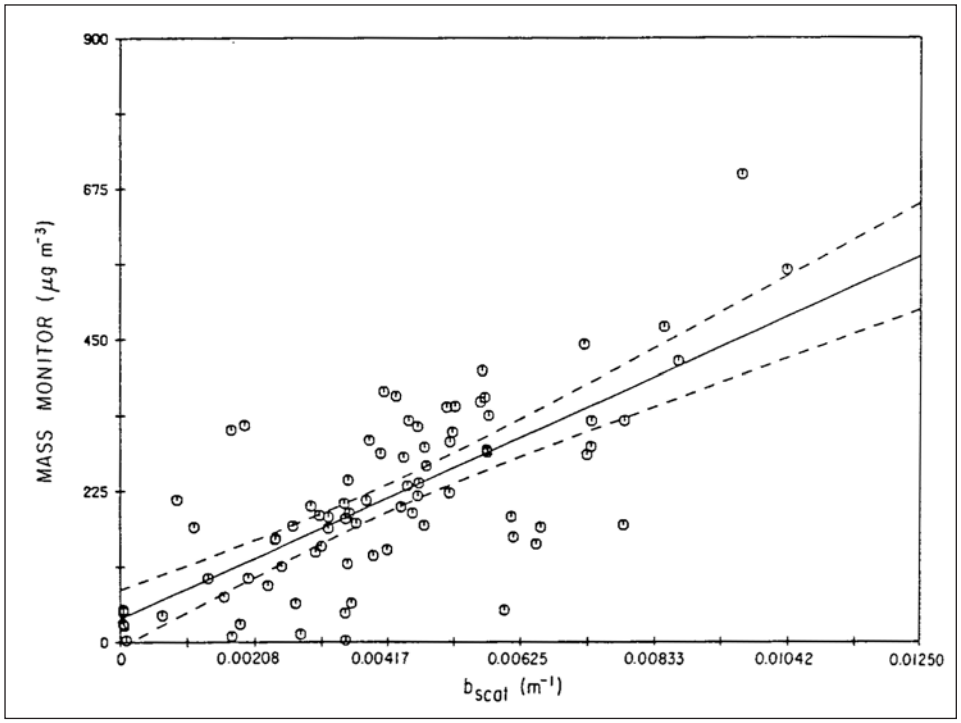

Figure 10—A plot of the mass monitor mass concentration versus the light-scattering coefficient (b_{scat}) with the linear regression and the 95-percent confidence interval for the Washington data set.

For both reasons, and also because of the historical use of the ratio method, we will use both the ratio method and the b_{scat}-linear algorithm method in later sections. As an aside, the b_{scat}-linear algorithm resulting from data of Anderson and others (1982) is:

mass concentration ($\mu g \bullet m^{-3}$) = -0.042 ($b_{scat} \bullet 10^{-6} \bullet m^{-1}$) + 990 ;

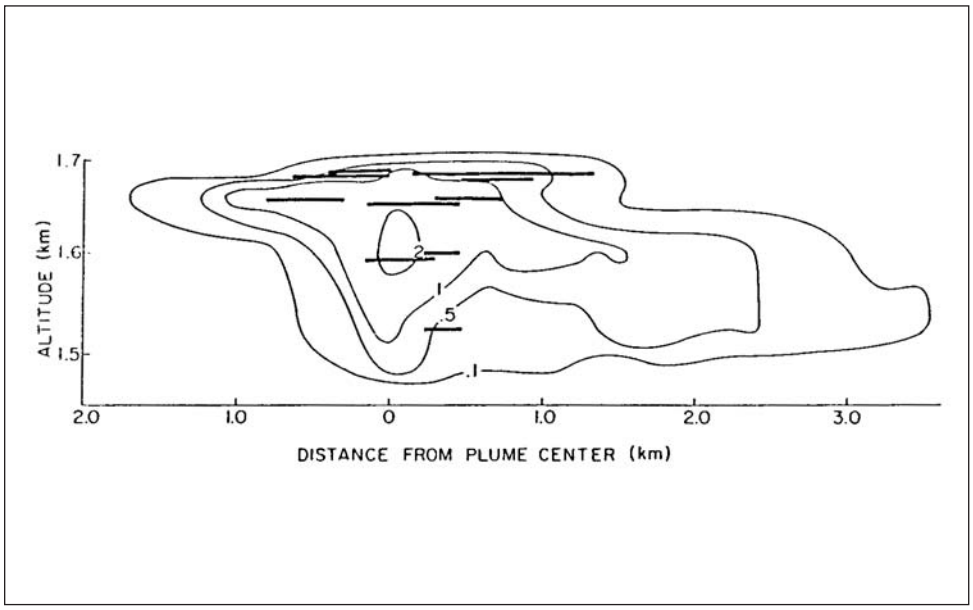

Figure 11—Vertical cross section of the light-scattering coefficient in units of $10^{-3} \cdot m^{-1}$ measured perpendicular to the long axis of the plume from the prescribed burn on July 23, 1982 at 3.3 km from the burn. The heavy bars indicated the regions over which the batch sampler on the B-23 aircraft was operated. The cross section is based on airborne measurements taken during sequence 1 between 1606 and 1644 PDT.

with a correlation coefficient of -0.13. This result does not have predictive value nor does it support a 1:1 relation between b_{scat} and mass. This further indicates the need for a substantial data set to reduce statistical uncertainties.

6. Preliminary Results and Analysis

Some of the data from the airborne measurements of the slash burns are presented in this section along with some preliminary interpretations.

6.1 Characterization of Cross Sections of the Plumes

Using the methods described in section 5.2, we assembled all the airborne measurements (except those clearly unsuitable because of nonperpendicular penetrations of the plumes or gross changes in burn characteristics) into cross sections of light-scattering coefficient. Illustrative examples are provided for each burn in this study.

July 23, 1982—This burn was on a hillside, just below a ridgeline in rough terrain. The plume initially rose nearly vertically through a boundary-layer inversion; it was then carried off horizontally, at an altitude of ≈1.7 km, by the winds aloft. The plume was initially only ≈250 m thick (vertical dimension) with a well-defined axial core (fig. 11). Additional fuel added to the burn after 1640 Pacific Daylight Time (PDT) increased the depth of the plume to ≈400 m (fig. 12);

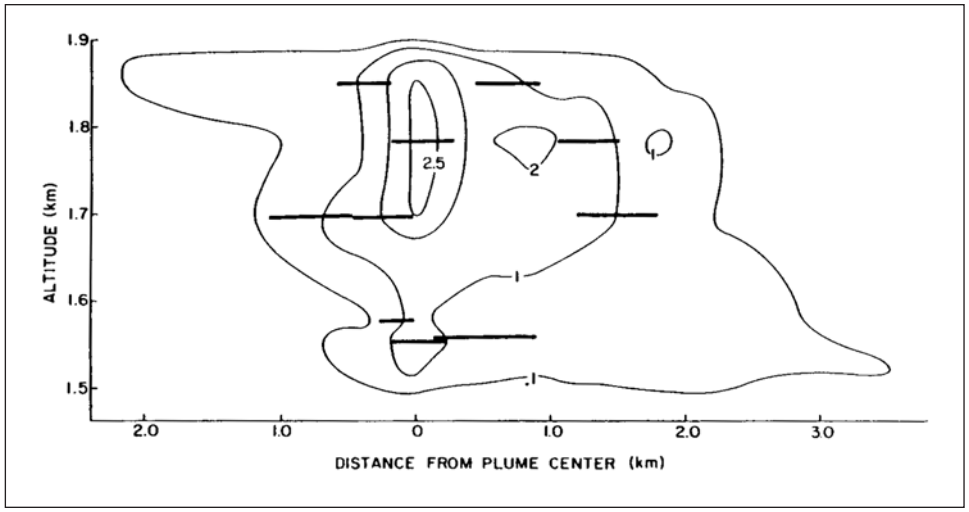

Figure 12—Vertical cross section of the light-scattering coefficient in units of $10^{-3} \cdot m^{-1}$ measured perpendicular to the long axis of the plume from the prescribed burn on July 23, 1982 at 3.3 km from the burn. The heavy bars indicated the regions over which the batch sampler on the B-23 aircraft was operated. The cross section is based on airborne measurements taken during sequence 2 between 1640-1814 PDT.

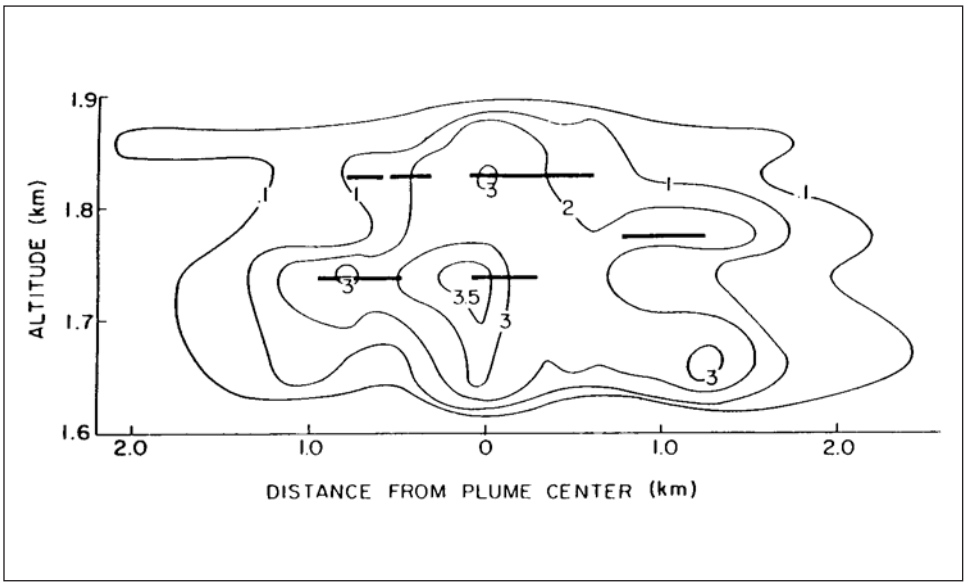

Figure 13—Vertical cross section of the light-scattering coefficient (in units of $10^{-3} \cdot m^{-1}$) measured perpendicular to the long axis of the plume from the prescribed burn on July 23, 1982, at 3.3 km from the burn. The heavy bars indicate the regions over which the batch sampler on the University of Washington B-23 aircraft was operated. The cross section is based on airborne measurements taken during sequence 3 between 1719 and 1745 PDT.

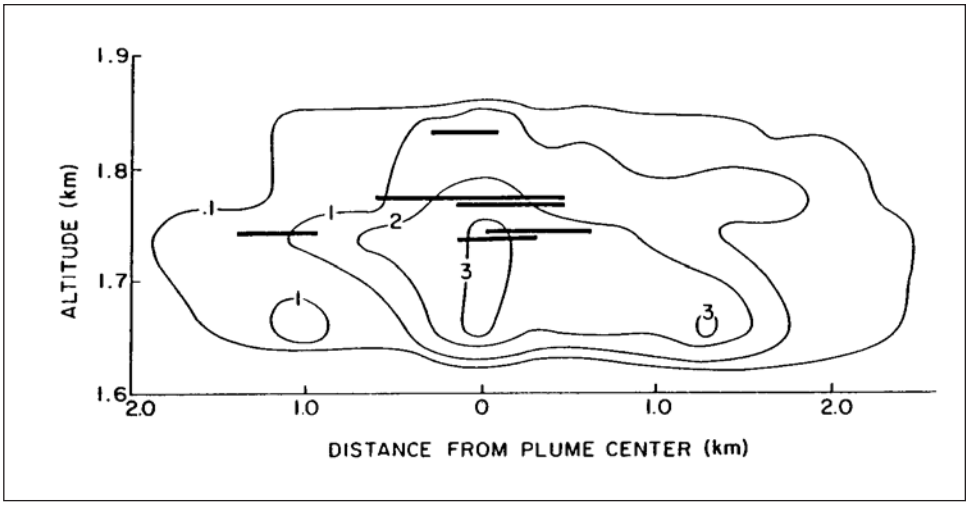

Figure 14—Vertical cross sections of the light-scattering coefficient (in units of $10^{-3} \cdot m^{-1}$) measured perpendicular to the long axis of the plume from the prescribed burn on July 23, 1982, at 3.3 km from the burn. The heavy bars indicate the regions over which the batch sampler on the University of Washington B-23 aircraft was operated. The cross section is based on airborne measurements taken during sequence 4 between 1744 and 1814 PDT.

but by 1720 PDT, the plume had stabilized back to a thickness of ≈280 m. By 1720 PDT, the plume was substantially more complex (fig. 13), with light winds and terrain features introducing portions of the plume from earlier in the day into the cross section. The secondary core of the plume, located at an altitude of 1.65 km and 1.2 km to right of center (fig. 13) was part of the "old" plume. During post-analysis, we removed from the data set encounters with smoke that were obviously separated from the main plume. In this case (and the following), where "old" smoke merged with "new" smoke, we were unable to objectively partition the data. Consequently, this cross section and the following (fig. 14) tend to exaggerate the emission fluxes. When the plume sketches and photographs from the patrol aircraft aloft become available, it may be possible, through further analysis, to remove this ambiguity.

July 24, 1982—This plume was low initially and did not rise above local ridgelines, which made airborne sampling nearly impossible. An attempt was made to rectify this by adding more fuel; this caused the plume to rise to more than 3500 m. Before a series of airborne cross-sectional measurements could be completed, however, the plume collapsed to much lower altitudes. A steady-state assumption for this burn, therefore was not justified, and no cross sections were compiled.

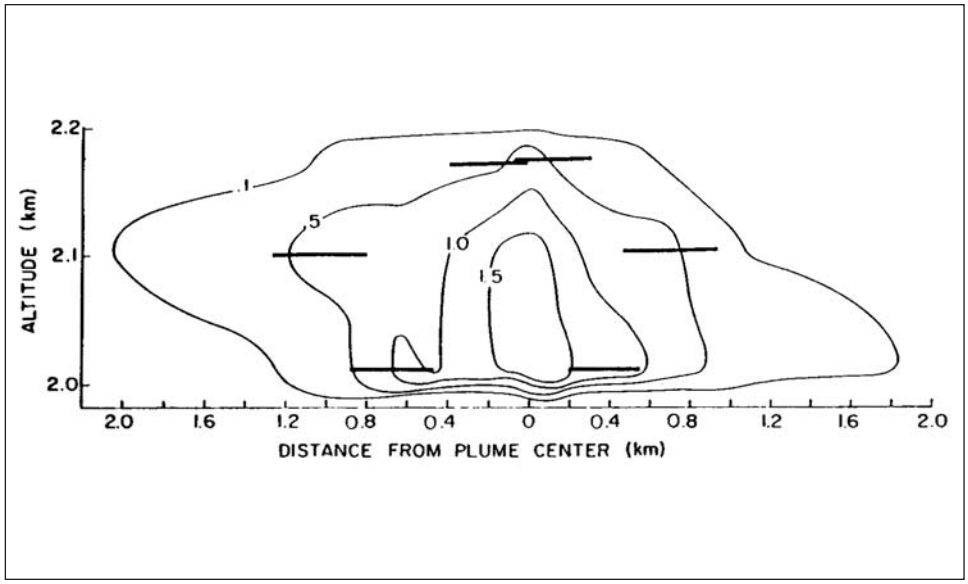

Figure 15—Vertical cross section of the light-scattering coefficient (in units of $10^{-3} \cdot m^{-1}$) measured perpendicular to the long axis of the plume from the prescribed burn on July 25 ,1982, at 3.3 km from the burn. The heavy bars indicate the regions over which the batch sampler on the University of Washington B-23 aircraft was operated. The cross section is based on airborne measurements taken during sequence 2 at 1021 and 1041 PDT.

July 25, 1982—This burn produced a good, stable plume for about 2.5 hours. The cross sections all look similar to the one shown in figure 15. Only sequence 3, taken between 1037 and 1054 PDT, departed from a completely stableappearance; the plume contained a significant amount of smoke ≈300 m below the average base of the plume at ≈900 m at mean sea level (MSL).

July 26, 1982—Stable weather conditions allowed good measurements to be obtained on July 23 and 25. On July 26, as broken cirrus and cirrocumulus and towering cumulus clouds on the horizon to the east invaded the sky, sampling conditions deteriorated. Despite changes in atmospheric stability, seven cross sections of good quality were obtained in the plume from this burn. Only sequences 3 and 4 (from 1114 to 1159 PDT) showed significant deviations from an otherwise visually steady plume. The thickness of the plume decreased during sequence 3 and increased during sequence 4; the other cross sections look very much like the one shown in figure 16.

September 15, 1982—This was the first burn in Washington, and it was significantly larger than any of the Oregon burns. The plume was visually rather stable and steady. The cross sections show a small plume initially, followed by a very steady period from 1500 to nearly 1600 PDT, followed, in turn, by a slowly shrinking plume. Figure 17 is representative of the large and complex plume encountered.

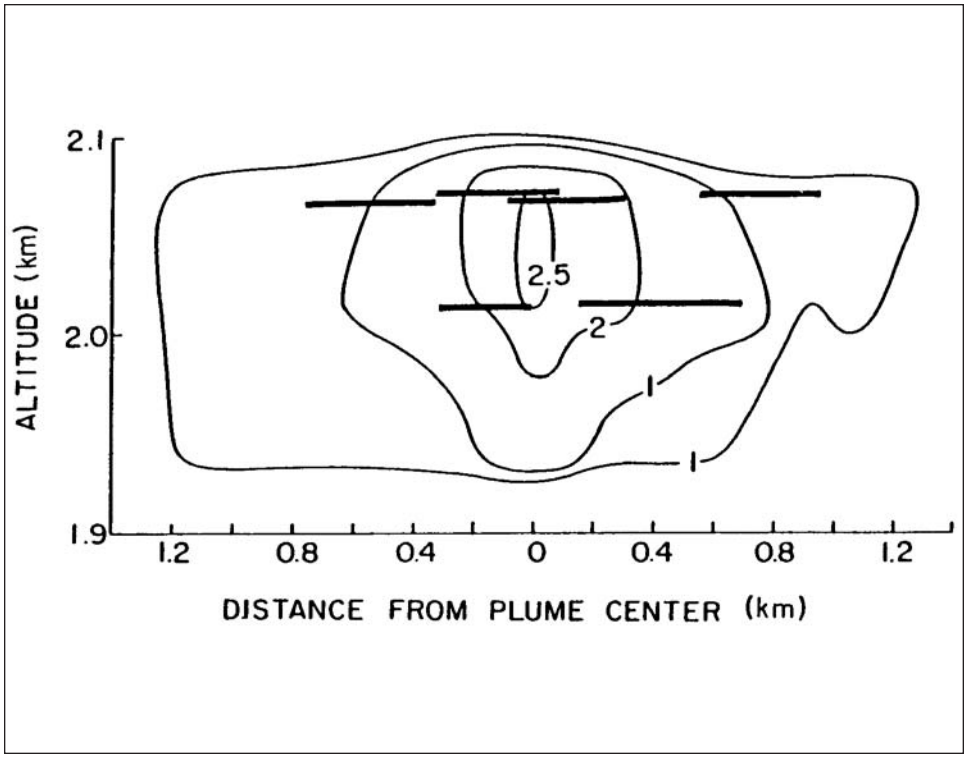

Figure 16—Vertical cross section of the light-scattering coefficient (in units of $10^{-3} \cdot m^{-1}$) measured perpendicular to the long axis of the plume from the prescribed burn on July 26, 1982, at 3.3 km from the burn. The heavy bars indicate the regions over which the batch sampler on the University of Washington B-23 aircraft was operated. The cross section is based on airborne measurements taken during sequence 5 between 1157 and 1219 PDT.

September 23, 1982—This plume showed large departures from visual steady state. This situation was further complicated by a substantial turning of the wind direction with height within the range of altitudes occupied by the plume. Obscuring of surface terrain features by smoke near the burn and off-scale readings of the light-scattering coefficient at a range of 3.3 km prompted us to move to a range of 6.6 km to obtain cross-sectional measurements. The results depicted in figure 18 are typical of the complex plume encountered.

Summary—The cross sections shown in figures 11 through 18 are important in quantifying the nature of the plumes. Further quantitative information is provided in table 7, which lists the average values of b_{scat} between contours (shown in the cross sections) and the area between that contour interval multiplied by the wind speed (the volume flux of air) for all valid cross sections. The information in table 7 can be used to compute the emission flux of any parameter that can be related to b_{scat}.

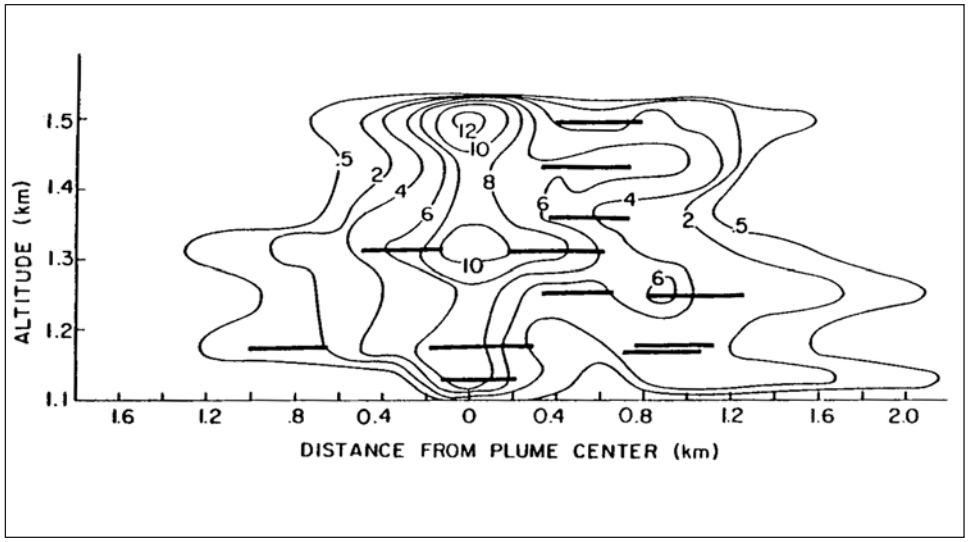

Figure 17—Vertical cross section of the light-scattering coefficient (in units of $10^{-3} \cdot m^{-1}$) measured perpendicular to the long axis of the plume from the prescribed burn on September 15, 1982, at 3 3 km from the burn. The heavy bars indicate the regions over which the batch sampler on the University of Washington B-23 aircraft was operated. The cross section is based on airborne measurements taken during sequence 4 between 1525 and 1610 PDT.

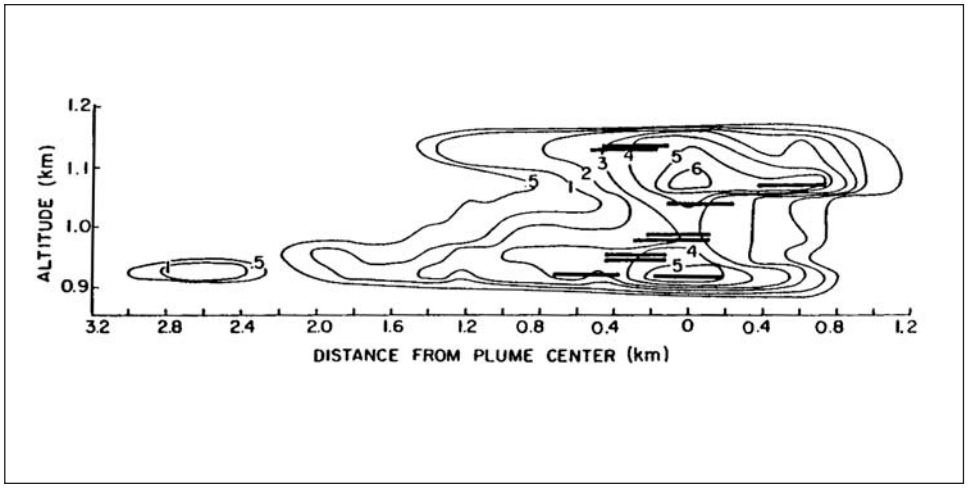

Figure 18—Vertical cross section of the light-scattering coefficient (in units of $10^{-3} \cdot m^{-1}$) measured perpendicular to the long axis of the plume from the prescribed burn on September 23, 1982, at 6.6 km from the burn. The heavy bars indicate the regions over which the batch sampler on the University of Washington B-23 aircraft was operated. The cross section is based on airborne measurements taken during sequence 3 at 1608 and 1647 PDT.

6.2 Some Characteristics of the Particles in the Plumes

In a previous series of airborne measurements obtained in the plumes from prescribed burns (Stith and others 1981), it was noted that both the number and the mass distributions of the particles in the plume are generally dominated by a concentration peak at -0.1 μm diameter; a much less prominent peak at ≈0.5 μm also occurs. With the instrumentation available in 1981, information on particles >10 μm present in number concentrations down to ≈0.1 cm^{-3} was uncertain. With the instrumentation available for the present study, relative measurements on particles >10 μm can be obtained at concentrations down to ≈0.1 cm^{-3}. The availability of new instruments to measure particle sizes (see section 2) extended our measurements to particles ≈3000 μm in diameter that were present in concentrations down to ≈10^{-5}•cm^{-3}. These new capabilities resulted in a revision in our view of the role of supermicron particles in smoke from prescribed burns.

Particle size distributions--The distribution of particle sizes shown in figure 19 illustrates many of the features typical of the smoke from the prescribed burns in this study. The distribution shown in figure 19 was obtained on July 23, 1982, at a range of 3.3 km for the burn and near the plume center on traverse "C."

As discussed in section 2.2, the use of the batch samples should resolve any timing difficulties arising because the four instruments for measuring particle sizes (EAA, ASAS, LAS, Royco 245) operate on different time sequences. Some loss of data accuracy nevertheless can occur through operational errors. For the data obtained to be considered valid, we required smooth transitions between measurements from the various instruments that measured particle sizes. Due to counting statistics and sedimentation, each instrument was most accurate for small-sized particles and generally least valid for large-sized particles. The most common concerns about the data were poor transitions between measurements obtained with the EAA and ASAS (about 20 percent of all cases) and a rough transition between measurements from the ASAS and LAS. lnstrument transition for these most regularly used particle-measuring instruments occurred at diameters of about 0.14, 0.85, and 6.4 μm. The instruments in the particle-measuring system produce, in total, concentrations for 100 different-sized, but not entirely discrete, particle intervals (see table 1 and fig. 2). To reduce the data, original data were merged into one 30-point spectrum for each sample. A correction factor also was applied to concentrations in several of the size ranges after we found that a laser was misaligned in one of the instruments. (This misalignment caused a negligible error in measuring particle size but a significant error in concentration of the particles.)

The measured particle-size distributions showed similar shapes and gross features throughout the duration of each burn and for all burns studied (for example, fig. 20). The predominant concentration peak at 0.15 μm diameter and volume peak at ≈0.25 μm diameter agree well with those of Stith and others (1981) who found corresponding values of 0.1 and 0.3 μm Measurements from the EAA show concentrations still increasing below 0.01 μm (the limit of this instrument), indicating the possibility of a (nucleation) peak in the number distribution

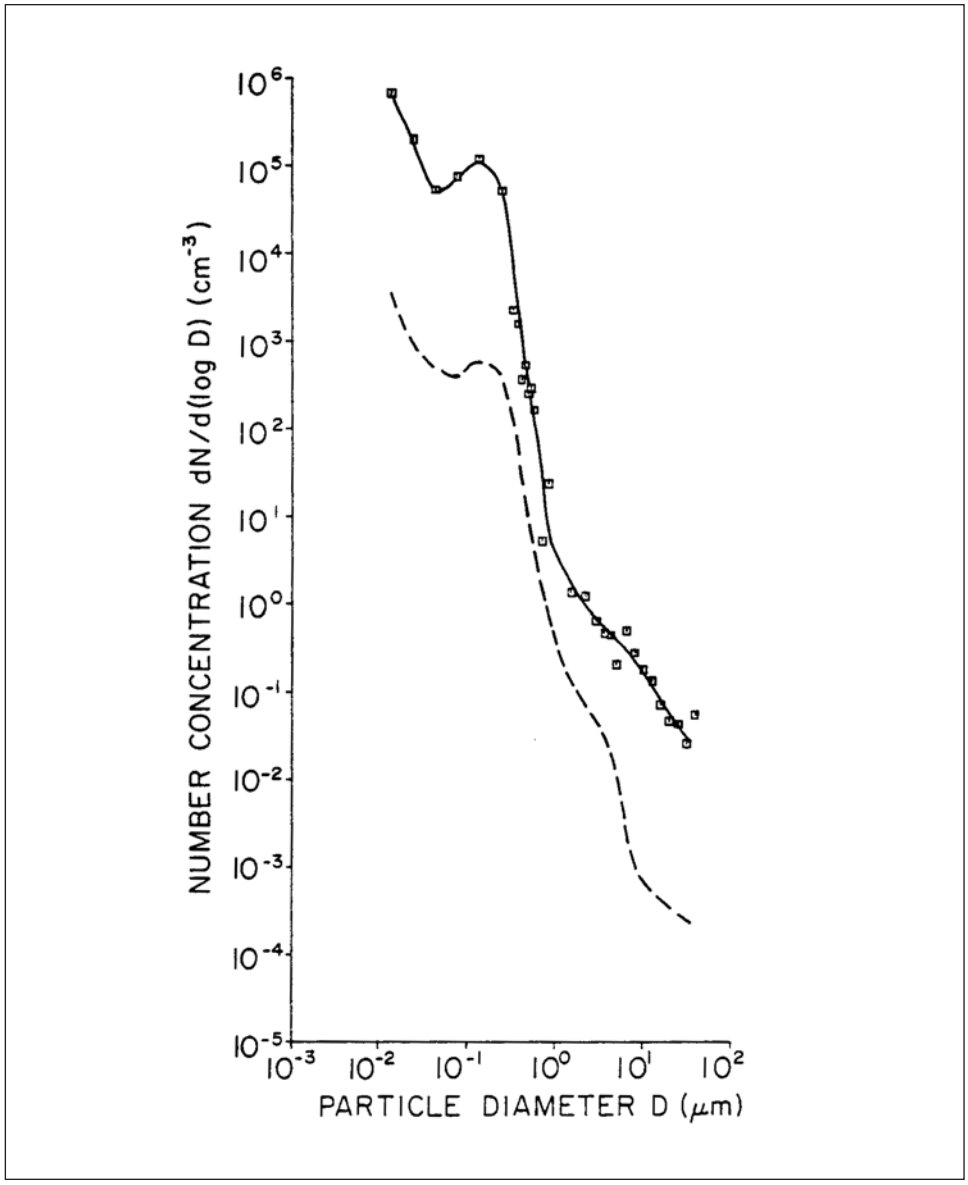

Figure 19—Number concentrations versus size of particle measured in the plume from the prescribed burn at 1742 PDT on July 23, 1982, at 3.3 km downwind of the burn (solid line). The dashed line shows the average ambient particle size distribution on that day.

below 0.01 μm. Because the cumulative particle number from the EAA is in reasonable agreement with the "total" aerosol concentration as measured by the Aitken nucleus counter, the peak must be near 0.01 μm. Furthermore, most of

In contrast to the spectra of Stith and others (1981), the present spectra lacked a small secondary concentration peak at 0.5 μm diameter. This may have been an artifact of the aerosol system used by Stith and others (1981). Our new system had an instrument transition point a little beyond (0.65 μm) that of the old system and made use of the ASAS, which has smaller sizing intervals. Our current data did not support a concentration peak at 0.5 μm diameter.

The most dramatic difference between the present measurements and those reported by Stith and others (1981) was in the supermicron particle volume distribution, for which our new particle-sampling system provided superior resolution for particles with diameters up to ≈45 μm Figure 20 shows that in our current data, the supermicron particle peak is not resolved; the volume continues to increase with increasing size to the limit of the measurements. Our previous smoke data showed a minor mass peak at ≈10 μm and the vast majority of the mass located in the submicron peak. The higher concentrations of supermicron particles measured in this study, as compared to measurements by Stith and others (1981), are almost certainly due to improved sampling techniques. These new observations affect estimates of total suspended particulates.

A substantial fraction of the particles in the plumes had diameters >45 μm; this was supported by the pilot observing that we were collecting millimeter-sized pieces (still smoldering?) under the windshield-wiper blades of the aircraft. The shapes of some of these particles are shown in figure 21. The largest particle in this sample was about 4 mm long.

The other three laser cameras aboard the B-23 also detected the large particles. Although the counting statistics of these three cameras were only just satisfactory, the shape of the distribution can be seen in the raw data plot taken near plume center at 1427 PDT on September 15, 1982 (fig. 22). The measurements from the instruments agree reasonably well with simultaneous measurements obtained from the aerosol system, but there is a change in the slope at the overlapping intersection of the two data sets (fig. 23). The point is, these curves show that the peak in the volume of the supermicron particles is still not resolved even by our extended size measurements; the total volume of the particles is still increasing for particles above 1000 μm in diameter. Although the submicron particles dominated visibility reduction by the plume and the impact of the plume over large distances, it was clear that at 3.3 km downwind of the prescribed burns that we studied, the supermicron particles dominated the total mass of particles in the plume. This result had a significant effect on our interpretation of the aerosol filter data (see section 6.5).

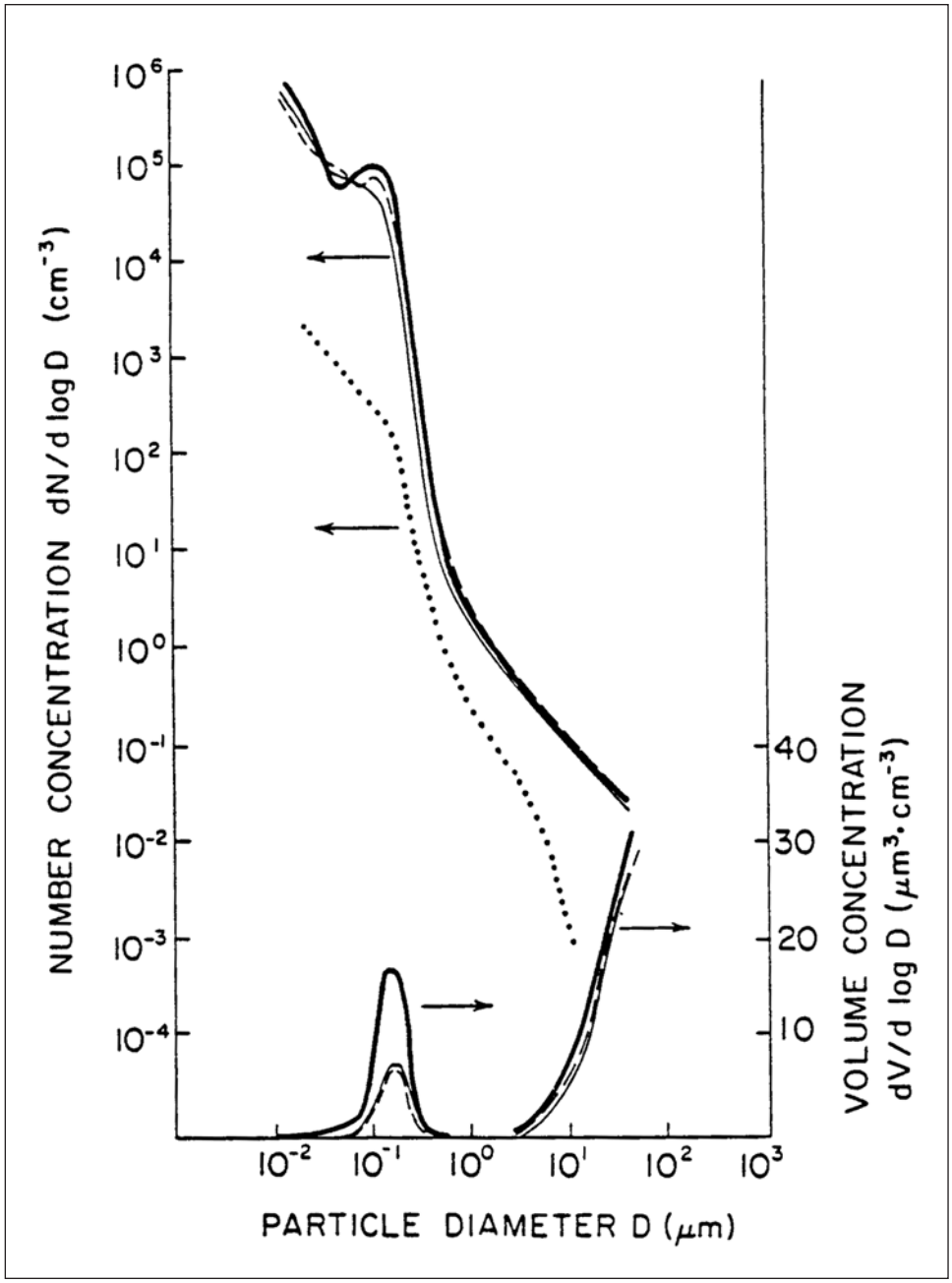

Figure 20—Number concentrations versus size of particles measured near the center of the plume and 3.3 km downwind of the burn on July 23, 1982, at 1636 PDT (heavy solid line), 1741 PDT(dashed line) and 1759 PDT (solid line). The ambient particle size distribution is also shown (dotted line).

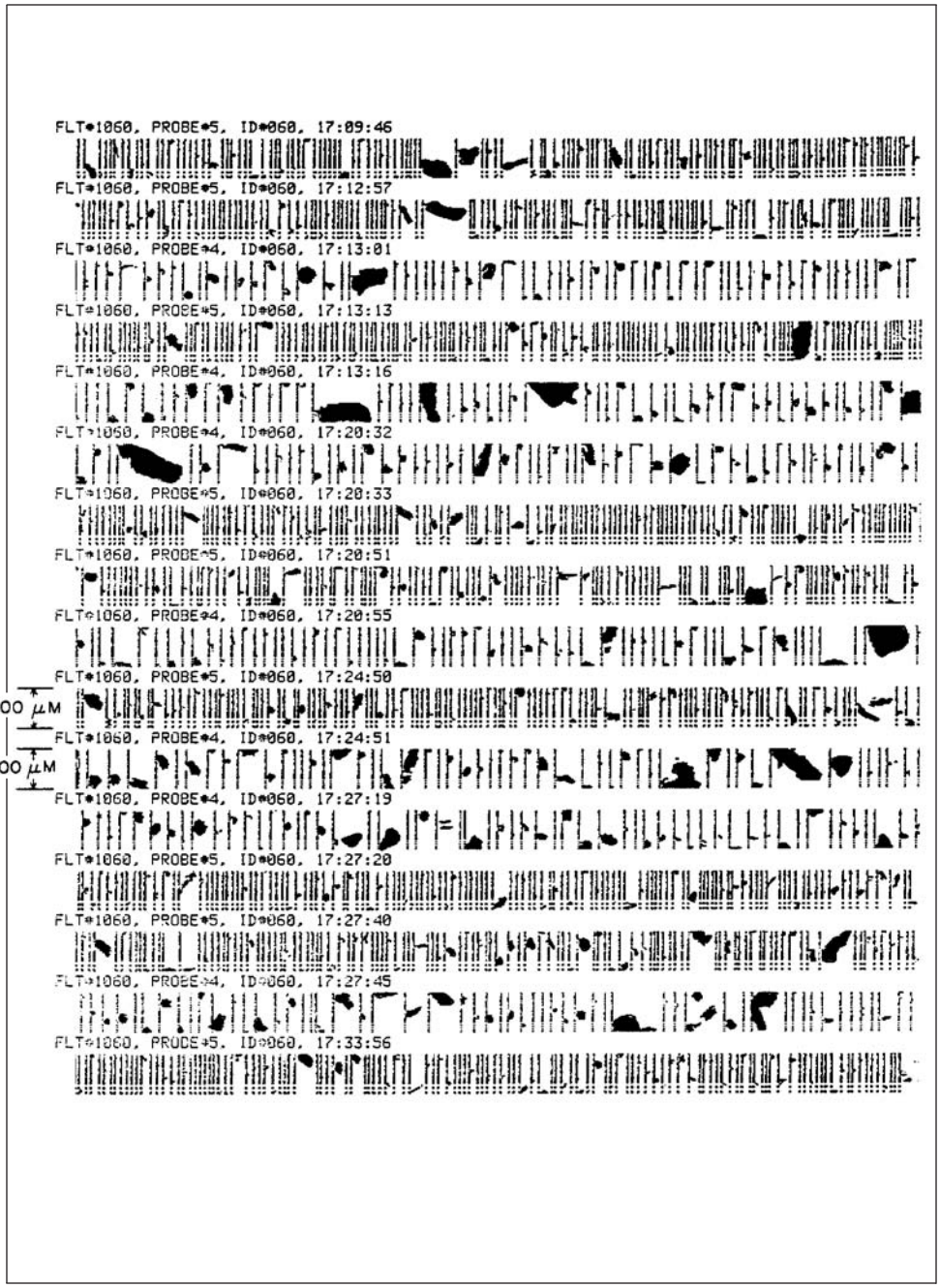

Figure 21—Shadow images of airborne particles observed with the laser camera in cross-sectional sequence 2 through the plume from the burn, ≈1727 PDT, September 15, 1982. For probe 4, the vertical frame size is 800 μm; for probe 5, it is 3200 μm.

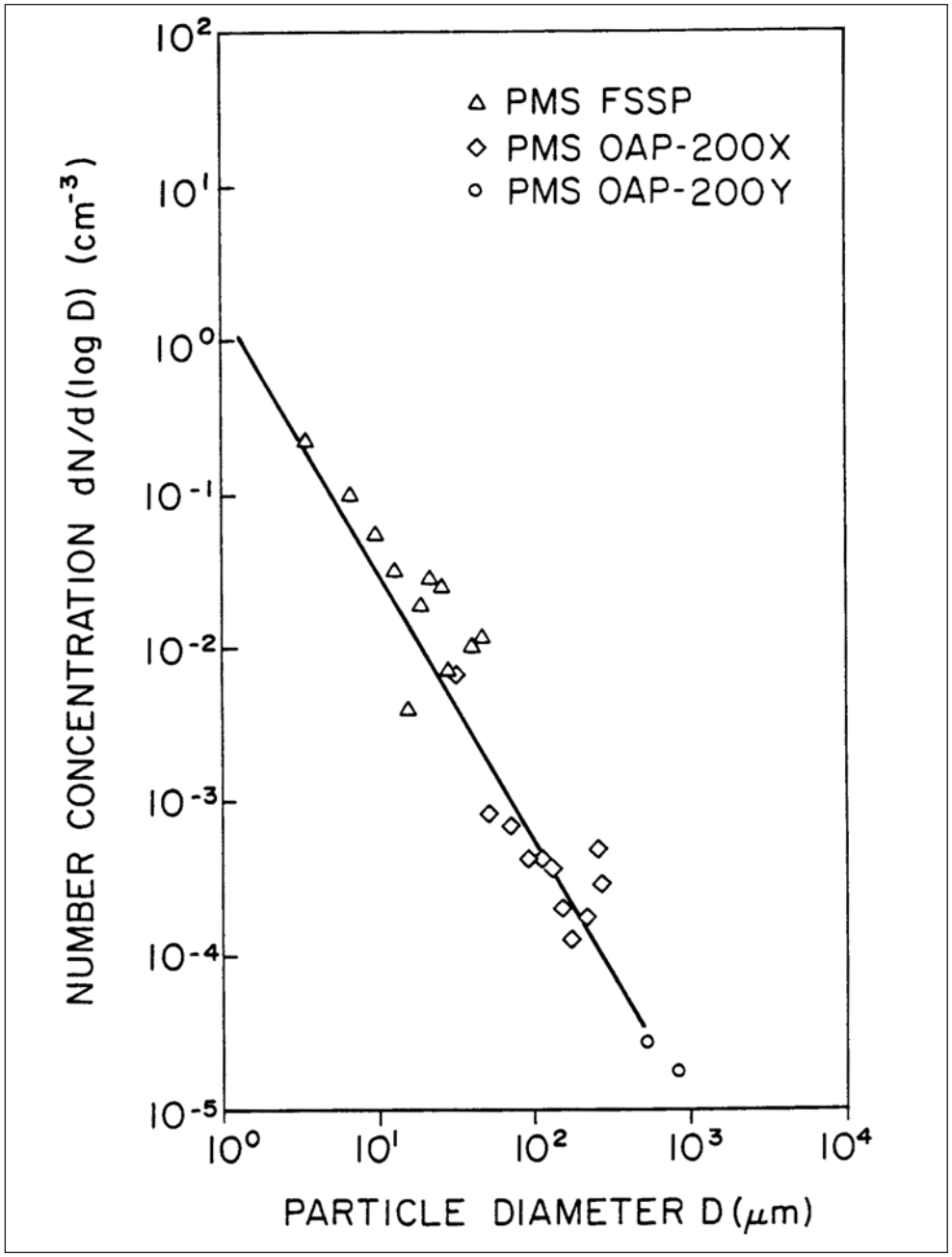

Figure 22—Number concentration versus size of particles measured with a laser camera on the University of Washington B-23 aircraft near the center of the plume 3.3 km downwind of the burn, 1427 PDT, September 15, 1982.

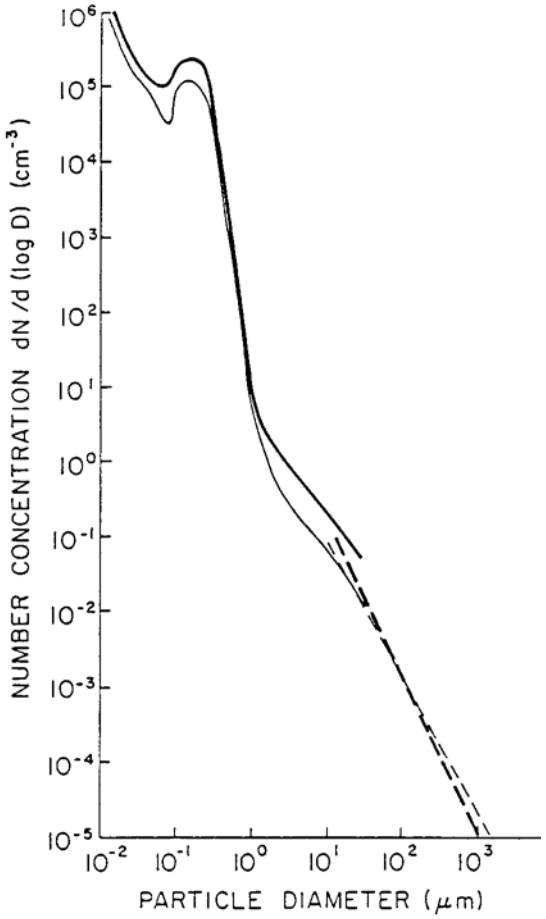

Figure 23—Number concentration versus the size of particles from the burn on September 15, 1982. Measurements were obtained with the aerosol system near the top of the plume at 3.3 km downwind of the bum at 1427 PDT (heavy line) and at plume center at 1727 PDT (lighter line). The dashed line extensions are measurements from the laser cameras.

Average characteristics of the particle-size distributions—The characteristics of the particle-size distributions are best seen in the averaged and summed characteristics of the mean number diameter (MND) of the particles, their mean volume diameter (MVD), and the total particle volume (TPV) for particles ≤43 μm in diameter. Plots of these parameters, as a function of time after burn ignition, reveal a number of significant differences among the burns that we studied.

Figure 24 indicates the generally steady-state nature of the plume from the burn on July 23, 1982, for 50-140 minutes after ignition; the MND is steady between 0.02 and 0.04 μm, and the TPV is steady near 300 $\mu m^3 \cdot cm^{-3}$ The MVD is more variable, ranging from 3 to 10 μm, and is evidently correlated with the TPV. The altitude of the plume center rose by less than 150 m during this period. In contrast, the "well-behaved" plume occurring on July 25, 1982, showed a general increase in MVD and TPV as a function of time after ignition (fig. 25), although it gained substantially in altitude as the burn progressed. This behavior was repeated on July 26, 1982 (fig. 26). In both cases, the MVD was initially

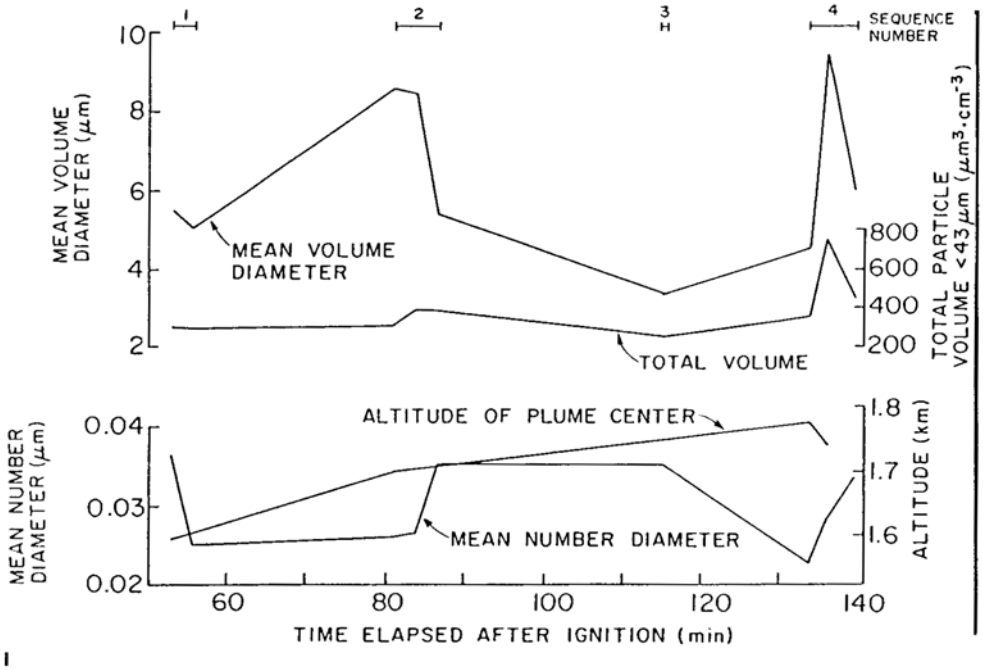

Figure 24—Characteristics of the particles near the center of the plume on traverse "C" 3.3 km downwind of the burn on July 23, 1982, as a function of time after ignition.

≈1 1μm and increased to ≈5 μm by about 2 hours after ignition. The MND's show little variation. The larger burn in Washington on September 15, 1982 (fig. 27) shows far more variability, despite a visually steady plume.

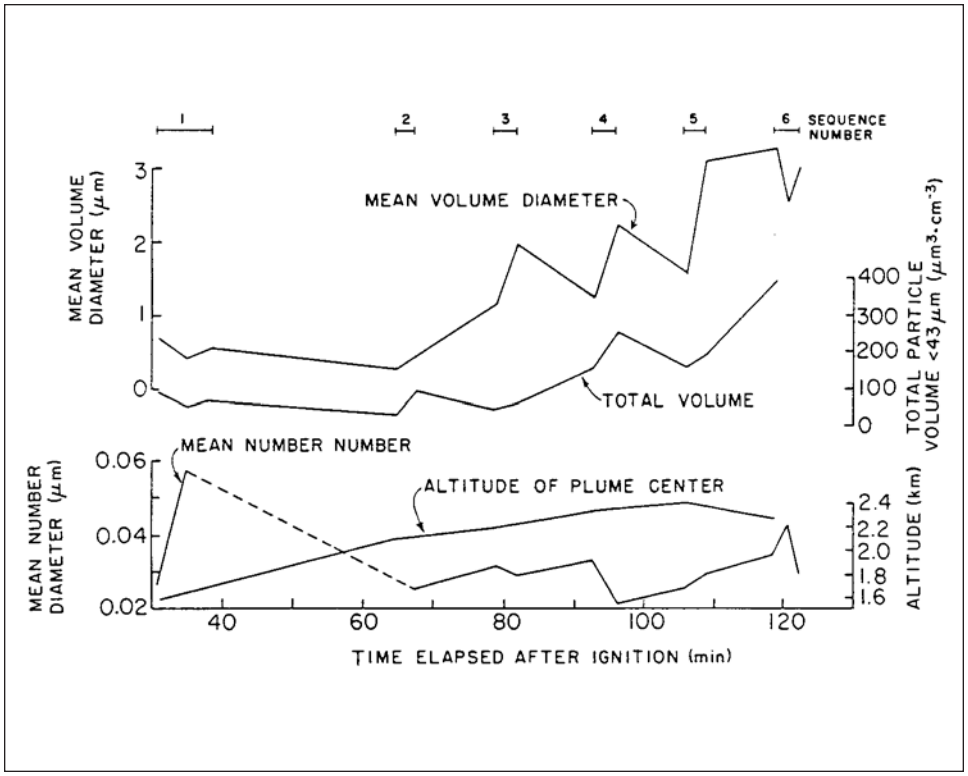

Figure 25—Characteristics of the particles near the center of the plume on traverse “C” 3.3 km downwind of the burn on July 25, 1982, as a function of time after ignition.

The second Washington burn on September 23, 1982, was studied at 6.6 km downwind (fig. 28). Visually, the plume was less steady than the plume on September 15; again, there was only slight correlation between MVD and TPV. The MVD decreased throughout the duration of the burn; it had an initial value ≈1.5 μm and finished at 0.5 μm, with a discontinuity at ≈100 minutes after ignition when both MVD and TPV increased sharply. The MND shows signs of being anticorrelated with MVD.

Interesting features of the data sets are the two cases of clear positive correlation among MVD, TPV, and plume rise and the other three cases in which these correlations are not evident. In the two cases of positive correlation, a relation seems to occur between the intensity of the burn (as indicated by plume rise) and the lofting of ever-larger debris into the plume. The fact that there are weak indications that the MND decreases as MVD and TPV increase (see the July 25 and 26 cases) suggests that combustion efficiency also played a role. As the intensities of the burns increased, more complete combustion produced smaller particles, but simultaneous increases in the velocity and turbulence of the air increased the concentrations of partially burned fuel and other debris in the plumes.

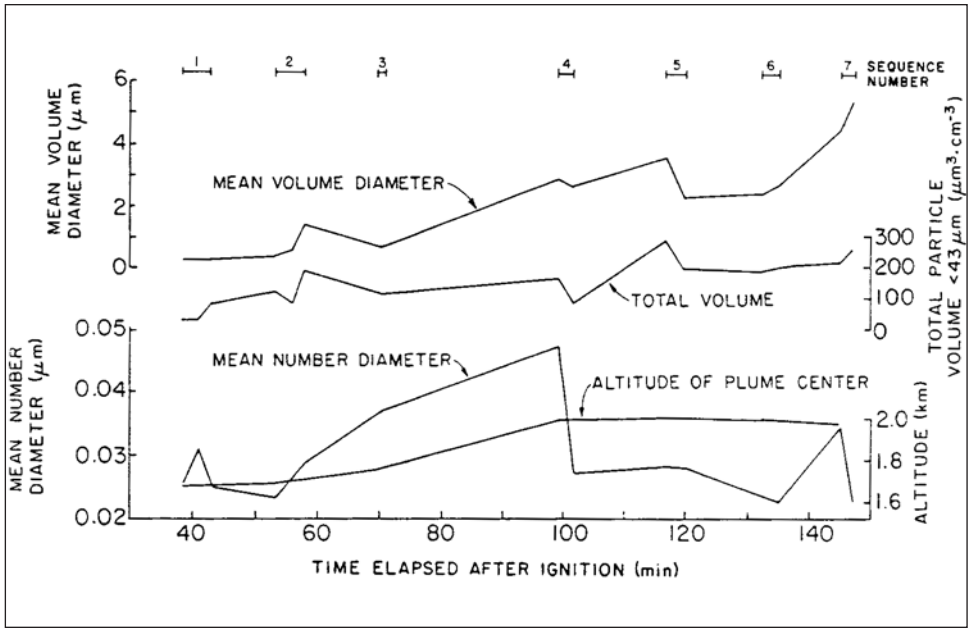

Figure 26—Characteristics of the particles near the center of the plume on traverse "C" 3.3 km downwind of the burn on July 26, 1982, as a function of time after ignition.

Apparent density of the particles—Simultaneous measurements of the particle size distribution (from which the particle volume distribution can be inferred), the particle mass distribution (with the cascade microbalance), and the mass of particles <2 μm (with the mass monitor) allow determination of the apparent density of the particles. Because the uncertainties in the responses of the instruments are less for smaller sized particles, we limited our calculations to particles with diameters <1.9 μm.

The equations resulting from linear fits to the data are given in table 8. The apparent particle density obtained from the mass monitor data was 0.98±0.03 g•cm^{-3}, and that from the microbalance data was 0.86±0.09 g•cm^{-3}. Using similar instruments (the same mass monitor) and techniques, Stith and others (1981) determined a particle density of ≈1 g•cm^{-3} in the plumes from the prescribed burns that they studied. Some systematic uncertainties may remain in the particle-density determinations (perhaps greater than the quoted standard deviations) because of the broad mix of instruments used. For this reason, we use the term "apparent density."

Because the correlation between particle volume distributions, derived from the particle size measurements and the particle mass distributions for particles <2 μm in diameter, as measured by the cascade microbalance, was barely satisfactory (correlation coefficient = 0.66; table 8), it is illustrative to compare the particle volume distributions with the mass distributions measured by the cascade

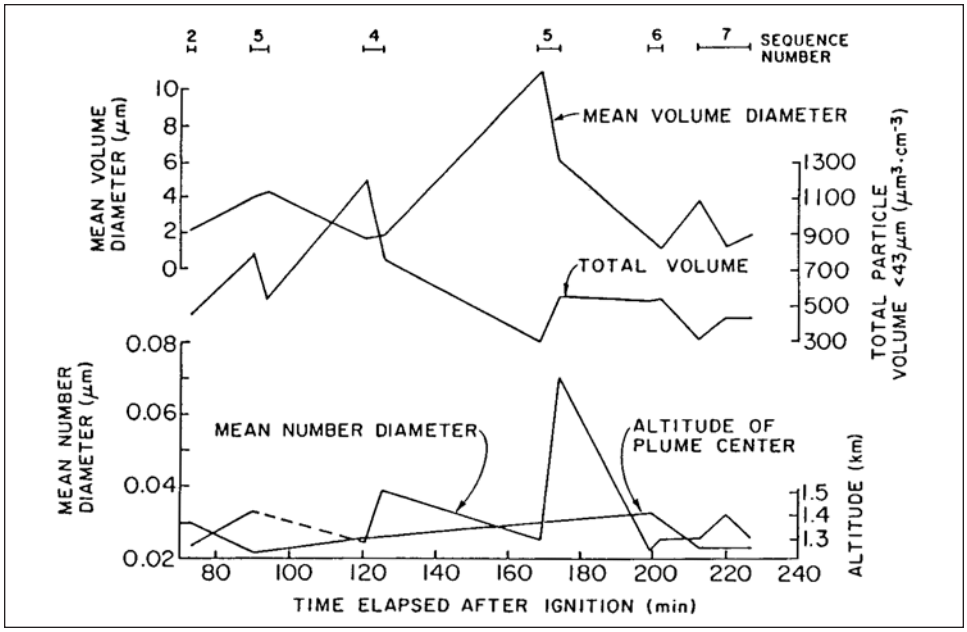

Figure 27—Characteristics of the particles near the center of the plume on traverse C" 3.3 km downwind of the burn on September 15, 1982, as a function of time after ignition.

microbalance over the full range of particle diameters from 0.05 to 25 μm To convert the cascade microbalance distributions to volume distributions, we divided by a (rounded-off) particle density of 1.0 g•cm^{-3}. (We will use this density in the remainder of this report.) Some results are shown in figure 29, where we see that the volume distributions derived from cascade microbalance measurements reproduce the submicron peak detected by the system for measuring particle sizes. The very small sample flow for the cascade microbalance prevents it from collecting a weighable sample for particles >5 μm, however.

We believe that the measurements of the size spectra of particles converted to a mass distribution, by using a derived apparent particle density, is a more valid approach to obtaining size-segregated mass distributions in the plumes than are the measurements from the cascade microbalance.

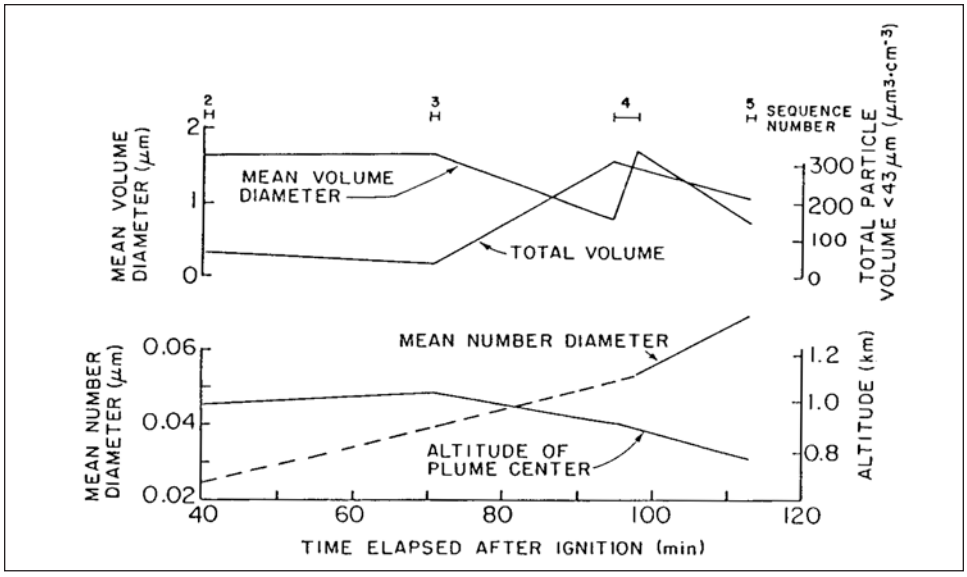

Figure 28—Characteristics of the particles near the center of the plume on traverse "C" 3.3 km downwind of the burn on September 23, 1982, as a function of time after ignition.

The effect of particle density on the mass of particles produced by fire conditions is not resolved here. Recent data suggest an increase in the elemental carbon content from near zero for smoldering fires to 20 percent for very high-intensity fires. Ward and Core (1984) report the percentage mass of elemental carbon (specific gravity 1.88 to 2.25) and trace elements of K and CI to be proportional to fire intensity. Although we concluded that the density of the aerosol from these prescribed fires is about 1 $g \cdot cm^{-3}$, the variance over the course of a fire may be a function of fire intensity.

Aerosol elemental analysis—In addition to weighing the filters, Crocker Laboratory performed an elemental analysis by Proton-Induced X Ray Emission (PIXE). We have applied the matrix correction factors for Na, Al, Si, and CI, which had correction factors >10 percent; all other elements had correction factors <10 percent, which were not applied. These data are shown in table 9 in a form suitable for factor analysis.

As expected, the filters show high concentrations of Ca and K (from the combusted biological materials). Significant S is emitted, although we have never seen significant SO_2 emitted from a slash fire.

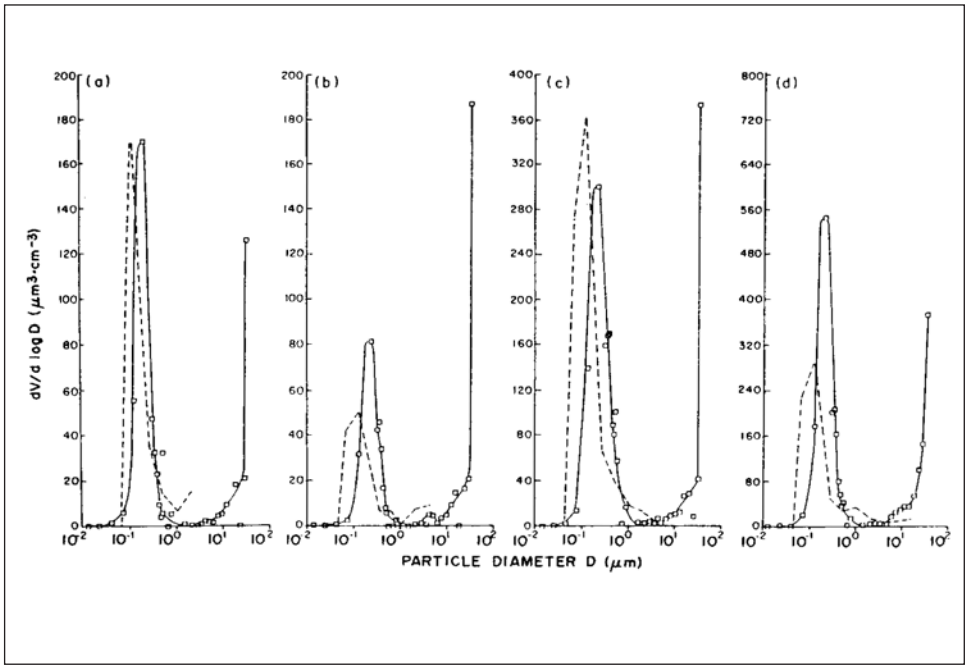

Figure 29—Volume concentration versus size of particles measured with the aerosol sizing system near the center of the plume from the burns: (a) 0954 PDT, July 25, 1982; (b) 1605 PDT, September 23, 1982; (c) 1718 PDT, September 23, 1982; and (d) 1700 PDT, September 23, 1982. The dashed lines show results derived from the cascade microbalance impactor (mass/density of particles).

6.3 Analysis and Cross Comparisons of Bulk Air Samples

In addition to the 6-L air samples collected in the 500-L polyethylene bag sampler for LEMSCO (the samples were used to determine CO and COp concentration in the plumes), a limited number of 6-L air samples were collected after passing through a stainless steel sample loop (see section 2.3). The later samples were analyzed for hydrocarbons and fluorocarbons by R. Rasmussen at OGC to determine if specific hydrocarbons or fluorocarbons could be used as plume tracers. These samples also served as quality control checks on the more numerous samples collected in the polyethylene bag for LEMSCO, as the stainless steel sample loop is much less subject to contamination than a polyethylene bag. Besides the intercomparison among samples collected from the two sampling systems, a limited number of samples collected from the polyethylene bag were analyzed by OGC after they had been analyzed by LEMSCO. Comparison of these samples allowed an evaluation of the LEMSCO system against what is essentially the standard reference system for such analyses (that is, gas chromatograph/mass spectrometer; gas chromatograph/electron capture; and gas chromatograph/flame ionization detector).

Table 10 lists the results of the LEMSCO and OGC analyses on the same samples collected with the polyethylene-bag sampler from the B-23. There is good agreement between the two data sets for CH_4, CO, and CO_2 with the concentrations measured by LEMSCO and OGC generally within about 10 percent of each other. But because of the relatively slight difference in concentrations of the CO_2 in the plume and the ambient air, a 10 percent error in CO_2 measurements can have a substantial impact on the derived CO_2 flux in a plume (see appendix A and tables 4 and 5). Furthermore, one of the two samples for which total nonmethane hydrocarbons (TNMHC) concentrations could be compared (sample 238) showed a marked discrepancy between the LEMSCO and OGC measurements, with the LEMSCO system measuring a TNMHC concentration ≈65 percent higher than the OGC measurement (despite the fact that the LEMSCO measurement does not include C_2 hydrocarbons and the OGC measurement does). Although it is conceivable that reactive hydrocarbons may have appreciably decayed between the LEMSCO and OGC measurements (reactive compounds such as isoprene were virtually absent from the OGC analysis), it is unlikely that this accounts for a discrepancy of this magnitude. Unfortunately, the limited number of samples available for comparison precludes any definitive comparison of the two measuring systems. Table 11 compares measurements made by LEMSCO on samples collected in the polyethylene bag with those made by OGC on samples collected using the stainless steel sampling loop. The CH_4 and CO_2 measurements were in reasonable agreement, but both the CO and TNMHC concentrations obtained from the polyethylene bag were generally significantly greater than those obtained from the canisters. This is almost certainly a result of contamination and suggests that the TNMHC concentrations measured by LEMSCO should be discarded. The CO concentrations measured by LEMSCO, although showing somewhat less disparity with the measurements for samples collected with the stainless steel sampling loop than with those shown by the TNMHC concentrations, should also be used with caution.

6.4 Plume Tracers

Although a rather large number of trace compounds were elevated over ambient levels in the plumes from the bums (for example, C_2H_4 and C_2H_2), the compounds most consistently elevated were the halocarbons (CH_3I and CH_3Cl). This was the case both for samples collected by the polyethylene bag sampler and those collected by the stainless steel loop. Enhancements in concentrations of these trace compounds in the plume ranged from a factor of 1.5 to a factor of 10 in both the Oregon and Washington field studies. This suggests that these compounds could be used as conservative tracers of slash burn smoke by using the halocarbons (CH_3I and CH_3Cl). This was the case both for samples collected by the polyethylene bag sampler and those collected by the stainless steel loop. Enhancements in concentrations of these trace compounds in the plume ranged from a factor of 1.5 to a factor of 10 in both the Oregon and Washington field studies.

6.5 Particle Emission Factors

Principle of the method for determining particle emission factors— The principle of the method for determining particle emission factors for fires is to measure the particle emission flux and to divide this by the fuel consumption rate. Because we did not have information on the rates of fuel consumption, this method was not used for this report. Instead, we determined particle emission factors by a carbon-balance method. This method requires measurements of the concentrations of carbonaceous gases and particles across a section of the plume and simultaneous measurements of the horizontal wind through this cross section. The procedure for the emission factor (EF) for particles (over any specified size range) is defined as:

$$EF = \frac{\text{mass flux of particles along the plume}}{\text{fuel consumption rate}}$$

Therefore:

$$EF = \frac{\bar{P} \bullet A \bullet V}{F} \quad (1)$$

where $\bar{P}$ is the average mass concentration of the particles across a section of the plume, A is the cross-sectional area of the plume, V is the horizontal wind speed through this section, and F is the fuel consumption rate. Because the carbon burned per unit of time (CB) is given by:

$$CB = F \bullet CF_w \; ; \quad (2)$$

where CF_w is the fractional mass of carbon in the fuel, we have from (1) and (2):

$$EF = \frac{\bar{P} \bullet A \bullet V \bullet CF_w}{CB} \quad (3)$$

If deposition of the particles is negligible and the plume is in steady state:

$$CB = [(\bar{P} \bullet CF_p) + (\overline{CO_2} \bullet CF_{CO2}) + (\overline{THC} \bullet CF_{THC}) + (\overline{CO} \bullet CF_{CO})]V \bullet A \; ; \quad (4)$$

where, $\overline{CO_2}$, $\overline{THC}$, and $\overline{CO}$ are, respectively, the average mass concentrations of C02, total hydrocarbons (THC), and CO across the section of the plume; and CFp, CF_{CO^2}, CF_{THC}, and CF_{CO} are the fractional masses of carbon in the airborne particulates, CO_2, THC, and CO, respectively. From(3) and (4):

$$EF = \frac{\bar{P} \cdot CF_w \quad (5)}{(\bar{P} \cdot CF_p) + (\overline{CO_2} \cdot CF_{CO^2}) + (\overline{THC} \cdot CF_{THC}) + (\overline{CO} \cdot CF_{CO})} \qquad (5)$$

In (5), the bar over the concentrations indicates an areal average over the plume cross section. If the particles and gases in the plume are mixed in a uniform ratio, the areal averages may be replaced by averages along the flight path (which are what are available in practice; see section 6.1). Using the airborne measurements and taking $CF_w = 0.497$ (Byram 1959) and $CF_p = 0.50$ (Ward and Hardy 1984), we can determine particulate emission factors from (5).

We will discuss below the results of applying this method to determine the emission factors for total suspended particulates and for particles in several size ranges for six of the burns studied.

Emission factors for total suspended particulates derived from filter measurements—We applied the above procedures to the canister data analyzed by LEMSCO for carbonaceous gases and the total suspended particles from weighed filters (part of the Crocker Laboratory analysis). These samples were obtained simultaneously from the large bag sampler, although most of the filter samples represented the average of several bag samples. Each bag sample that was analyzed had a canister sample that was averaged over the same period for which the filter was exposed.

The Oregon burns (missions 1-4) yielded 18 estimates of the emission factor for total suspended particulates. The Washington burns (missions 5 and 6) produced an additional 20 estimates. These derived emission factors for total suspended particulates are listed in table 12 (the data used to calculate these emission factors are given in appendix A).

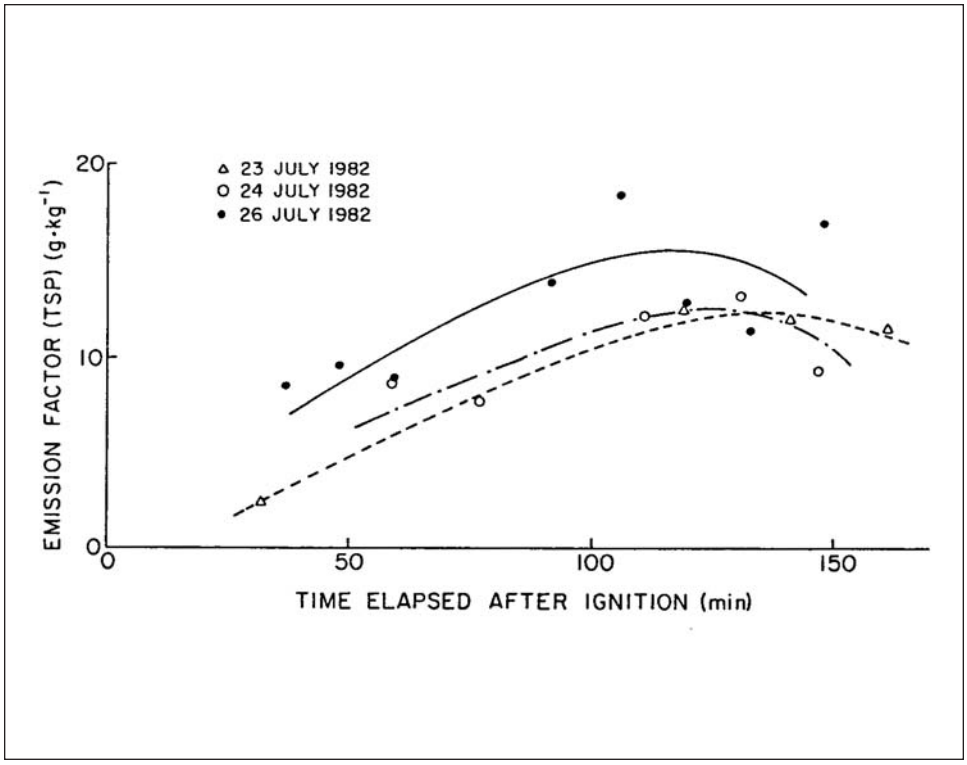

Figure 30—Emission factors for TSP as a function of time after ignition for the Oregon burns.

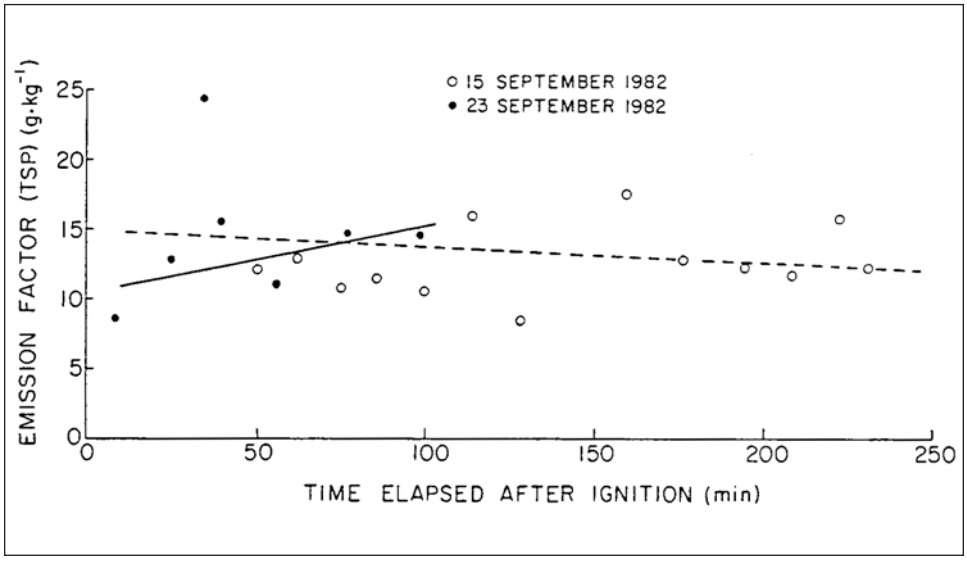

Figure 31—Emission factors for TSP as a function of time after ignition for the Washington burns.

When the emission factors are plotted as a function of time after ignition, the rather similar-sized Oregon burns show a clear pattern (fig. 30). At about 50 minutes after ignition, the emission factors ranged from ≈3 to 9 g•kg^{-1} (0.3 to 0.9 percent), they reached peak values of ≈11 to 15 g•kg^{-1} (1.1 to 1.5 percent) about 125 minutes after ignition, and they appeared to decline slightly between ≈125 to 150 minutes after ignition. Interestingly, the emission factors peaked at about the same time as the centers of the plumes reached their maximum heights (see section 6.1). The emission factors for total suspended particulates for the larger Washington burns show little functional tendency with time (fig. 31).

The emission factors for total suspended particulates for the Oregon burns averaged 11.0±3.5 g•kg^{-1} (1.1±0.4 percent) compared to an average of 13.3±3.4 g.kg^{-1} (1.3±0.3 percent) for the Washington burns.

In assessing the accuracy of the emission factors for total suspended particulates listed in table 12, the following points should be considered:

1. All filters noted by the Crocker Laboratory to have been damaged or to have had missing portions were excluded from the analysis. Data loss from this source was severe only for July 26, 1982 (mission 3).

2. Measurements of THC, NMHC, and CH_4 made by LEMSCO were of uneven quality, both in consistency and accuracy (see sections 4.2 and 6.3). Most notable was the failure of NMHC + CH_4 to equal THC (even when the C_2 compounds, thought to be excluded in the LEMSCO analysis, were estimated and included in the LEMSCO results). Our estimates of carbon content in hydrocarbons were obtained by using the THC for missions 2, 3, 4, and 6 and NMHC + CH_4 for mission 1. The THC and NMHC measurements taken with Mylar bags on mission 5 were obviously faulty[4] and showed no correlation with emissions. Calculations for mission 5 were made without hydrocarbon estimates. The impact of these uncertainties on the calculation of the emission factors was only a few percentage points.

3. The uncertainty in the CO_2 fluxes (discussed in section 6.3) was potentially a larger problem than the THC problem discussed above, but it was not well quantified.

4. The mass collection efficiency of the filters was better than 99 percent over the entire submicron range. The primary uncertainty in estimating the emission factors for total suspended particulates may be the result of uncertainties in the collection efficiencies of large particles on the filters. The filter sample train for the bag sampler should have a reasonably high collection efficiency for particles

[4] Because of a lack of stainless steel canisters, Mylar bags were substituted for the canisters on mission 5.

up to about 10 μm diameter. While sampling at the very short range of 3-4 km, we encountered unexpectedly high concentrations of ash particles and other debris larger than 100 μm (see section 6.2). Because of its rapid removal from the atmosphere by sedimentation, this material would not normally be considered a part of the total suspended particulates, but some small fraction of this material likely was captured by the filters.[5]

The results, shown in table 13, are compared to the emission factors for total suspended particulates calculated from the filter data. Average emission factors are as follows: for total suspended particulates (filters) 12.2±3.6 $g \bullet kg^{-1}$, for particles ≤43 μm in diameter 6.0±3.4 $g \bullet kg^{-1}$, and for particles <2 μm in diameter 4.1±1.5 $g \bullet kg^{-1}$ from the mass monitor and 3.7±1.7 $g \bullet kg^{-1}$ from the cascade impactor measurements. The largest burn was mission 5; this burn also produced the best visual steady-state plume.

The average emission factors for all three size categories were higher in this burn than in the other five burns; they were for total suspended particulates 13.4±3.7 $g \bullet kg^{-1}$, for particles ≤43 μm in diameter 8.7±3.8 $g \bullet kg^{-1}$, and for particles <2 μm in diameter 4.8±1.4 $g \bullet kg^{-1}$.

Calculations based on total suspended particulate (filter) measurements yielded the largest emission factors and tended to confirm the role of particles >43 μm in diameter in determining the weight of the filters. Comparisons of emission factors derived from the filter data with those calculated for particles ≤43 μm in diameter, from mass monitor, and from cascade impactor data produced linear correlation coefficient of 0.85, 0.81, and 0.65, respectively. The correlation coefficient among emission factors for particles <2 μm in diameter (mass monitor) and for particles ≤43 μm in diameter was 0.76; a comparison of emission factors from the mass monitor and cascade impactor (both particles <2 μm in diameter) produced a correlation coefficient of 0.58.

Because we are uncertain about the upper limit of the particles collected on the filters, we conclude that the emission factors and values of total suspended particulates derived from the filters must be used with caution. Measurements obtained from the other techniques discussed above, although they may be more closely defined, also have accuracy limitations. We emphasize that none of the estimates for emission factors and TSP listed in table 13 represent the actual total particulate in the plume.

---

[5] We suspect that the larger particles collected were primarily the products of the breakup of the supermicron ash particles in the intake tube. Large particles inducted intact would have a very low probability of being collected on the filter because of impaction or sedimentation in the sample train. Resuspension of supermicron particles within the bag at the next fill cycle and turbulent or mechanical breakup into smaller particles, and hence their appearance in subsequent samples, are also possibilities.

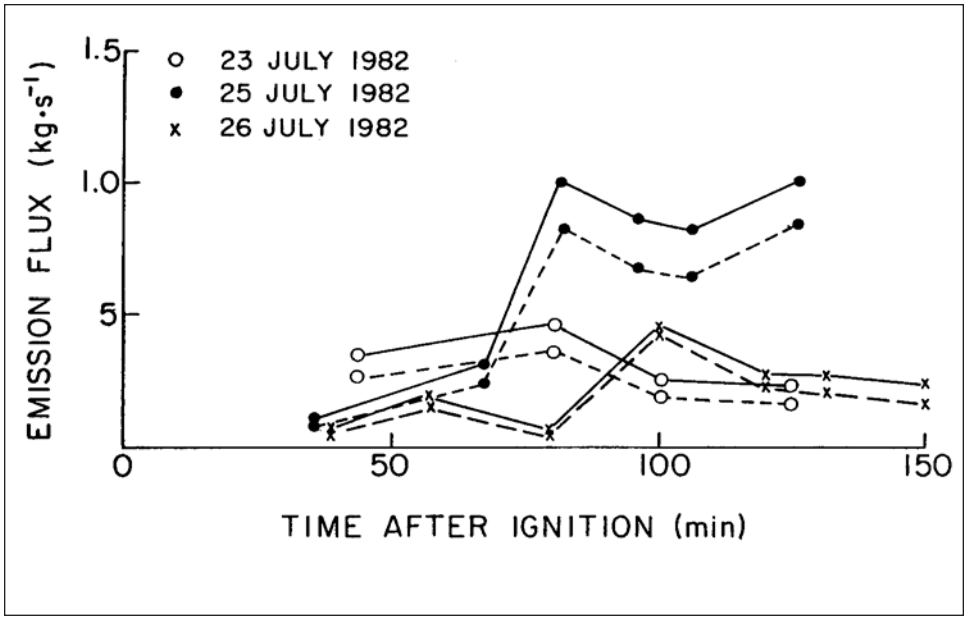

Figure 32—Particle mass fluxes derived from particle mass measurements ≤43 μm (solid lines) and particle mass measurements <2 μm for the Oregon burns.

In another study (Ward and Hardy 1984), emission factors for particulate matter were determined by using samplers suspended from cables strung between towers over prescribed fires. The size-selective emission factors for total particulate matter and particulate matter <2.5 μm in mean mass diameter are in reasonable agreement with the results reported here. Ward and Hardy's measurements show the difference between total particulate matter and particulate matter <2.5 μm, to be a function of fire intensity (r=0.90). Most of the emissions sampled for this paper originated from the flaming combustion phase before the onset of the collapse of the convection column, when the difference between the emission factor for total suspended particulates and that for particles <2 μm in diameter would likely be at a maximum.

6.6 Particle Mass Fluxes

Although it will not be possible to calculate emission factors using the flux method until the fuel consumption data are available, this section describes the first step, namely, the calculation of particle mass fluxes. As for emission factors, we have calculated particle mass fluxes for total suspended particulates (from the filters), for particles ≤43 μm (from the UW particle-size measuring system, assuming a particle density of 1 $g \cdot cm^{-3}$) and for particles <2 μm (from the mass monitor).

The particle mass fluxes for total suspended particulates (TSP) were calculated by using the appropriate value of the "volume flux of air," as listed in table 7, together with the appropriate algorithms relating b_{scat} and TSP particle mass concentration for "all data" as given in table 6. These results are shown in the fourth column of

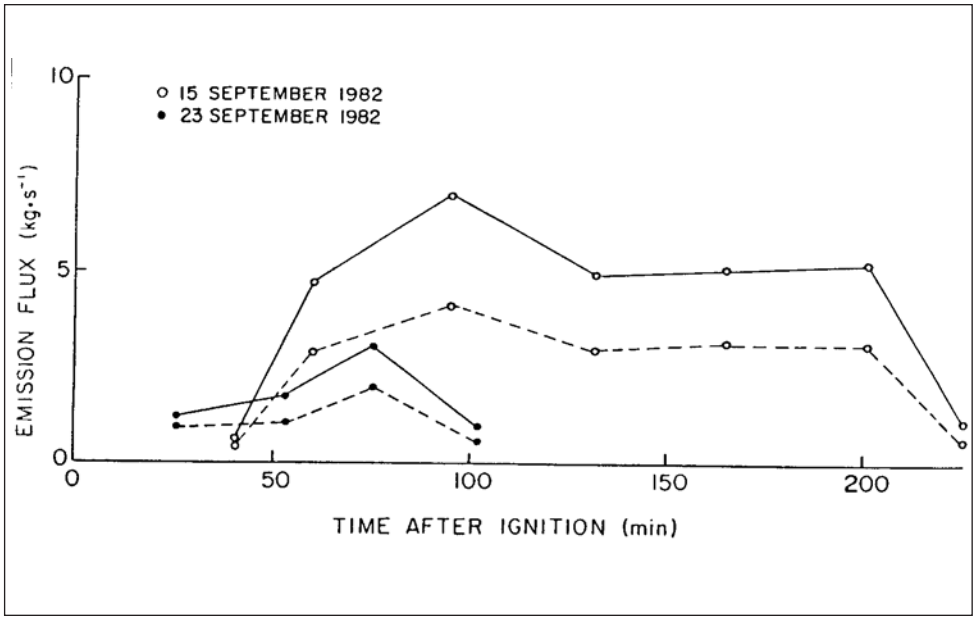

Figure 33—Particle mass fluxes derived from particle mass measurements ≤43μm (solid lines) and particle mass measurements <2 μm for the Washington burns.

table 14. The particle emission fluxes for TSP were also calculated with the ratio method by using the appropriate ratios of b_{scat} to aerosol mass for the Oregon and Washington fires (see section 5.3). The results are listed in the fifth column of table 14. Shown in the last two columns of table 14 are the particle mass fluxes for particles ≤43 μm and <2 μm in diameter as derived from the particle spectra and mass monitor data, respectively. The particle mass fluxes for the total suspended particulates are about twice those for particles ≤43 μm in diameter and about three times for particles <2 μm in diameter.

Plots of the particle mass fluxes for the burns in Oregon (fig. 32) and Washington (fig. 33) show a number of interesting features when compared to the time histories of particle volume at plume center (see section 6.2) and to the emission factors (section 6.5). Figure 32 shows that the peak particle mass flux for the Oregon burns occurred 80-100 minutes after ignition; the total particle volumes at plume center and the emission factors tended to peak later in the burn. For both the Oregon and Washington burns, the particle volume (≤43 μm) at plume center was not a very good predictor of the integrated flux over the cross section.
The following topics deserve further study:

7. Topics For Further Study

1. The airborne data collected on July 24, 1982, were only partially analyzed because visual observations indicated that a steady-state assumption was not warranted. Despite this limitation, some good data were obtained on this flight. These data need further analysis.

Study

because visual observations indicated that a steady-state assumption was not warranted. Despite this limitation, some good data were obtained on this flight. These data need further analysis.

2. Data collected on July 25, 1982, were not fully analyzed (despite the excellent plume on this day) because the filters were damaged. The remaining data should be fully analyzed.

3. In determining the particle emission factors presented in this report, we used CO_2 and CO measurements from the canister samples; however, continuous measurements of $C0_2$ and CO were also made. Calculations of particulate emission factors using these continuous measurements are needed. By using the continuous data, we could obtain measurements of particle emission factors in all cases where particle samples were obtained rather than just those where a canister sample was available. Accuracy would not be improved because canister samples would be needed to calibrate the CO_2 data (see section 4.2), but this would result in an approximate doubling of the number of estimates of the emission factors.

4. The nitrogen oxides and ozone data have not been analyzed, although they appear to be of good quality. This should be done.

5. The measurements of the particle size distributions from 0.01 to 4500 μm in diameter permit particle fluxes to be determined over any reasonable number of size intervals for all of the cross sections (independent of b_{scat} or other continuous measurements). These fluxes have not been calculated, but this could be done to assess the mass of particles in the plume by size fractions.

6. We have made only limited use of the elemental analysis of the material collected on the filters. The data are now organized for factor analysis, which could be useful in establishing elemental “fingerprints.”

7. When the fuel consumption rates become available, independent estimates need to be made of the emission factors for the burns; these can then be compared with those determined from the carbon-balance technique used in this report.

8. The yarding and ignition characteristics of the burns need to be compared with the information about the plumes provided by the airborne measurements.

9. Additional knowledge is needed on the density of the material in the emissions over various particle size intervals to compute more accurately the mass fluxes of aerosols from the particle volume distribution data.

8. Conclusions

In this report, we have presented the results of airborne measurements on the particulate and gaseous emissions from a series of prescribed burns of forest residues. The measurements were used to obtain quantitative data on plume

dimensions, particle size distributions, particle densities, and size-dependent particle emission fluxes and emission factors.

Our airborne measurements of particle size distributions produced some surprises. As in previous studies, a peak in the mass concentration of particles centered around particles 0.25-0.3 μm in diameter. Particle concentrations were dominated by large numbers of Aitken nuclei (median number diameter ≈0.15 μm). Although submicron particles dominated the visibility characteristics of the plumes, they did not dominate the total emissions from the burns. Even more surprrsing was the observation that the mass flux 3.3 km downwind of the burn may have been dominated by millimeter-sized debris.

The effective density of the submicron particles in the plumes was determined by two independent techniques to be 0.86±0.09 $g \bullet cm^{-3}$ and 0.98±0.03 $g \bullet cm^{-3}$. Some uncertainty exists as to the absolute accuracy of these determinations. Recent studies suggest that the density of the particles may be a function of fire intensity.

Emission factors have been determined, by using the carbon-balance method, for total suspended particulates (with some uncertainty as to the upper limit for particle size), particles with diameters ≤43 μm, and particles <2 μm in diameter. The derived average emission factors, based on numerous measurements in six burns, were 12.2±3.6 $g \bullet kg^{-1}$ for the total suspended particulates, 6.0±3.4 $g \bullet kg^{-1}$ for particles ≤43 μm in diameter, and 4.1+1.5 $g \bullet kg^{-1}$ and 3.7±.7 $g \bullet kg^{-1}$ from two independent measurements of particles with diameter <2 μm. The Washington burns showed no significant trend with time, but the Oregon burns showed marked and consistent temporal variations.

Particle mass fluxes for total suspended particulates, particles ≤43 μm in diameter, and particles <2 μm in diameter ranged from 0.1 to 2.4 $kg \bullet s^{-1}$, 0.1 to 1.1 $kg \bullet s^{-1}$, and 0.1 to 0.8 $kg \bullet s^{-1}$, respectively, for the smaller Oregon burns, and 1.1 to 11.7 $kg \bullet s^{-1}$, 0.6 to 7.0 $kg \bullet s^{-1}$, and 0.4 to 4.1 $kg \bullet s^{-1}$ respectively, for the larger Washington burns.

English Equivalents

Centigrade (°C)	1.8 degrees Fahrenheit + 32
centimeter (cm)	0.3937 inch
cubic centimeter (cm^3)	.061 cubic inches
garam (g)	0.03527 ounce
hectare (ha)	2.471 acres
kilometer (km)	0.6214 statute mile or 0.5396 nautical mile
liter (L)	33.814 ounces (liquid) or 6.00353 ft^3

meter (m)	39.37 inches
metric ton (t)	2204.623 pounds
micrometer (μm)	$1 \cdot 10^{-6}$ meters
millimeter (mm)	0.0394 inch
square meter (m^2)	10.76 square feet

Literature Cited

Anderson, J.A.; Waters, N.; Richards,L.W. [and others]. 1982. Air quality sampling during the Green Mountain smoke characterization study. [location of publisher unknown]: [publisher unknown]; Report to the Environmental Protection Agency; contract TS-AM D-8194.

Byram, G.M. 1959. Forest fire control and use. Davis, K. P., ed. New York: McGraw-Hill. 321 p.

Ewing, G.W. 1975. Instrumented methods of chemical analysis. New York: McGraw-Hill.

Sandberg, D.V.; Ward, D.E. [1982]. Increased wood utilization reduces emission from prescribed burning. In: Air quality protection aspects of forestry management. Tech. Bull. 390. New York: National Council of the Paper Industry for Air and Stream Improvement, Inc.

SCEP. 1970. Man's impact on the global environment. Cambridge, Mass.: MIT Press. 319 p.

Stith, J.L.; Radke, L.F.; Hobbs, P.V. 1981. Particle emissions and the production of ozone and nitrogen oxides from the burning of forest slash. Atmospheric Environment. 7: 73-82.

Ward, D.E.; Core, J.E. 1984. Source emission profiles for Douglas-fir and hemlock slash burning. In: Papers, 21st annual meeting of the Air Pollution Control Association, Pacific Northwest International Section, 1984 November 12-14, Portland,OR. Pap. 84-19. Portland,OR: Air Pollution Control Association: [not paged].

Ward, D.E.; Hardy, C.C. 1984. Advances in the characterization and control of emissions from prescribed fires. In: Papers, 77th annual meeting of the Air Pollution Control Association, 1984 June 24-29, San Francisco, CA. Pap. 84-36.3. Portland, OR: Air Pollution Control Association: [not paged].

Ward, D.E.; McMahon, C.K.; Johansen, R.W, 1976. An update on particulate emissions from forest fires. In: Papers, 69th annual meeting of the Air Pollution Control Association, 1976 June 27-July 1, Portland, OR. Pap. 76-2.2. Portland, OR: Air Pollution Control Association: [not paged].

Ward, D.E.; Sandberg, D.V. 1982. Measurement of smoke from prescribed fires in the Pacific Northwest: A progress report. In: Papers, the Pacific Northwest Air Pollution Control Association Meeting, 1982, Vancouver, BC. Portland, OR: Air Pollution Control Association: [not paged].

Ward, D.E.; Sandberg, D. V.; Ottmar, R, D. 1982. Measurement of smoke from two prescribed fires in the Pacific Northwest. In: Papers, 75th annual meeting of the Air Pollution Control Association, 1982 June 20-25, New Orleans, LA. Pap. 82-8.4. Portland, OR: Air Pollution Control Association: [not paged].

White, W.H. 1981. The role of particulate sulfates and nitrates in reducing visibility. In: Papers, 74th annual meeting of the Air Pollution Control Association, 1981 June 21-26, Philadelphia, PA. Portland, OR: Air Pollution Control Association: [not paged].

Appendix A Data used in the calculation of emission factors for total suspended particulates (TSP), Particles ≤43 μm in diameter, and particles 2μm in diameter.

Table 15–Data used in the calculation of emission factors for TSP by the carbon-balance method, by mission number

Mission	Sample time (PDT)	Canister number	Filter mass	THC	Carbon	NMHC	Carbon	CO_2	Carbon	CH_4	Carbon	CO	Carbon
			μg•m^{-3}	ppm C	mg•m^{-3}	ppm C	mg•m^{-3}	ppm	mg•m^{-3}	ppm	mg•m^{-3}	ppm	mg•m^{-3}
1	1526 (amb)[a]	148		3.38		0.69		332.6		1.54			0.45
	1603	265	213.63	6.74	1.80	1.16	0.25	474.3	75.9	1.52		1.01	.30
	1611	229		3.01		1.23	.18	374.3	22.3	1.45		1.78	.71
	1621	170		3.78	.21	1.66	.52	382.6	26.8	1.81	0.14	3.65	1.71
	1631	309		3.01		1.30	.33	332.1		1.71	.09	1.70	.67
	1641	227		3.36		1.90	.64	351.5	10.0	1.85	.17	3.53	1.65
	1651	297	371.64	3.26		1.78	.58	323.1		1.60	.03	1.26	.43
	1701	40		3.28		1.27	.19	384.8	28.0	1.96	.22	4.16	1.99
	1710	114		3.73	.19	1.21	.17	406.3	39.5	1.95	.22	6.15	3.05
	1720	244		3.72	.18	1.35	.35	399.0	35.6	2.04	.27	6.50	3.24
	1733	217S		3.59	.11	1.23	.29	389.4	30.4	2.07	.28	6.09	3.02
	1738	157	875.82	3.90	.78	1.61	.49	388.9	30.2	2.16	.33	7.28	3.66
	1745	220		4.09	.38	1.50	.26	391.4	31.5	2.14	.32	6.90	3.46
	1753	293	504.00	3.75	.20	1.58	.47	365.1	17.4	1.99	.24	4.95	2.41
	1803	208		3.28		.94	.43	366.7	18.3	1.92	.20	4.14	1.98
	1818	146		3.65	.14	1.25	.30	393.0	32.4	1.99	.24	5.12	2.50
	1825	255	484.14	2.81		1.97	.68	340.6	4.3	1.77	.12	1.97	.81
2	1612	238		3.06	.38	1.47	.43	321.4		1.53	.02	1.96	.81
	1621	133		2.98	.34	.69	.01	347.2	13.6	1.63	.07	1.51	.57
	1633	280	372	3.33	.53	.70	.02	374.2	28.0	1.72	.12	3.17	1.46
	1641	77		2.75	.22	.57		343.0	11.3	1.58	.04	1.81	.73
	1650	316	286	3.01	.36	.59		364.5	22.8	1.68	.10	2.48	1.09
	1659	292		2.86	.28	.62		343.9	11.8	1.62	.06	1.80	.73
	1710	301		3.01	.36	.62		336.2	7.7	1.73	.12	2.53	1.12
	1723	283	110	2.87	.28	.60		329.4	4.0	1.55	.03	.98	.29
	1735	112		2.51	.09	.50		329.4	4.0	1.56	.03	.87	.23
	1745	186	777	4.06	.92	.89	.12	371.6	26.6	2.23	.39	7.65	3.86

Table 15–(continued)

Mission	Sample time (PDT)	Canister number	Filter mass	THC	Carbon	NMHC	Carbon	CO_2	Carbon	CH_4	Carbon	CO	Carbon
			$\mu g \cdot m^{-3}$	ppm C	$mg \cdot m^{-3}$	ppm C	$mg \cdot m^{-3}$	ppm	$mg \cdot m^{-3}$	ppm	$mg \cdot m^{-3}$	ppm	$mg \cdot m^{-3}$
2	1754	155		4.08	.93	1.00	.18	362.5	21.8	2.19	.37	6.85	3.43
	1801	308	120	2.97	.34	.66		340.2	9.8	1.78	.15	2.60	1.16
	1810	198		2.72	.20	.48		324.2	1.2	1.52	.01	.44	
	1820(amb)	147		2.34		.67		321.9		1.50		.44	
3	0846(amb)	195	81	2.77		.76		327.7		1.54		.59	
	0953	231	165	2.71		.38		330.2	1.3	1.54		.38	
	1000	110		3.05	.15	.56		357.1	15.7	1.64	.05	1.35	.41
	1009	315		3.18	.22	1.01	.13	335.4	4.1	1.60	.03	1.00	.22
	1021	12		3.33	.30	1.03	.14	336.0	4.4	1.59	.03	1.14	.29
	1030	219		2.90	.07	.52		338.3	5.7	1.66	.06	.82	.12
	1037	163		3.15	.20	.46		351.2	12.6	1.69	.08	1.96	.73
	1044	123		2.64		.57		329.9	1.2	1.58	.02	.75	.08
	1051	102		2.96	.10	.43		346.6	10.1	1.705	.09	2.05	.78
	1058	76		2.92	.08	.54		346.4	10.0	1.75	.11	2.67	1.11
	1104	230		3.09	.17	.57		331.8	2.2	1.67	.07	1.43	.45
	1111	289		2.78	.01	.58		343.5	8.5	1.67	.07	2.34	.94
	1117	296		3.04	.14	.47		350.3	12.1	1.72	.10	2.43	.98
	1124	305		3.41	.34	.56		360.3	17.5	1.86	.17	3.88	1.76
	1130	93		3.35	.31	.52							
	1137	111		3.02	.13	.49		337.8	5.4	1.77	.12	2.27	.90
	1144	271S		2.57		.46		326.9		1.60	.03	.79	.11
4	1012(amb)	245		2.49		.38		335.9		1.58		.38	
	1041	97	86	3.08	.32	.38		350.6	7.9	1.59	1.04	.35	
	1049	267S		2.87	.20	.38		337.9	1.1	1.53	.74	.19	
	1056	74	105	3.21	.38	.38		344.8	4.8	1.55	.96	.31	
	1104	319	481	3.21	.39	.38		370.9	18.8	1.74	.08	2.01	.87
	1111	124		3.38	.48	.38		394.5	31.4	1.85	.14	3.76	1.81
	1117	4		3.06	.31	.38		388.4	28.1	1.77	.10	2.93	1.37
	1127	99		2.70	.11	.38		336.8	.5	1.56		.58	.11
	1134	41	508	2.72	.12	.38		350.6	7.9	1.60	.01	1.30	.49
	1140	183		3.80	.70	.38		382.6	25.0	1.92	.18	4.69	2.31
	1146	234		3.21	.39	.38		364.3	15.2	1.80	.12	3.54	1.69

Table 15–(continued)

Mission	Sample time (PDT)	Canister number	Filter mass	THC	Carbon	NMHC	Carbon	CO_2	Carbon	CH_4	Carbon	CO	Carbon
			$\mu g \cdot m^{-3}$	ppm C	$mg \cdot m^{-3}$	ppm C	$mg \cdot m^{-3}$	ppm	$mg \cdot m^{-3}$	ppm	$mg \cdot m^{-3}$	ppm	$mg \cdot m^{-3}$
4	1154	13	317	2.68	.10	.38		350.7	7.9	1.56		1.03	.35
	1202	250	487	3.19	.37	.38		372.3	19.5	1.81	.12	3.70	1.78
	1208	252		3.05	.30	.38		362.1	14.0	1.78	.11	3.11	1.46
	1217	236	566	3.59	.59	.38		390.3	29.1	1.87	.16	4.71	2.32
	1225	290		3.36	.47	.38		363.3	14.7	1.80	.12	3.31	1.57
	1233	318	499	3.20	.38	.38		361.3	13.6	1.87	.16	3.50	1.67
	1240	156		3.26	.41	.38		355.9	10.7	1.84	.14	3.79	1.83
	1250	201		3.33	.45	.38		359.1	12.4	1.82	.13	3.14	1.48
5	1402(amb)	1		207.1		0		343.6		.46		0	
	1415	3	672.44	211.5		0		362.1	12.8	.87	.21	1.15	.62
	1426	4		250.8	13.3	0		447.6	58.6	1.21	.40	9.01	4.8
	1435	5	1614.28	242.2	8.53	0		417.4	42.4	1.19	.38	6.27	3.36
	1440	6		196.4		0		354.6	8.7	.71	.13	.17	.09
	1445	7	1057.35	204.6		0		456.0	63.0	1.86	.74	14.13	7.57
	1455	8	913.54	237.9	6.23	0		396.9	31.4	1.45	.52	6.57	3.52
	1502	9		155.0		0		430.5	49.4	1.47	.54	7.09	3.80
	1509	10	1017.27	193.6		0		395.8	30.8	1.23	.41	5.81	3.11
	1517	11		15.9		1.40	0.75	519.6	97.1	2.19	.92	15.23	8.16
	1524	12	1618.98	182.0		0		409.8	38.3	1.21	.40	5.16	2.76
	1530	13		125.7		0		383.4	24.2	1.37	.48	5.31	2.84
	1536	14	912.73	182.4		0		384.6	24.8	1.30	.44	6.43	3.45
	1546	15		200.7		0		440.2	54.6	1.16	.37	6.77	3.63
	1553	16	520.35	181.3		0		333.0		.77	.16	-.00	
	1600	17		181.3		0		339.1	.4	.77	.16	.09	.05T
	1607	18		178.1		0		346.2	4.2	.95	.26	.50	.27
	1614	19		192.7		.02	.01	404.8	35.6	1.14	.36	6.37	3.41
	1625	20	703.55	190.8		0		337.4	.81	.18	-.00		
	1633	21		166.9		0		384.4	24.7	1.05	.31	3.42	1.83
	1640	22	652.30	202.6		0		378.2	21.4	.98	.27	2.66	1.42
	1651	23		177.5		.02	.01	401.2	33.7	1.18	.38	5.86	3.14

Table 15–(continued)

Mission	Sample time (PDT)	Canister number	Filter mass	THC	Carbon	NMHC	Carbon	CO_2	Carbon	CH_4	Carbon	CO	Carbon
			$\mu g \cdot m^{-3}$	ppm C	$mg \cdot m^{-3}$	ppm C	$mg \cdot m^{-3}$	ppm	$mg \cdot m^{-3}$	ppm	$mg \cdot m^{-3}$	ppm	$mg \cdot m^{-3}$
5	1658	24	878.53	161.3		0		396.8	31.3	1.24	.41	5.04	2.70
	1705	25		161.3		0		374.7	19.5	1.06	.31	3.48	1.86
	1711	26	414.98	186.1		.01	.005	361.7	12.5	.83	.19	1.99	1.07
	1719	27		176.5		.01	.005	368.6	16.2	1.12	.35	4.85	2.60
	1726	28	867.49	185.2		0		395.7	30.8	1.49	.73	8.49	4.55
	1731	29	455.06	209.3		0		365.7	14.7	1.67	.64	5.82	3.12
	1750(amb)	30		245.4		0		333.0		.48		-.00	
6	1531	301		3.31	.28	.53	.01	408.5	29.0	1.77	.08	3.11	1.66
	1535(amb)	294		2.79		.51		354.3		1.61			
	1537	111	391.43	3.16	.20	.49		376.8	12.0	1.79	.10	2.27	1.22
	1547	102		3.48	.37	.51		401.5	25.3	1.91	.16	4.84	2.59
	1554	231	601.76	3.28	.26	.53	.01	383.8	15.8	1.88	.14	3.32	1.78
	1559	146		3.68	.48	.43		406.8	28.1	2.00	.21	5.39	2.89
	1604	208		2.66		.38		342.2		1.51		1.20	.64
	1612	310	600.36	3.54	.40	.63	.06	394.7	21.6	1.93	.17	4.80	2.57
	1619	309		3.19	.21	.55	.02	391.3	19.8	1.88	.14	3.36	1.80
	1624	45	322.44	2.86	.04	.45		365.4	6.0	1.70	.05	1.85	.99Ta
	1639	40		3.43	.34	.48		403.5	26.4	2.00	.21	5.44	2.91
	1656	289		3.83	.556	.69	.096	407.7	28.6	2.16	.29	7.50	4.02
	1703	305		3.22	.23	.58	.04	381.6	14.3	2.03	.22	4.27	2.29
	1710	170	692.31	3.49	.37	.57	.03	385.3	16.6	2.01	.21	5.04	2.70

[a] Sample of ambient air

Table 16–Data used in the calculation of emission factors for particles ≤43 μm and <2 μm diameter, by date

Date, mission, and UW flight	Sample interval (PDT)	Mass concentration of particles ≤43 μm diameter	Mass concentration of particles <2 μm diameter from mass monitor	Mass concentration of particles <2 μm diameter from cascade microbalance
		μg•m^{-3}		
July 23, 1982, mission 1, flight 1054	1603-1621	196.1	119.1	132.0
	1631-1651	316.3	145.6	103.1
	1733-1745	551.3	247.4	187.2
	1753-1810	289.3	181.1	115.2
	1818-1825	145.7	277.0	178.9
July 24, 1982, mission 2, flight 1055	1612-1621	33.1	0	57
	1633-1641	99.4	44.2	307.0
	1650-1659	103.4	69.8	106.7
	1723-1735	52.4	30.0	57.8
	1745-1754	297.1	240.7	128.9
	1801-1810	54.4	66.2	63.2
July 25, 1982, mission 3, flight 1056	1041-1049	29.2	55.9	21.7
	1056	39.9	25.7	23.0
	1104-1111	215.9	128.6	130.8
	1134-1146	129.1	133.0	78.4
	1154	491.1	55.4	51.1
	1202-1208	176.3	113.5	94.7
	1217-1225	205.4	137.5	201.7
	1233-1240	207.6	142.7	194.4
Sept. 15, 1982, mission 5, flight 1060	1415	486.9	0	0
	1426-1435	803.4	0	0
	1440-1445	645.5	0	0
	1455	593.6	323.0	0
	1502-1509	766.1	311.8	0
	1517-1524	805.2	351.2	0
	1530-1536	743.7	314.5	0
	1546-1553	43.9	404.2	0
	1614-1625	368.0	257.1	0
	1633-1640	417.0	190.7	0
	1651-1658	602.7	373.5	0
	1706-1711	308.0	170.5	0
	1719-1726	431.1	344.0	0
	1731	514.5	169.8	0
Sept. 23, 1982, mission 6, flight 1061	1531-1537	137.8	142.8	0
	1547-1554	269.8	175.9	220.2
	1559-1612	194.2	211.5	282.2
	1619-1624	167.4	101.1	118.4
	1639-1646	200.9	177.9	76.7
	1656-1710	349.6	261.4	159.4

Appendix B General information on aircraft passes for missions 1 through 6.

Table 17–Sample information table, by mission number

Mission number	Sequence number	Time (PDT)	Altitude	Altitude	Number of passes	Canister or Mylar bag number	Position with respect to plume[a]
			km	ft			
1		1526	1.80	5900		148	amb
		1603	1.80	5900		265	
	1	1606-1617	1.68	5500	5	229	A
	1	1618-1627	1.66	5430	4	170	
	1	1630-1636	1.59	5230	3	309	C
	1	1640-1644	1.52	5000	2	227	
	1	1638-1639	1.49	4890	1	297	E
	2	1640-1644	1.52	5000	2	227	E
	2	1646-1652	1.55	5100	3		
	2	1654-1655	1.58	5180	1		
	2	1657-1707	1.70	5575	4	40	C
	2	1710-1713	1.79	5860	2	114	
	2	1719-1723	1.85	6080	2	244	A
	3	1719-1723	1.85	6080	2	244	A
	3	1729-1733	1.83	6000	2	217S	
	3	1734-1735	1.77	5820	1		
	3	1738-1741	1.74	5710	2	157	C
	3	1744-1745	1.66	5440	1	220	E
	4	1744-1745	1.66	5440	1	220	E
	4	1753-1759	1.74	5700	5	293	C
	4	1800-1806	1.77	5800	2	208	
	4	1810-1814	1.83	6000	2		A
		1818	1.77	5800		146	
		1825	1.76	5775		255	

Table 17–(continued)

Mission number	Sequence number	Time (PDT)	Altitude	Altitude	Number of passes	Canister or Mylar bag number	Position with respect to plume[a]
			km	ft			
2	No sequences	1612	1.83	6000		238	
		1621	1.80	5900		133	
		1633	2.93	9600		280	
		1641	2.83	9280		77	
		1650	2.77	9090		316	
		1659	2.64	8660		292	
		1710	2.93	9600		301	
		1723	2.59	8500		283	
		1735	1.80	5900		112	
		1745	1.68	5500		186	
		1754	1.52	5000		155	
		1801	1.61	5280		308	
		1810	1.68	5500		198	
		1820	1.58	5200		147	amb
3		0846	1.66	5440		195	amb
	1	0950-0953	1.66	5440	2	231	A
	1	0956-1003	1.59	5220	3	110	C
	1	1008-1009	1.49	4900	1	315	E
	2	1021-1025	2.18	7140	2	12	A
	2	1029-1033	2.10	6900	2	19	C
	2	1037-1041	2.01	6600	2	163	E
	3	1037-1041	2.01	6600	2	163	E
	3	1044-1047	2.21	7250	2	123	C
	3	1051-1054	2.51	8250	2	102	A
	4	1051-1054	2.51	8250	2	102	A
	4	1057-1102	2.33	7640	3	76	C
	4	1104-1108	2.19	7200	3	230	E

Table 17–(continued)

Mission number	Sequence number	Time (PDT)	Altitude	Altitude	Number of passes	Canister or Mylar bag number	Position with respect to plume[a]
			km	ft			
3	5	1104-1108	2.19	7200	3	230	E
	5	1110-1114	2.35	7700	2	289	C
	5	1117-1120	2.55	8360	2	296	A
	6	1117-1120	2.55	8360	2	296	A
	6	1123-1138	2.27	7460	3	305	C
	6	1130-1133	2.22	7300	2	93	E
		1137	2.29	7500		111	
		1144	2.29	7500		271S	
4		1012	1.69	5540		245	amb
	1	1041-1045	1.75	5750	2	97	A
	1	1046-1052	1.69	5540	3	267S	C
	1	1053-1059	1.63	5340	3	74	E
	2	1053-1059	1.63	5340	3	74	E
	2	1101-1107	1.69	5560	3	319	C
	2	1109-1112	1.76	5780	2	124	
	2	1114-1118	1.80	5900	2	4	A
	3	1114-1118	1.80	5900	2	4	A
	3	1118-1121	1.76	5780	2		C
	3	1121-1124	2.33	5660	2		E
		1127	1.74	5700		99	
		1134	2.04	6700		41	
	4	1140-1143	2.19	7200	2	183	A
	4	1143-1144	2.13	7000	1		
		1147-1150	2.00	6560	2	234	C
	4	1152-1155	1.98	6500	2	13	
	4	1157-1200	1.94	6360	2		E
	5	1202-1208	2.01	6600	2	250,252	C

Table 17–(continued)

Mission number	Sequence number	Time (PDT)	Altitude km	Altitude ft	Number of passes	Canister or Mylar bag number	Position with respect to plume[a]
4	5	1210-1219	2.07	6800	4	236	A
	6	1210-1219	2.07	6800	4	236	A
	6	1220-1223	2.00	6560	2		C
	6	1225-1231	1.92	6300	3	290	E
	7	1225-1231	1.92	6300	3	290	E
	7	1233-1236	1.99	6520	2	318	C
	7	1238-1245	2.04	6700	4	156	A
		1250	1.98	6500		201	
5		1402	1.64	5400		1	amb
		1415	1.62	5300			
	1	1416-1417	1.62	5300	1	3	E
	1	1421-1428	1.64	5400	3	4	A
	2	1421-1428	1.64	5400	3	4	A
	2	1431-1438	1.55	5100	3	5	
	2	1441-1445	1.49	4900	2	6,7	
	2	1448-1453	1.38	4540	2		C
	2	1456-1457	1.00	3300	1	8	
	2	1459-1501	.98	3200	1		E
	3	1459-1501	.98	3200	1		E
	3	1503-1506	1.10	3600	2	9	
	3	1510-1515	1.25	4100	2	10	C
	3	1518-1522	1.35	4440	2	11	
	3	1525-1529	1.49	4900	2	12	A
	4	1525-1529	1.49	4900	2	12	A
	4	1531-1532	1.43	4700	1	13	
	4	1534-1538	1.36	4450	2	14	
	4	1541-1546	1.31	4300	2	15	C
	4	1548-1552	1.25	4100	2		
	4	1554-1606	1.17	3850	4	16,17	

Table 17–(continued)

Mission number	Sequence number	Time (PDT)	Altitude	Altitude	Number of passes	Canister or Mylar bag number	Position with respect to plume[a]
			km	ft			
	4	1608-1610	1.13	3700	1	18	E
	5	1608-1610	1.13	3700	1	18	E
	5	1615-1616	1.16	3800	1	19	
	5	1612-1613	1.19	3900	1		
	5	1619-1620	1.22	4000	1		
	5	1622-1626	1.28	4200	2	20	
	5	1629-1635	1.37	4500	2	21	C
	5	1637-1638	1.40	4600	1		
	5	1641-1642	1.55	5100	1	22	
	5	1644-1645	1.58	5200	1		A
	6	1644-1645	1.58	5200	1		A
5	6	1652-1658	1.41	4640	2	23	C
	6	1659-1703	1.37	4500	2	24	
	6	1706-1710	1.34	4400	2	25	
	6	1713-1721	1.23	4050	2	26,27	E
	7	1713-1721	1.23	4050	2	26,27	C
	7	1724-1731	1.26	4150	3	28,29	C
	7	1734-1735	1.31	4300	1		A
		1750	.79	2600		30	amb

Table 17–(continued)

Mission number	Sequence number	Time (PDT)	Altitude	Altitude	Number of passes	Canister or Mylar bag number	Position with respect to plume[a]
			km	ft			
6		1531	.55	1800		301	
		1535	.64	2100		294	amb
		1537	.64	2100		111	
		1547	1.04	3400		102	
		1554	1.05	3440		231	
	2	1558-1602	1.13	3700	2	146	A
	2	1605-1606	.99	3250	1	208	C
	2	1608-1612	.91	3000	2	310	E
	3	1608-1612	.91	3000	2	310	E
	3	1614-1620	.94	3100	2	309	
	3	1624-1628	.98	3200	2	45	
	3	1632-1636	1.04	3400	2		C
	3	1638-1639	1.07	3500	1	40	
	3	1641-1647	1.13	3700	2	276	A
	4	1642-1647	1.13	3700	2	276	A
	4	1649-1650	1.07	3500	1		
	4	1653-1656	1.00	3300	2	289	
	4	1700-1703	.91	3000	2	305	C
	4	1706-1707	.76	2500	1		
	4	1709-1710	.73	2400	1	170	E
	5	1709-1710	.73	2400	1	170	E
	5	1718-1719	.78	2550	1		C
	5	1713-1716	.82	2700	2		A

[a]A = top; C = center; E = bottom; amb = ambient

Abbreviations

ASAS	active scattering laser probe
b_{scat}	light-scattering coefficient
EAA	electrical aerosol analyzer
FSSP	forward scattering spectrometer probe
EF	emission factor
EPA	Environmental Protection Agency
LAS	laser aerosol spectrometer
LEMSCO	Lockheed Engineering and Management Services Co.
MCI	microbalance cascade impactor
MND	mean number diameter
MSL	mean sea level
MVD	mean volume diameter
NMHC	nonmethane hydrocarbons
OGC	Oregon Graduate Center
PDT	Pacific Daylight Time
PIXE	proton-induced X-ray emission
PMS	particle measuring system
RTI	Research Triangle lnstitute
S	sulfur
THC	total hydrocarbons
TNMHC	total nonmethane hydrocarbons
TPV	total particle volume
TSP	total suspended particulates
USDA	U.S. Department of Agriculture
UW	University of Washington

Table 1–Specifications of research instruments aboard the University of Washington B-23 aircraft

Parameter	Instrument type	Manufacturer	Range (and error)[a]
Total air temperature[b]	Platinum wire resistance	Rosemount, model 102CY2CG + 414 L	-70 to 30 °C (<0.2 °C)
Static air temperature[b]	Computer value	In-house	-70 to 30 °C (<0.5 °C)
Dew point[b]	Dew condensation	Cambridge Systems, model th73-244	-40 TO 50 °C (<1 °C)
Pressure altitude[f]	Variable capacitance	Rosemount, model 831 BA	150 to 1060 mb (<0.2%)
True airspeed	Variable capacitance	Rosemount, model 831 BA	0 to 230 $m \cdot s^{-1}$ (<0.2%)
Air turbulence[b]	Differential	Meteorology Research, Inc., model 1120	0 to 10 $cm^{2/3} \cdot s^{-1}$ (<10%)
Electric field[b]	Rotary field mill	Meteorology Research, Inc. model 611	0 to 110 kV (<10%)
Types and sizes of hydrometers	Metal foil impactor	Meteorology Research, Inc. model 1220A	Detects particles (>250 μm)
Ice particle[b] concentrations	Optical polarization technique	In-house	0 to 1000 L^{-1} detects particles (>50 μm)
Cloud condensation nucleus-concentrations[b]	Four vertical thermal diffusion chambers	In-house	0 to 5000 cm^{-3} (<10%) Simultaneous measurements at 0.2, 0.5, 1.0, and 1.5% supersaturation
Ice nucleus concentrations[bc]	Acoustical counter	In-house	0.01 to 500 L^{-1}
Ice nucleus concentrations[bc]	Polarizing	Mee Industries	0.1 to 10,000 L^{-1}
Concentrations of sodium-containing particles[bc]	Flame spectrometer	In-house	0 to 10,000 L^{-1} (<1%)
Altitude above terrain[b]	Radar altimeter	AM/APN22	0 to 6 km (<5%)
Weather radar[b]	5 cm gyrostabilized	Radio Corp. of America, AVQ-10	100 km
Aircraft position and course plotter[b]	Works off DME and VOR	In-house	180 km (1 km)

Table 1–(continued)

Parameter	Instrument type	Manufacturer	Range (and error)[a]
Time[b]	Time code generator	Systron Donner model 8220	h, min, s ($1:10^5$)
	Radio WWV	Gertsch RHF 1	min
Ground communication[b]	FM transceiver	Motorola	200 km
Light-scattering coefficient	Integrating nephelometer	Meteorology Res. Inc., model 1567 (modified for increased stability and better response time)	0 to $10 \cdot 10^{-4}$ m^{-1} or 0 to 2.5 $10^{-3} \cdot m^{-1}$
Heading[b]	Gyrocompass	Sperry, model C-2	0 to 360 ° (<2%)
Ground speed and drift angle[b]	Doppler navigator	Bendix, model DRA-12	0 to 6 km altitude
Ultraviolet radiation[b]	Barrier-layer photoelectric cell	Eppley Laboratory Inc., model 14042	0.7 $J \cdot m^{-2} \cdot s^{-1}$ (<5%)
Angle of attack[b]	Potentiometer	Rosemount, model 861	±23 ° (<0.5 °)
Photographs[b]	35-mm time-lapse camera	Automax, model GS-2D-111	1 s to 10 min
Total gaseous sulfur[b]	FPD flame photometric detector	Meloy, model 285	0.5 ppb - 1ppm
Ozone[b]	Chemiluminescence (C_2H_4)	Monitor Labs, model 8410 A	0 to 5 ppm (<7 ppb)
NH_3, NO, NO_2, NO_x[b](O3)	Chemiluminescence model 8440	Monitor Labs,	0 to 5 ppm (<10 ppb)
Size spectrum of aerosol[b]	Electrical aerosol analyzer	Thermal Systems, Inc., model 3030	0.0032 to 1.0 μm
Size spectrum of aerosol particles[b]	90° light-scattering[b]	Particle Measuring System (LAS-200)	0.5 to 11 μm
	Forward light-scattering[b]	Royco (modified in-house)	1.5 to 40 μm
	Diffusion battery	Thermal Systems, Inc., model 3040 with in-house automatic valves and sequencing	0.01 to 0.2 μm
	35-120° light-scattering Spectrometer (ASAS)	Particle Measuring Systems, Active Scattering Aerosol	0.09 to 3.0 μm (<0.007 μm)

Table 1–(continued)

Parameter	Instrument type	Manufacturer	Range (and error)[a]
Size spectrum aerosol and cloud particles[b]	Forward light-scattering Probe (FSSP)	Particle Measuring Systems, Forward Scattering Spectrometer	2 to 47 μm
Size spectrum cloud particles[b]	Diode occulation	Particle Measuring Systems, model OAP-200X	20 to 300 μm
Size spectrum of precipitation particles[b]	Diode occulation	Particle Measuring Systems, model OAP-200Y	300 to 4500 μm
Images of cloud particles[b]	Diode occulation imaging	Particle Measuring systems, model OAP-2D-C	Resolution 25 μm
Images of precipitation particles[b]	Diode imaging	Particle Measuring Systems, model OAP-2D-P	Resolution 200 μm
Concentrations of Aitken nuclei[b]	Light transmission	General Electric, model CNC II	10^2 to 10^6 cm^{-3} (particles >0.005 μm)
Concentrations of Aitken nuclei[b]	Rapid expansion	Gardner	$2 \cdot 10^2$ to 10^7 cm
Sizes and types of aerosol particles[b]	Direct impaction	Glass slides	5 to 100 μm
Concentrations of ice nuclei[c]	Direct impaction	Nuclepore/ Millipore	
Mass concentration aerosol particles[b]	Electrostatic deposition onto matched oscillators	Thermal Systems, Inc., model 3205	0.1 to 3000 $\mu g \cdot m^{-3}$ (<0.1 $\mu g \cdot m^{-3}$)
Particulate matter[c] (sulfur, $SO_4^=$, NO_3^-, Cl^-, Na^+,	Teflon filters CSI and Dionex XRF spectroscopy and ion exchange	In-house	0.1 to 50 $\mu m \cdot m^{-3}$ (for 500-L air sample)
K^+, NH_4^+ and other trace materials.)	chromatography		
Cloud water samples[c]	Centrifuge	In-house	Collects cloud droplets >3 μm radius with an efficiency >50%
Size-segregated concentrations of aerosol particles[d]	Cascade impaction onto matched oscillators	California Instruments	0.05 to 25 μm
	Cascade impactor	Sierra Instruments, Inc.	0.1 to 3 μm (6 size

Table 1–(continued)

Parameter	Instrument type	Manufacturer	Range (and error)[a]
HNO_3[c]	Nylon filters with Teflon prefilter followed by ion chromatography	Dionex	Variable
Hydrocarbons[b]	Gas chromatograph (flame ionization detection)	Analytical Instrument Development, Inc., model 511	0.5 to 110 ppm (as CH_4)
CO_2[d]	Electrochemical oxidation	Ecolyzer model 2000	0 to 300 ppm
CO_2[b]	IR absorption	Foxboro Miran IA	3 to $2 \cdot 10^4$ ppm
Total suspended particulate[c]	High-volume sampler	Nucleonic Corp., model HA69	
Total suspended particulate (TSP)	25-mm Teflon filter (electrobalance analysis)	Analysis to be provided by LEMSCO	

[a] All particle sizes refer to maximum particle dimensions.
[b] Data displayed or available aboard the aircraft.
[c] Not relevant to this study.
[d] Supplied by EPA/LEMSCO.

Table 2–Research flights by date

Date	UW flight number	Mission number	Duration (local times)	Activity
July 2, 1982	—	—	—	Quality control instrumentation check on ground.
July 19, 1982	1052		1137-1506	Airborrne instrumentation flight check.
July 22, 1982	1053		1312-1528	Ferry flight from Seattle to Eugene.
July 23, 1982	1054	1	1449-1909	Slash burn flight (Oregon).
July 24, 1982	1055	2	1508-1904	Slash burn flight (Oregon).
July 25, 1982	1056	3	0809-1223	Slash burn flight (Oregon).
July 26, 1982	1057	4	0926-1328	Slash burn flight (Oregon).
July 26, 1982	—	—	—	Quality control instrumentation check on ground.
July 27, 1982	1058		0858-1147	Ferry flight from Eugene to Seattle.
Sept. 15, 1982	1060	5	1313-1845	Slash burn flight (Washington)
Sept. 23, 1982	1061	6	1417-1806	Slash burn flight (Washington)
Oct. 5, 1982	1064		1310-1506	Slash burn flight (Washington); flight aborted enroute to fire because of aircraft engine malfunction

Table 3–Summary of audit of instrumentation

Organization	Manufacturer of Instrument, model, and serial numbers	Parameter	Regression of instrumentation response to auditor's standard (y=mx+c)			
			Range of measurement	Slope	Intercept	Correlation coefficient
				m	c	
University of Washington's B-23 Aircraft Instrumentation (At Mahlon Sweet Field, Eugene, Oregon)	Foxboro Miran IA	Carbon dioxide	0-5000 ppm	0.8877[a]	+ 14.5 .6097[b]	0.9927 + 263.9.9645
	Ecolyzer 2700, S/N 1686	Carbon monoxide	0-10 ppm	.8573	+ .11	.9996
	Monitor Labs 8440 S/N 169	Nitric oxide	0-0.2 ppm	1.1685	- .011	.9994
		Nitrogen dioxide	0-0.2 ppm	AUDIT INCOMPLETE (see text)		
		Total oxides of nitrogen	0-0.2 ppm	.9366	- .007	.9974
	Monitor Labs, S/N 1686	Ozone	0-0.2 ppm	1.1548	+ .001	.9999
	MRI Nephelometer, model 1567	b_{scat}			Satisfactory	
	Rosemount	Temperature			Satisfactory	
	Cambridge Systems, model TH73-244	Dew point			Satisfactory	
	TSI Quartz Crystal Microbalance, Model 3205	Flow rate	0-1 Lpm	Satisfactory		
	Ghia Filter Sampler	Flow rate	0-100 Lpm	Satisfactory		
	Byron 401 S/N 0306	Total hydrocarbons (as methane)	0-20 ppm	1.0821	+ .18	.9997
		Total hydrocarbons (as propane)	0-20 ppm	.8514	+ .11	.9984
LEMSCO	Byron 401 S/N 0306	Nonmethane hydrocarbon	0-10 ppm	.963	- .46	.9936
		Methane	0-5 ppm	.9247	- .11	.9987
		Carbon monoxide	0-10 ppm	.9403	- .28	.9973
		Carbon dioxide	0-500 ppm	.9709	- 2.53	.9998

[a] Linear regression of CO_2 based only on lower range of concentrations (0-2700 ppm) as measured by instrument.
[b] Linear regression of CO_2 based on full range of concentrations (0-5000 ppm) as measured by instrument.

Table 4–Comparison of measurements by Oregon Graduate Center and LEMSCO of plume minus ambient $C0_2$ concentrations collected in stainless steel canisters via the polyethylene bag, by date

Date	Sample number	Oregon Graduate Center	Lemsco	Ratio LEMSCO/ Oregon Graduate Center
		----------ppm----------		
July 23, 1982	261	62	74	0.19
July 24, 1982	147			
July 24, 1982	155	43	41	.95
July 24, 1982	308	16	18	1.13
July 24, 1982	186	46	50	1.09
July 24, 1982	112	9	8	.89
July 24, 1982	283	14	8	.57
July 24, 1982	292	18	22	1.22

Table 5–Comparison of measurements by Oregon Graduate Center and LEMSCO measurements of plume minus ambient $C0_2$ concentrations collected in stainless steel canisters via the stainless steel loop with those collected in stainless steel canisters via the polyethylene bag, by date

Date	Oregon Graduate Center	LEMSCO	Ratio LEMSCO/ Oregon Graduate Center
	----------ppm----------		
July 25, 1982	6.0	13.3	2.22
July 26, 1982	17.0	25.0	1.47

Table 6–Algorithms relating b_{scat} to mass concentration

Source of data	Equation	Number of samples	Correlation coefficient	Mean mass concentration ÷ mean b_{scat}
TSP (from filter measurements):				
Combined	$(\mu g \cdot m^{-3}) = [b_{scat}\ (m^{-1})]\ (1.30 \cdot 10^5) + 150$	44[a]	.78	$1.77 \cdot 10^5\ \mu g \cdot m^{-2}$
Oregon	$(\mu g \cdot m^{-3}) = [b_{scat}\ (m^{-1})]\ (2.32 \cdot 10^5) + 24$	20[b]	.88	$2.44 \cdot 10^5\ \mu g \cdot m^{-2}$
Washington	$(\mu g \cdot m^{-3}) = [b_{scat}\ (m^{-1})]\ (1.68 \cdot 10^5) - 119$	18[c]	.92	$1.44 \cdot 10^5\ \mu g \cdot m^{-2}$
Particles <2 μm in diameter (from mass monitor):				
Combined	$(\mu g \cdot m^{-3}) = [b_{scat}\ (m^{-1})]\ (4.30 \cdot 10^4) + 48$	241[b]	.77	
Oregon	$(\mu g \cdot m^{-3}) = [b_{scat}\ (m^{-1})]\ (5.85 \cdot 10^4) + 31$	160[b]	.71	
Washington	$(\mu g \cdot m^{-3}) = [b_{scat}\ (m^{-1})]\ (4.31 \cdot 10^4) + 35$	81	.72	
Particles <43 μm in diameter (from particle-size measurements):				
Combined[d]	$(\mu m^3 \cdot cm^{-3}) = [b_{scat}\ (m^{-1})]\ (7.9 \cdot 10^4) + 35$	295	.78	
Oregon	$(\mu m^3 \cdot cm^{-3}) = [b_{scat}\ (m^{-1})]\ (1.0 \cdot 10^5) + 14$	195	.70	
Washington	$(\mu m^3 \cdot cm^{-3}) = [b_{scat}\ (m^{-1})]\ (7.8 \cdot 10^5) + 27$	100	.74	

[a] All data included.
[b] Two extreme values deleted.
[c] Four extreme values deleted.
[d] Multiplying the particle density (in $g \cdot cm^{-3}$) by the volume concentration (in $\mu m^3 \cdot cm^{-3}$) gives the mass concentration (in $\mu g \cdot m^{-3}$).

Table 7–Compilation of the volume flux of air and the associated value of the light-scattering coefficient (b_{scat}) taken from the contoured cross sections of b_{scat} and the measured horizontal winds, by date

Date, mission number, and UW flight number	Cross section sequence number	Time interval (PDT)	Average b_{scat} value for contour interval	Area of contour interval	Wind speed of air	Volume flux
			$10^{-3} \cdot m^{-1}$	$10^{5} \cdot m^{2}$	$m \cdot s^{-1}$	$10^{5} \cdot m^{3} \cdot s^{-1}$
July 23, 1982, mission 1, flight 1054	1	1606-1644	2.45	0.134	5.0	0.670
			1.45	1.584	4.6	7.288
			.725	3.040	4.7	14.290
			.225	2.638	4.8	12.664
	2	1640-1723	2.725	.249	3.0	.747
			2.225	1.255	3.0	3.735
			1.45	3.308	3.1	10.256
			.43	8.968	3.5	31.390
	3	1719-1745	3.725	.104	1.0	.104
			3.225	.420	1.6	.673
			2.45	2.882	1.7	4.899
			1.45	2.334	1.7	3.968
			.43	3.650	1.9	6.934
	4	1744-1814	3.725	.006	2.0	.012
			3.225	.219	2.0	.437
			2.45	1.731	2.0	3.461
			1.45	2.382	2.0	4.764
			.43	3.991	2.0	7.981
July 25, 1982, mission 3, flight 1056	1	0950-1009	1.225	.351	4.9	1.722
			.725	.968	4.4	4.260
			.225	1.545	4.7	7.263
	2	1021-1041	1.725	.341	7.0	2.385
			1.225	.685	7.0	4.794
			.725	1.545	7.0	10.818
			.225	2.723	6.8	18.508
	3	1037-1054	2.45	.007	11.0	.079
			1.45	3.421	9.7	33.183
			.725	3.453	10.0	34.532
			.225	4.213	10.1	42.555
	4	1051-1108	2.45	6.17	10.8	6.660
			1.45	3.058	10.8	33.030
			.43	2.984	10.	832.227
	5	1104-1120	2.225	.036	9.0	.323
			1.725	1.033	10.4	10.740
			1.225	2.567	10.0	25.674
			.43	4.016	10.2	40.963
	6	1117-1133	2.45	1.370	9.8	13.426
			1.45	3.000	10.1	30.300
			.43	4.430	9.8	43.411

Table 7–(continued)

Date, mission number, and UW flight number	Cross section sequence number	Time interval (PDT)	Average b_{scat} value for contour interval	Area of contour interval	Wind speed of air	Volume flux
			$10^{-3} \cdot m^{-1}$	$10^{5} \cdot m^{2}$	$m \cdot s^{-1}$	$10^{5} \cdot m^{3} \cdot s^{-1}$
July 25, 1982, mission 4, flight 1057	1	1041-1059	1.225	.158	5.0	.789
			.725	.835	5.0	4.177
			.225	1.122	5.0	5.612
	2	1053-1118	2.725	.054	5.9	.317
			2.225	.316	5.6	1.767
			1.45	1.008	5.4	5.441
			.43	1.782	5.3	9.446
	3	1114-1124	2.45	.014	5.0	.072
			1.45	.412	5.0	2.062
			.43	.818	5.0	4.088
	4	1140-1200	3.225	.032	8.0	.257
			2.725	.315	7.5	2.366
			2.225	.835	6.2	5.180
			1.45	1.761	6.0	10.566
			.43	2.980	6.2	18.475
	5	1157-1219	2.725	.050	6.8	.341
			2.225	.412	7.0	2.886
			1.45	1.022	7.2	7.358
			.43	1.789	7.3	13.062
	6	1210-1231	2.725	.158	5.7	.900
			2.225	.563	5.5	3.096
			1.45	1.119	5.5	6.154
			.43	2.170	5.4	11.715
	7	1225-1245	2.725	.097	5.0	.484
			2.225	.520	5.0	2.60
			1.45	1.101	5.0	5.504
			.43	1.972	5.0	9.861
Sept. 15, 1982, mission 5, flight 1060	1	1416-1428	12.90	.057	16.0	.912
			10.90	.074	16.0	1.184
			8.90	.095	16.0	1.520
			6.90	.136	16.0	2.176
			3.25	.373	16.0	5.968
			.725	.151	16.0	2.416
	2	1421-1501	10.90	.358	13.3	4.761
			8.90	.646	11.9	7.687
			6.90	1.657	11.8	19.553
			4.90	2.467	11.2	27.630
			2.90	3.703	10.0	37.030
			1.175	3.641	9.7	35.318
	3	1459-1529	12.9	.244	14.4	3.514
			10.9	.767	11.3	8.667
			8.9	1.635	11.4	18.639
			6.9	2.310	10.7	24.717
			4.9	3.679	10.3	37.894
			2.9	2.998	12.3	36.875
			1.175	3.808	10.3	39.222
	4	1525-1610	12.9	.036	17.0	.612
			10.9	.236	15.8	3.729
			8.9	.560	16.0	8.960
			6.9	1.290	14.9	19.340
			4.9	1.850	15.6	28.860
			2.9	2.869	14.0	40.166
			1.175	2.639	13.9	36.682

Table 7–(continued)

Date, mission number, and UW flight number	Cross section sequence number	Time interval (PDT)	Average b_{scat} value for contour interval	Area of contour interval	Wind speed of air	Volume flux
			$10^{-3} \cdot m^{-1}$	$10^{5} \cdot m^{2}$	$m \cdot s^{-1}$	$10^{5} \cdot m^{3} \cdot s^{-1}$
	5	1608-1645	12.9	.151	11.0	1.661
			10.9	.107	11.1	1.188
			8.9	.502	12.6	6.325
			6.9	1.499	12.6	18.887
			4.9	3.012	13.0	39.156
			2.9	3.851	12.9	49.678
			1.175	3.292	12.2	40.162
	6	1644-1721	10.9	.122	12.7	1.549
			8.9	.323	12.6	4.069
			6.9	.796	13.2	10.507
			4.9	4.174	14.3	59.688
			2.9	3.478	13.5	46.953
			1.175	2.374	13.7	32.524
	7	1713-1735	8.9	.086	13.0	1.118
			6.9	.115	13.6	1.564
			4.9	.602	14.3	8.609
			2.9	1.004	14.1	14.156
			1.175	.889	14.1	12.535
Sept. 23, 1982, mission 6, flight 1061	2	1558-1612	6.45	.021	13.0	.273
			5.45	.287	12.1	3.473
			4.45	.596	11.9	7.092
			3.45	.688	12.0	8.256
			2.45	1.155	11.6	13.398
			1.45	1.563	11.8	18.443
			.725	1.112	11.9	13.233
	3	1608-1647	6.45	.064	13.0	.832
			5.45	.366	12.2	4.465
			4.45	.588	12.3	7.232
			3.45	.890	11.9	10.591
			2.45	1.412	11.7	16.520
			1.45	1.507	12.2	18.385
			.725	1.369	11.6	15.880
	4	1642-1710	7.45	.043	12.0	.515
			6.45	.373	12.2	4.551
			5.45	.609	12.2	7.430
			4.45	1.564	11.2	17.517
			3.45	1.606	12.0	19.272
			2.45	2.611	11.4	29.765
			1.45	2.460	11.5	28.290
			.725	1.879	11.6	21.796
	5	1709-1716	5.45	.186	10.0	1.860
			4.45	.682	10.1	6.343
			3.45	.466	10.3	4.800
			2.45	.703	10.2	7.171
			1.45	.968	10.2	9.874
			.725	.839	10.4	8.726
				3.040	4.71	4.290
			.225	2.638	4.81	2.664

Table 8–Apparent density of the particles in the plumes, by source

Source	Mass Concentration	Number of samples	Correlation coefficient	Density of particles
	$\mu g \cdot m^{-3}$			$g \cdot cm^{-3}$
Mass monitor	[a]	247	0.89	.98±0.03
Cascade microbalance	[b]	115	0.66	.86±.09

[a]0.98 (aerosol volume in $\mu m^3 \cdot cm^{-3}$) + 41.
[b]0.86 (aerosol volume in $\mu m^3 \cdot cm^{-3}$) + 35.

Table 9–PIXE analysis of emissions from slash burns[a]

Filter	Time	Na+	Mg	Al+	Si+	P	S	Cl+	K
Flight 1054 on July 23, 1982[b]									
A5(Amb)	1526-1535	—	—	—	1.7±0.70	—	0.5±0.4	—	—
A6	1603-1621	—	—	—	1.0±0.58	—	1.5±0.4	0.72±0.46	2.9±0.5
A7	1631-1651	2.5±1.3	0.77±0.39	1.6±0.5	1.4±0.44	1.6±0.34	1.7±0.37	0.88±0.41	3.2±0.5
A8	1733-1745	—	1.01±0.68	3.7±0.94	3.1±0.71	2.1±0.55	2.5±0.56	1.80±0.67	7.6±0.9
A9	1753-1810	—	—	1.2±0.95	2.5±0.72	2.0±0.53	3.2±0.76	—	4.9±0.8
A10	1818-1825	—	—	—	1.2±1.0	2.2±0.65	1.9±0.74	—	5.96±0.9
Flight 1055 on July 24, 1982[c]									
A1(Amb)	1557-1601	4.2±1.4	—	—	0.76±0.66	0.46±0.34	0.61±0.40	—	1.1±0.35
A2	1612-1621	—	1.3±0.76	1.0±0.77	2.6±0.86	—	1.5±0.64	0.86±0.54	1.6±0.47
A3	1633-1641	—	—	—	—	1.3±0.88	—	1.70±0.94	6.1±1.1
A4	1650-1659	—	1.4±0.92	1.9±0.93	2.2±0.87	1.6±0.59	1.8±0.69	—	4.9±0.72
A11	1710	—	—	3.7±2.5	—	5.3±1.5	—	2.10±1.4	6.4±1.4
A12	1723-1735	—	—	—	—	—	1.5 ±0.8	—	2.4±0.72
A13	1745-1754	—	1.6±0.68	2.9±1.0	—	2.5±0.73	2.9±0.61	0.62±0.52	7.2±0.92
A14	1801-1824	—	—	—	—	0.68±0.50	1.2±0.61	—	1.9±0.4
A15(Amb)	1820-1824	—	—	—	1.9±0.59	0.77±0.37	0.91±0.54	—	0.70±0.32

Ca	Pb	Cr	Mn	Fe	Ni	Zn	Cu
—	—	0.3±0.25	—	5.6±0.6	—	—	0.26±0.15
6.5±0.74	—	0.37±0.27	1.5±0.36	5.7±0.65	0.47±0.2	0.44±0.18	—
19.7±2.0	—	—	2.0±0.31	4.8±0.55	0.33±0.1	10.7±1.16	—
43.1±4.4	—	—	5.4±0.68	7.9±0.90	0.57±0.2	0.45±0.22	—
17.4±1.8	—	1.1±0.39	2.4±0.43	8.6±0.97	—	0.64±0.28	—
15.1±1.7	—	—	2.6±0.55	5.3±0.72	—	—	—
2.1±0.34	—	0.46±0.26	—	4.8±0.59	—	15.6±1.7	0.23±0.16
2.2±0.41	—	—	—	2.8±0.49	0.59±0.25	—	—
16.8±1.8	2.9±1.1	—	3.2±0.65	7.7±0.99	1.4±0.40	6.4±0.90	—
17.6±1.9	—	—	4.1±0.64	7.5±0.90	0.46±0.22	—	—
12.5±1.6	6.7±2.2	—	2.0±0.76	.4±1.0	—	—	—
7.5±0.99	—	—	2.0±0.50	4.4±0.62	0.51±0.22	—	—
16.9±1.8	—	0.53±0.33	3.4±0.52	4.5±0.60	0.37±0.23	—	—
4.5±0.73	—	—	0.72±0.23	2.8±0.48	—	—	—
—	—	0.34±0.28	—	2.7±0.41	—	—	—

Table 9–(continued)

Filter	Time	Na+	Mg	Al+	Si+	P	S	Cl+	K
Flight 1056 on July 25, 1982									
A17	0842-0846	—	1.2±0.58	—	2.4±0.83	—	1.1±0.52	1.0±0.54	0.83±0.38
A18	0953-1000	—	—	—	—	1.8±0.88	1.4±0.65	1.3±0.77	2.6±0.6
A19	1009	—	2.3±1.9	—	3.4±1.8	2.7±1.0	2.8±1.1	—	—
A20	1021-1037	—	—	—	—	—	0.92±0.45	—	0.77±0.35
A21	1044-1058	—	—	—	1.1±0.70	0.86±0.33	1.0±0.38	0.96±0.41	1.6±0.39
A23	1137-1144	—	—	—	1.9±0.68	—	0.81±0.39	—	1.2±0.37
Flight 1057 on July 26, 1982[d]									
A36	1012-1015	—	1.2±0.53	2.3±0.90	—	—	0.61±0.53	—	0.77±0.29
A37	1041-1049	—	2.9±0.75	—	—	—	1.0±0.42	—	0.59±0.30
A38	1056	1.8±1.6	2.2±0.85	5.3±1.7	5.2±1.5	—	1.2±0.71	—	2.1±0.62
A39	1104-1111	—	—	2.5±1.1	—	—	2.0±0.50	1.4±0.49	3.2±0.
A40	1127	—	—	—	—	1.3±0.87	1.0±0.82	—	—
A41	1134-1146	—	1.8±0.37	1.6±0.64	1.7±0.44	1.4±0.34	0.75±0.41	1.0±0.34	2.9±0.44
A42	1154	5.9±2.1	—	5.1±1.8	—	2.4±0.93	1.2±0.68	—	2.6±0.84
A43	1202-1206	—	—	3.8±1.1	1.4±0.64	1.1±0.38	0.73±0.54	—	2.7±0.49
A44	1217-1225	—	1.7±0.67	2.4±0.70	1.2±0.59	1.5±0.40	1.3±0.43	0.86±0.50	3.1±0.56
A45	1233-1240	—	1.2±0.70	2.2±0.85	—	2.0±0.63	1.7±0.69	—	3.1±0.56

	Ca	Pb	Cr	Mn	Fe	Ni	Zn	Cu
	0.58±0.28	—	—	—	2.7±0.43	—	—	—
	1.1±0.44	—	1.2±0.46	—	2.2±0.45	—	—	—
	1.0±0.75	—	—	—	5.2±0.98	1.8±0.60	—	—
	1.1±0.37	—	—	—	3.5±0.48	—	—	—
	4.0±0.54	—	0.32±0.29	0.90±0.28	2.9±0.41	—	—	—
	1.5±0.36	—	—	—	1.3±0.29	—	—	—
	1.0±0.29	3.0±0.85	0.32±0.26	—	3.7±0.46	—	—	1.5±0.45
	2.2±0.37	—	—	—	2.4±0.37	—	—	—
	5.3±0.75	—	2.56±0.50	—	2.6±0.51	0.72±0.35	—	—
	6.4±0.75	—	—	1.5±0.34	3.3±0.45	—	2.0±0.37	1.1±0.33
	3.3±0.64	—	—	—	3.5±0.67	0.72±0.34	—	2.2±0.58
	12.1±1.3	2.6±0.66	—	1.5±0.26	4.6±0.52	—	1.5±0.27	1.4±0.30
	11.3±1.3	—	—	0.63±0.40	3.8±0.63	—	2.5±0.55	2.1±0.60
	8.5±0.94	2.0±0.64	0.47±0.26	0.99±0.26	2.6±0.39	0.38±0.17	—	—
	11.0±1.2	—	—	1.4±0.31	3.9±0.50	0.19±0.16	—	—
	9.2±1.0	—	0.89±0.33	1.1±0.32	2.9±0.46	0.73±0.22	—	—

Table 9--(continued)

Filter	Time	Na+	Mg	Al+	Si+	P	S	Cl+	K
Flight 1060 on September 15, 1982[e]									
UW1(Amb) 1402		5.1±1.3	—	2.8±1.2	—	—	—	0.92±0.46	—
UW2	1407-1415	—	0.5±0.34	—	0.46±0.39	0.4±0.26	1.3±0.35	3.2±0.49	8.3±0.89
UW3	1426-1435	4.6±1.5	1.6±0.41	3.6±0.81	4.0 ±0.62	1.8±0.36	4.0±0.62	9.3±1.0	18.5±1.9
UW4	1440-1445	—	1.2±0.51	—	0.60±0.39	1.3±0.31	3.9±0.49	6.5±0.74	12.5±1.3
UW5	1445	—	4.4±0.84	4.2±1.2	4.1±0.76	1.6±0.48	4.5±0.71	3.8±0.71	12.5±1.4
UW6	1502-1509	—	1.2±0.46	1.7±0.69	1.3±0.44	1.5±0.34	3.1±0.51	5.4±0.68	11.4±1.2
UW7	1517-1524	—	1.7±0.46	1.9±0.86	2.3±0.60	1.7±0.36	5.1±0.76	10.2±1.1	20.7±2.
UW8	1530-1536	—	3.2±0.70	3.5±0.76	2.0±0.46	1.8±0.33	3.8±0.53	4.2±0.56	12.8±1.4
UW9	1546-1553	—	2.2±0.59	2.5±0.58	2.2±0.52	1.0±0.30	2.6±0.40	2.9±0.48	9.6±1.0
UW10	1614-1625	—	2.9±0.56	5.2±0.86	2.5±0.57	1.5±0.30	3.0±0.48	2.9±0.45	8.8±0.92
UW11	1633-1640	—	—	—	—	0.73±0.41	2.7±0.49	3.8±0.56	11.9±1.3
UW12	1651-1658	—	4.4±0.66	3.1±1.2	1.7±0.40	1.5±0.30	4.5±0.82	4.8±0.58	11.1±1.1
UW13	1705-1711	—	2.4±0.58	2.0±0.68	0.5±0.40	0.85±0.28	2.4±0.49	2.2±0.40	7.0±0.74
UW14	1719-1726	—	3.2±0.66	2.7±0.82	1.7±0.43	1.7±0.31	3.7±0.58	3.1±0.46	11.4±1.3
UW15	1731	—	—	2.2±1.6	—	—	1.3±0.83	3.0±0.62	8.9±1.0
UW16	1742	—	3.3±0.98	7.1±1.3	3.8±0.83	2.2±0.54	3.4±0.72	2.4±0.64	15.9±1.7

Ca	Pb	Cv	Mn	Fe	Ni	Zn	Br
1.0±0.43	—	—	—	9.4±1.0	0.29±0.17	5.9±0.69	0.66±0.31
11.7±1.2	1.5±0.48	0.40±0.17	2.0±0.27	8.1±0.85	—	1.1±0.18	1.1±0.2
23.4±2.4	1.8±0.51	0.21±0.20	3.2±0.38	10.3±1.1	—	15.8±1.6	1.6±0.34
16.0±1.6	—	0.25±0.18	2.4±0.32	4.1±0.46	—	0.81±0.17	3.8±0.53
17.1±1.8	1.4±0.76	—	2.1±0.37	8.4±0.52	—	2.5±0.36	2.3±0.58
13.3±1.4	1.4±0.50	0.23±0.20	2.2±0.30	4.9±0.54	0.23±0.13	0.87±0.18	1.4±0.31
23.2±2.3	2.0±0.57	—	4.0±0.48	6.5±0.70	—	5.9±0.70	2.0±0.38
11.8±1.2	1.0±0.44	—	2.1±0.28	3.1±0.36	0.13±0.10	0.75±0.18	0.83±0.24
9.4±0.99	0.60±0.40	0.22±0.19	1.4±0.23	4.7±0.52	—	1.5±0.23	—
15.9±1.6	1.2±0.43	—	2.5±0.32	4.3±0.47	0.13±0.10	0.97±0.17	1.3±0.29
13.7±1.4	1.0±0.49	0.48±0.18	2.1±0.31	4.9±0.55	—	1.3 ±0.20	1.4±0.37
7.6±0.81	4.2±0.71	—	1.5±1.22	2.1±0.25	0.11±0.88	0.36±0.10	3.8±0.5
7.7±0.82	2.0±0.54	0.18±0.13	1.7±0.24	2.3±0.30	0.17±0.12	0.18±0.10	1.7±0.34
12.8±1.3	1.8±0.49	—	1.8±0.25	3.9±0.43	—	1.3 ±0.20	1.8±0.34
5.4±0.63	6.5±1.2	—	1.0±0.32	1.8±0.33	0.26±0.18	—	4.9±0.73
12.3±1.3	2.2±0.73	—	2.5±0.40	5.2±0.61	0.25±0.16	4.4±0.53	1.3±0.38

Table 9–(continued)

Filter	Time	Na[a]	Mg	Al[a]	Si[a]	P	S	Cl[a]	K
Flight 1061 on September 23, 1982[f]									
UW17(Amb)	1535	—	—	—	—	—	—	—	1.2±0.62
UW18	1531-1537	—	—	—	1.6 ±0.45	0.57±0.25	2.5±0.42	3.3±0.52	7.7±0.82
UW19	1547-1554	—	0.81±0.40	0.59±0.48	0.99±0.40	0.91±0.28	2.6±0.40	4.0±0.55	10.4±1.1
UW20	1559-1612	1.4±0.76	2.2±0.45	2.1±0.59	2.1±0.33	0.61±0.16	2.3±0.39	2.5±0.34	8.0±0.82
UW21	1619-1624	—	0.78±0.48	2.3 ±0.51	1.0±0.42	0.40±0.25	1.9±0.35	1.3±0.38	6.9±0.76
UW22	1639-1646	—	—	—	—	—	2.3±0.43	1.4±0.40	7.1±0.80
UW23	1656-1710	—	—	—	—	0.51±0.23	1.2±0.44	2.8±0.36	8.9±0.92

	Ca	Pb	Cv	Mn	Fe	Ni	Zn	Br
	1.9±0.44	—	0.97±0.30	—	6.6±0.81	—	4.1±0.56	—
	6.0±0.65	0.79±0.37	0.22±0.15	1.3±0.22	2.3±0.29	—	0.52±0.15	—
	9.7±1.0	—	—	2.0±0.29	2.8±0.34	0.30±0.12	3.3±0.3	0.47±0.21
	7.4±0.76	1.5±0.42	0.09±0.09	1.1±0.14	2.7±0.29	0.09±0.06	0.54±0.10	1.2±0.28
	5.6±0.61	—	0.33±0.20	0.98±0.20	2.4±0.30	0.13±0.11	0.91±0.18	—
	4.4±0.53	—	0.29±0.21	0.87±0.20	2.1±0.29	0.16±0.14	0.36±0.15	0.36±0.20
	6.2±0.64	3.2±0.28	0.14±0.12	1.3±0.18	3.8±0.41	—	1.6±0.20	0.56±0.15

[a] The numbers in the body of the table are the concentrations of the specified element in $\mu g \cdot m^{-3}$. Matrix correction factors have been applied only in cases in which they are ≥10 percent. The correction factors are: Na=1.45, Al=1.70, Si=1.39, Cl=1.13, K=1.09, Ca=1.085, Ti=1.057.

[b] V, Br, and Ti were not detected.

[c] Filter A3 had Br = 1.7±0.55 $\mu g \cdot m^{-3}$. Br was not detected on remaining filters.

[d] No Cu measured on this flight.

[e] No Cr or Cu measured on this flight.

[f] Cu on UW19 was 0.12±0.12.

Table 10--Comparisons of Oregon Graduate Center (OGC) and LEMSCO measurements on air samples collected in canisters from the polyethylene bag sampler, by sample

Sample[a]	Date	CH_4	CO	CO_2	Total nonmethane hydrocarbons[b] (TNMHC)[b]
		---------- ppb----------		ppm	$\mu g \cdot m^{-3}$
148 L	July 23, 1982	1540	450	332.6	
148 OGC	July 23, 1982	1651	324	359.6	
114 L	July 23, 1982	1950	6150	406.3	
114 OGC	July 23, 1982	2110	5855	421.6	
58 L	July 24, 1982	1530	4640	424.5	
58 OGC	July 24, 1982	1653	4385	442.8	
238 L	July 24, 1982	1530	1950	424.5	788
238 OGC	July 24, 1982	1681	570	350.5	476.9
12 L	July 25, 1982	1590	1140	336.0	
12 OGC	July 25, 1982	1628	1222	354.6	
271 L	July 25, 1982	1600	790	326.9	
271 OGC	July 25, 1982	1693	785	349.6	
250 L	July 26, 1982	1810	3700	372.3	204
250 OGC	July 26, 1982	1896	3540	379.2	188.2
267 L	July 26, 1982	1530	740	337.9	
267 OGC	July 26, 1982	1680	807	360.0	

[a] The number refers to the labeled canister number; L = LEMSCO and OGC = Oregon Graduate Center.

[b] TNMHC = Total nonmethane hydrocarbons
The LEMSCO analysis did not include the C^2 hydrocarbons. OGC did not present a value for total hydrocarbons, and we have not evaluated the LEMSCO measurements of THC. We note that the technique employed by LEMSCO (an FID detector with no precolumn separation into individual hydrocarbons) is no longer generally accepted as a reliable method.

Table 11--Comparison of Oregon Graduate Center (OGC) measurements on samples collected in canisters from the stainless sampling oop with the LEMSCO measurements on samples collected in canisters from the polyethylene bag sampler, by sample

Sample[a]	Date	CH_4	CO	CO_2	Total nonmethane hydrocarbons (TNMHC)[b]
		---------- ppb ---------		ppm	($\mu g \cdot m^{-3}$)
L	July 23, 1982	1850	3903	376	734±177
OGC	July 23, 1982	1928	2925	373	168.5
L	July 24, 1982	1690	2649	349	396±139
OGC	July 24, 1982	1749	1197	351	71.3
L (ambient air)	July 25, 1982	1540	590	327.7	407
OGC (ambient air)	July 25, 1982	1639	148	343	6.3
L (plume)	July 25, 1982	1667	1633	341	305±96
OGC (plume)	July 25, 1982	1725	1165	349	52.7
L (plume)	July 26, 1982	1900	2538	361	±204
OGC (plume)	July 26, 1982	1897	2838	363	133.2
L (ambient air)	July 26, 1982	1580	380	336	±204
OGC (ambient air)	July 26, 1982	1607	144	346	7.2

[a] L = LEMSCO and OGC = Oregon Graduate Center.

[b] The LEMSCO analysis did not include the C_2 hydrocarbons. OGC did not present a value for total hydrocarbons, and we have not evaluated the LEMSCO measurements of THC. We note that the technique employed by LEMSCO (an FID detector with no precolumn separation into individual hydrocarbons) is no longer generally accepted as a reliable method.

Table 12–Emission factors for total suspended particulates derived by the carbon-balance method by using weighed filters, by mission number

Mission number	Date	UW flight number	Ignition time	Time interval (PDT)	Emissions factor
					$g \cdot kg^{-1}$
1	July 23, 1982	1054	1540	1603-1621	2.4
				1631-1651	36.6[a]
				1733-1745	12.4
				1753-1810	11.9
				1818-1825	11.5
2	July 24, 1983	1055	1538	1633-1641	8.7
				1650-1659	7.6
				1723-1735	12.1
				1745-1754	13.2
				1801-1810	9.3
3	July 25, 1982	1056	0925	0953-1000	9.2
4	July 26, 1982	1057	1008	1041-1049	8.5
				1056	9.5
				1104-1111	8.8
				1134-1146	13.9
				1154	18.4
5	Sept. 15, 1982	1060	1340 (est)	1415	24.4
				1426-1435	12.1
				1440-1445	12.9
				1445	10.9
				1502-1509	11.4
				1517-1524	10.7
				1530-1536	15.9
				1546-1553	8.7
				1614-1625	17.4
				1633-1640	12.8
				1651-1658	12.0
				1705-1711	11.5
				1719-1726	15.4
				1731	12.1
6	Sept. 23, 1982	1061	1525	1531-1537	8.7
				1547-1554	12.8
				1559-1612	15.5
				1619-1624	11.0
				1639-1646	14.7
				1656-1710	14.6

[a] Co_2 concentrations are suspect; therefore, emission factor is questionable and has been omitted in calculating the mean emission factor given in the text.

Table 13–Emission factors for various sizes of particle, by date

Date, mission, and UW flight	Sample intervals (PDT)	Emission factors: For total suspended particulates (from filter measurements)	Emission factors: For particles ≤43 µm diameter (from particle measurements)	Emission factors: For particles <2 µm diameter (from mass monitor)	Emission factors: For particles <2 µm diameter (from cascade microbalance)
		g/kg			
July 23, 1982, mission 1, flight 1054	1603-1621	2.4	2.2	1.4	1.5
	1631-1651[a]	36.6	31.3	14.9	10.4
	1733-1745	12.4	7.8	3.5	2.7
	1753-1810	11.9	6.9	4.3	2.8
	1818-1825	11.5	3.5	6.6	4.3
July 24, 1982, mission 2, flight 1055	1612-1621	—	2.1	—	3.6
	1633-1641	8.7	2.3	1.0	7.2
	1650-1659	7.6	2.8	1.9	2.8
	1723-1735	12.1	5.8	3.3	6.4
	1745-1754	13.2	5.1	4.1	2.2
	1801-1810	9.3	4.2	5.1	4.9
July 25, 1982, mission 3, flight 1056	0953-1000	9.2	3.0	—	2.2
July 26, 1982, mission 4, flight 1057	1041-1049	8.5	2.9	5.5	2.2
	1056	9.5	3.6	2.3	2.1
	1104-1111	8.8	4.0	2.4	2.4
	1134-1146	13.9	3.6	3.7	2.2
	1154	18.4	2.9	3.3	3.0
	1202-1208	12.8	4.6	3.0	2.5
	1217-1225	11.4	4.2	2.8	4.1
	1233-1240	17.0	7.2	4.9	6.7
Sept 15, 1982, mission 5, flight 1060	1415	24.4	17.5	—	
	1426-1435	12.1	6.1	—	—
	1440-1445	12.9	8.0	—	—
	1455	10.9	7.1	3.9	—
	1502-1509	11.4	8.6	3.5	—

Table 13–(continued)

Date, mission, and UW flight	Sample intervals (PDT)	Emission factors: For total suspended particulates (from filter measurements)	For particles ≤43 μm diameter (from particle measurements)	For particles <2 μm diameter (from mass monitor)	For particles <2 μm diameter (from cascade microbalance)
		g/kg			
	1517-1524	10.7	5.4	2.3	—
	1530-1536	15.9	13.0	5.5	—
	1546-1553	8.7	.7	6.8	—
	1614-1625	17.4	9.2	6.4	—
	1633-1640	12.8	8.2	3.8	—
	1651-1658	12.0	8.3	5.2	—
	1705-1711	11.5	8.5	4.8	—
	1719-1726	15.4	7.7	6.2	—
	1731	12.1	13.7	4.6	—
Sept 23, 1982, mission 6, flight 1061	1531-1537	8.7	3.1	3.2	—
	1547-1554	12.8	5.8	3.8	4.7
	1559-1612	15.5	5.1	5.5	7.4
	1619-1624	11.0	5.7	3.5	4.1
	1639-1646	14.7	6.6	5.8	2.5
	1656-1710	14.6	7.4	5.6	3.4

[a] CO_2 concentrations are suspect; therefore, emission factor is questionable and has been omitted in calculating the mean emission factors given in the text.

Table 14–Particle mass fluxes in the plumes for various particle sizes, by date

Date, mission, and UW flight	Cross section sequence number	Time interval (PDT)	For total suspended particulates (from filters)		For particles ≤43 μm diameter (from particle size spectra data)	For particles <2 μm diameter (from mass monitor data)
			Using the TSP b_{scat} algorithm	Using the ratio method		
			---------- Kilograms per second ----------			
July 23, 1982, mission 1, flight 1054	1	1606-1644	0.852	0.617	0.323	0.256
	2	1640-1723	1.195	.945	.467	.368
	3	1719-1745	.552	.568	.242	.187
	4	1744-1814	.513	.495	.218	.170
July 25, 1982, mission 3, flight 1056	1	0950-1009	.287	.167	.100	.081
	2	1021-2041	.833	.537	.302	.241
	3	1037-1054	2.733	2.023	1.041	.824
	4	1051-1108	2.102	1.921	.868	.677
	5	1103-1120	2.064	1.687	.812	.638
	6	1113-1144	2.560	2.351	1.059	.826
July 26, 1982, mission 4, flight 1057	1	1041-1059	.227	.128	.078	.063
	2	1053-1118	.475	.413	.192	.150
	3	1114-1143	.158	.122	.061	.048
	4	1140-1159	1.104	1.035	.461	.359
	5	1157-1219	.665	.583	.269	.211
	6	1209-1231	.634	.574	.261	.203
	7	1227-1248	.531	.476	.217	.170
Sept. 15, 1982, mission 5, flight 1060	1	1415-1428	1.179	1.071	.637	.370
	2	1422-1500	8.993	7.769	4.724	2.787
	3	1500-1529	13.137	11.735	7.031	4.106
	4	1525-1610	9.391	8.103	4.930	2.909
Sept 15, 1982, mission 5, flight 1060	5	1608-1645	10.209	8.699	5.106	3.153
	6	1644-1721	10.031	8.531	5.224	3.096
	7	1713-1735	2.113	1.709	1.071	.644
Sept 23, 1982, mission 6, flight 1061	2	1558-1612	2.283	2.158	1.274	.870
	3	1608-1647	3.410	2.550	1.657	1.022
	4	1642-1710	6.459	5.009	3.006	1.951
	5	1713-1719	1.792	1.341	.871	.537

Radke, Lawrence F.; Lyons, Jamie H.; Hobbs, Peter V.; Hegg, Dean A.; Sandberg, David V.; Ward, Darold E. 1990. Airborne monitoring and smoke characterization of prescribed fires on forest lands in western Washington and Oregon. Gen. Tech. Rep. PNW-GTR-251. Portland, OR: U.S. Department of Agriculture, Forest Service, Pacific Northwest Research Station. 81 p.

Detailed airborne measurements of smoke plumes from seven prescribed burns of forest biomass residues leftover from timber harvests in Washington and Oregon are described. Measurements of particle size distributions in the plumes at ≈3.3 km downwind of the burns showed a prominent peak in the mass concentration for particles ≈0.25-0.30 µm in diameter. The total mass of particles in the plume was dominated, however, by supermicron-sized particles. The particle number distributions were dominated by large numbers of Aitken nuclei (median number diameter ≈0.15 µm).

Based on numerous airborne measurements from six burns, the following average emission factors were determined using the carbon balance method: for total suspended particulates 1.2±0.4 percent, for particles ≤43 µm in diameter 0.6l±0.3 percent, and for particles <0.2 µm in diameter 0.4±0.2 percent. Particle mass fluxes for total suspended particulates, particles ≤43 µm diameter, and particles <2 µm diameter ranged from 0.1 to 2.4 $kg \cdot s^{-1}$, 0.1 to 1.1 $kg \cdot s^{-1}$ and 0.1 to 0.8 $kg \cdot s^{-1}$, respectively, for the smaller Oregon burns and from 1.1 to 11.7 $kg \cdot s^{-1}$, 0.6 to 7.0 $kg \cdot s^{-1}$, and 0.4 to 14.1 $kg \cdot s^{-1}$ respectively, for the larger Washington burns.

Other samples collected in conjunction with the airborne work included those for trace gas analysis, particulate matter for trace element analysis, and gas concentration measurements for carbon-mass analysis (oxides of nitrogen, ozone, and hydrocarbons). Mass concentration-to-light scattering coefficient algorithms and ratios, which can be used to convert integrating nephelometer response to mass concentration units, are also reported.

Keywords: Emissions, prescribed burning, smoke management.

Pacific Northwest Research Station
319 S.W. Pine St.
P.O. Box 3890
Portland, Oregon 97208

U.S. Department of Agriculture
Pacific Northwest Research Station
319 S.W. Pine Street
P.O. Box 3890
Portland, Oregon 97208

BULK RATE
POSTAGE +
FEES PAID
USDA-FS
PERMIT No. G-40

Official Business
Penalty for Private Use, $300

do NOT detach label